Inaugural dissertation

FOR

obtaining the doctoral degree

OF THE

Combined Faculty of Mathematics, Engineering and Natural Sciences

OF THE

Ruprecht – Karls – University

Heidelberg

Presented by
M.Sc. Naëmi Sarah Kuehn
Born in Heidelberg, Germany
Oral examination: 23.05.2023

Kainic acid-induced lumbar spinal cord damage leads to coordination deficits for the examination of cellular replacement therapies

Referees: Prof. Dr. Sabine Chourbaji
Dr. Radhika Puttagunta
Dr. Moritz Mall
Prof. Dr. Hilmar Bading

To my parents and Johannes

Abstract

Damage to the spinal cord can result in life-long deficits including locomotion. Most spinal cord injury cellular therapies focus on the regeneration of long-distance white matter descending motor tracts. However, locomotion is a complex task involving excitatory and inhibitory circuitry also in the spinal gray matter. The aim of this study was to create a discrete, gray matter lesion in the lumbar spinal cord to investigate the role of spinal interneurons in this region, as well as to establish a model that can evaluate proof-of principle targeted cell replacement therapies. A kainic acid lesion was modified to damage intermediate gray matter (laminae V-VII) in the lumbar spinal enlargement (spinal L2-L4) in 10-week-old female Fischer rats. A thorough, tailored behavioral evaluation revealed deficits in gross hindlimb function, skilled walking, coordination, balance and gait two-weeks post-injury. These deficits strongly correlated with structural deficits in the rostro-caudal axis. Machine-learning quantification confirmed interneuronal damage to laminae V-VII in spinal L2-L4 correlates with hindlimb dysfunction. White matter area and lower motoneuron numbers at lesion epicenters did not correlate with behavioral deficits. Animals do not regain lost sensorimotor function three months after injury, indicating that natural recovery mechanisms of the spinal cord cannot compensate for loss of laminae V-VII neurons. Together, this established model is ideal to evaluate cellular transplantation therapies that replace these lost neuronal pools vital to sensorimotor function.

Rat spinal cells taken from embryos age 14 contain a mix of neural stem cells and neural precursor cells and have shown potential to aid functional recovery. Studies have shown that they survive and differentiate into gray matter interneurons both *in vitro* and *in vivo,* despite being transplanted into white matter lesions. Using the newly established KA-model, E14 spinal graft survival in a lumbar gray matter lesion could be evaluated, for future proof-of-principle, targeted cell replacement experiments. Histological analysis revealed that grafted cells survive well both in the intact and KA-lesioned lumbar spinal cord without additional growth factors. Furthermore, grafts differentiate into neuronal NeuN+ cells both in the white and the gray matter. While future experiments will need to adjust injection parameters as well as evaluate graft differentiation and functional

benefits, this work lays the groundwork to assess the potential cellular replacement has to restore lost function after a lumbar spinal cord injury.

Zusammenfassung

Eine Schädigung des Rückenmarks kann zu lebenslangen Defiziten führen, auch bei der Fortbewegung. Die meisten zellulären Therapien für Rückenmarksverletzungen konzentrieren sich darauf, die absteigenden motorischen Langstreckenbahnen der weißen Substanz wiederherzustellen. Die Fortbewegung ist jedoch eine komplexe Aufgabe, an der auch erregende und hemmende Schaltkreise beteiligt sind, die in der grauen Substanz der Wirbelsäule vorhanden sind. Das Ziel dieser Studie war es, eine diskrete Läsion der grauen Substanz im lumbalen Rückenmark zu erzeugen, was ermöglicht die Rolle der spinalen Interneuronen in dieser Region zu untersuchen und ein Modell zu etablieren, mit dem sich der Nachweis von zielgerichteten Zellersatztherapien erbringen lässt. Eine Kainsäure-Läsion wurde modifiziert, um eine Schädigung der intermediären grauen Substanz (Laminae V-VII) in der lumbalen Rückenmarksvergrößerung (L2-L4) in 10 Wochen alten weiblichen Fischer-Ratten zu erreichen. Eine gründliche, maßgeschneiderte Verhaltensbeurteilung zeigte zwei Wochen nach der Verletzung Defizite bei der Funktion der Hinterläufer, beim geschickten Gehen, bei der Koordination, beim Gleichgewicht und beim Gangbild. Diese Defizite korrelierten stark mit strukturellen Defiziten in der rostro-caudalen Achse. Die Quantifizierung mittels maschinellen Lernens bestätigte, dass die Schädigung der Interneuronen in den Laminae V-VII der Wirbelsäule L2-L4 mit der Dysfunktion der Hintergliedmaßen korreliert. Die Fläche der weißen Substanz und unteren Motoneuronen in den Epizentren der Läsion korrelierten nicht mit Verhaltensdefiziten. Die Tiere erlangen die verlorenen sensomotorischen Funktionen drei Monate nach der Verletzung nicht wieder, was darauf hindeutet, dass die natürlichen Regenerationsmechanismen des Rückenmarks den Verlust der Neuronen der Laminae V-VII nicht kompensieren können. Zusammengenommen bietet dieses Modell eine ideale Bewertung neuer neuroregenerativer Therapien, um diese verlorenen Neuronenpools zu ersetzen, die für die sensomotorische Funktion wichtig sind.

Ratten-Rückenmarkszellen, die 14-tägigen Embryonen entnommen wurden, enthalten eine Mischung aus neuralen Stammzellen und neuralen Vorläuferzellen und haben das Potenzial, die funktionelle Erholung zu unterstützen. Studien haben gezeigt, dass sie

sowohl *in vitro* als auch *in vivo* überleben und sich in Interneuronen der grauen Substanz differenzieren, obwohl sie in Läsionen der weißen Substanz transplantiert wurden. Mit Hilfe des neu etablierten KA-Modells wollte ich das Überleben von E14-Transplantaten aus der Wirbelsäule in einer Läsion der grauen Substanz der Lendenwirbelsäule untersuchen, um zukünftige Experimente zum gezielten Zellersatz zu ermöglichen. Die histologische Analyse ergab, dass die transplantierten Zellen sowohl im intakten als auch im KA-läsonierten lumbalen Rückenmark ohne zusätzliche Wachstumsfaktoren gut überleben. Außerdem differenzieren sie sich sowohl in der weißen als auch in der grauen Substanz zu neuronalen NeuN+-Zellen. Obwohl die Injektionsparameter noch angepasst und die funktionellen Vorteile langfristig bewertet werden müssen, legt diese Arbeit den Grundstein für die Bewertung des Potenzials von Zellersatztherapien zur Wiederherstellung verlorener Funktionen nach einer Verletzung des lumbalen Rückenmarks.

Acknowledgements

I would like to express my deepest gratitude to all who have helped me and been there for me during my PhD. Without all of their support, I would not have gotten to where I am or become the person I am today.

I would like to especially thank my PI and supervisor, Dr. Radhika Puttagunta. Radhika gave me the opportunity to first do a rotation in her lab in 2017 which started my interest in cell transplantation and SCI, and continue on to do my master's thesis and PhD in her lab. I have learned a lot over these last few years and in particular how to think and write more critically. I am very grateful for her mentorship, persistence and openness to try new ideas and collaborate with others.
I would also like to thank Prof. Dr. Norbert Weidner for the opportunity to do my PhD in the Spinal Cord Injury Center at the Heidelberg University Hospital as well as for the expertise and clinical perspective he brought to this project.

I would like to thank my TAC members for agreeing to be on my TAC committee and providing guidance over the last years. I am especially grateful to Prof. Dr. Sabine Chourabji for being my first examiner and for sharing her passion for communicating a culture of care regarding animal research. I would also like to thank Dr. Moritz Mall for his quick feedback and Prof Dr. Hilmar Bading for being on my thesis committee.

I would like to thank my collaborators for their time and help in pushing this project forward. I would like to thank Dr. Jennifer Dulin and her lab for hosting me and teaching me how to isolate E14 spinal cells. I am also very grateful for Dr. David Magnuson and Alice Shum-Siu for sharing their expertise on developing this kainic acid lesion. I would like to thank Dr. Carlo Beretta for his expertise in image analysis and for setting up the NeuN quantification workflow. I am grateful for his expertise and for allowing me to do the analysis on his computers. I would also like to thank Dr. Andreas Schwarz for creating the Random Forest models and providing new insight into animal behavioral tests and classification. Both of their work adds new dimensions and insights to this project and future experiments. I would also like to thank the INBC for allowing me to do the CatWalk experiments in their facility, and in particular Barbara Kurpiers for explaining the program to me.

I am also very grateful to the Puttagunta laboratory members for all of their support along the way. I would like to especially thank Dr. Thomas Schackel for mentoring me during my rotation and teaching me how to culture cells, process tissue and other lab basics and for answering all of my questions. I would also like to thank Dr. Vasileios Kampanis for his help with the DREZ experiments, for the many conversations and advice he gave me. I would like to thank Melanie Motsch for her help with the animal work, for taking care of the lab managerial things, and for the time we spent together during the NISCI drug preparation. Without her help, things would not have gone as smoothly! I would like to thank Bahardokht Tolou-Dabbaghian for the pleasant conversations and friendship in the lab; Jing for her help with the cell transplantation experiment and Yifeng for his calm presence in the lab. I have really enjoyed our group dinners in Marstall and the time spent together. I would also like to thank Nicolas Rodemer, Francesca Schmitt and Yvonne Schwarte for their support establishing and characterizing this new model. I am also very grateful for Paul Ruf and Andrea Gunther for their animal expertise, help with animal breeding and tips for calmly handling animals.

Finally, I would like to thank my family and husband for all of their love and support during my PhD. To my family, even though we were on separate continents, I have felt their constant support. All of the texts, Skype dinner meals and visits brought so much laughter and have meant so much to me. I wouldn't be here today without all of their encouragement. I would like to thank my brother Noah for his quick wit. And I would especially like to express my deepest gratitude to my parents. I cannot properly express how grateful I am for the love, wisdom, support and grace they have shown me. They have always been there for me and have given me the opportunity to follow my dreams. They have shaped me into the person I am today and I hope I can become more like them.

And last but not least, I would like to thank Johannes for encouraging me every step of the way. I wouldn't be here without him. Thank you for celebrating all the highs together and carrying me through all the lows and for being there for everything else in between. I am forever grateful.

Table of Contents

Abbreviations

ABR	Ampicillin-buprenorphine-ringer
Ab	Antibody
AMPA	α-amino-3-hydroxy-5-methyl-4-isoxazolepropionic acid
ANOVA	Analysis of variance
BBB	Basso, Beattie, Bresnahan motor score
BDA	Biotinylated dextran amine
BMP	Bone morphogenetic protein
CGRP	Calcitonin gene-related peptide
Cm	Centimeter
CNS	Central nervous system
CSA	Cross-sectional area
CST	Corticospinal tract
CTB	Cholera-toxin b
DAPI	4’6-Diamidino-2-phenylindole
ddH_2O	Double distilled water
DMEM	Dulbecco’s modified Eagle medium
DPBS	Dulbecco’s phosphate buffered salt solution
DPI	Days post-injury
DRG	Dorsal root ganglia
EC	Eriochrome cyanine
EES	Epidural electrical stimulation
E	Embryonic day
FBS	Fetal bovine serum
FGF	Fibroblast growth factor
Foxp2	Forkhead box protein p2
Gad2	Glutamate decarboxylase 2
GFAP	Glial fibrillary acidic protein
GFP	Green fluorescent protein
gp	Guinea pig

gt	Goat
H_2O	Water
HBSS	Hank’s buffered salt solution
Hoxa10	Homeobox A10
Iba1	Ionized calcium-binding adaptor molecule 1
ICC	Immunocytochemistry
IgG	Immunoglobulin G
IHC	Immunohistochemistry
Il-1ß	Interleukin 1 beta
IM	Intramuscularly
INs	Interneurons
IP	Interperitoneally
iPSCs	Induced pluripotent stem cells
KA	Kainic acid
Kg	Kilogram
LHRH	LHRH
µm	Micrometer
mg	Milligram
ml	Milliliter
MIP	Maximum intensity projection
mm	Millimeter
mM	Millimolar
MN	Motoneuron
ms	Mouse
Na	Sodium
NaCl	Sodium chloride
NaOH	Sodium hydroxide
NBM	Neurobasal medium
NeuN	Neuronal nuclei
Nf1b	Nuclear factor 1 B-type
NOS	Native oxygen species

N.S.	Not significant
NSC	Neural stem cell
NPC	Neural progenitor cell
Olig2	Oligodendrocyte transcription factor 2
Pax 6	Paired box 6
Pax 7	Paired box 7
PB	Phosphate buffer
PBS	Phosphate buffered salt solution
PDL	Poly-d-lysine
Pen/Strep	Penicillin/streptomycin
PFA	Paraformaldehyde
pLDA	Parameter linear discriminant analysis
PNS	Peripheral nervous system
PRV	Pseudorabies virus
RA	Retinoic acid
RI	Regularity Index
Rb	Rabbit
ROI	Region of interest
r.p.m.	Rotations per minute
Satb1	Special T-Reich sequence bding protein -1
Sec	Seconds
SEM	Standard error of the mean
SCI	Spinal cord injury
Shh	Sonic hedgehog
Sox 2	Sex-determining region Y-box 2
SpINs	Spinal interneurons
TBS	TRIS-buffered salt solution
TNFα	Tumor necrosis factor alpha
TRIS	Tris(hydroxymethyl)aminomethane
Vs	Versus
Vsx2	Variable charge x-linked 2

Wnt	Wingless /integrated
w/v	Weight per volume
2D	Two-dimensional
3D	Three-dimensional

List of Figures

List of Tables

1 Introduction

1.1.1 Locomotion

Locomotion is a highly complex task involving intricate circuits in the central nervous system (CNS). Supraspinal input and afferent information converge in the spinal cord and are modified to ultimately induce a motor output in the periphery. The spinal cord is composed of white and gray matter which is structured into ten laminae. These laminae are composed of spinal interneurons (SpINs) and propriospinal interneurons (INs) which span short and long distances to connect segments within the spinal cord. Short SpINs span 1-3 spinal segments while long ones span more than three (Jankowska et al., 1974; Laliberte et al., 2019). Previous experiments using genetic and histological methods have shown that SpINs and propriospinal INs in the intermediate gray matter of the lumbar cord play an important role in spinal reflexes, rhythmic locomotion and the transmission of information to other parts of the cord (Crone et al., 2008; Dai et al., 2005; Gosgnach et al., 2006; Lanuza et al., 2004; Lundfald et al., 2007; Viala et al., 1988; Zavvarian et al., 2020; Zholudeva et al., 2018). There is evidence that circuitry within the gray matter of the lumbar enlargement can create rhythmic locomotion without supraspinal input. Early studies in cats and dogs that received a complete transection in the thoracic area were still able to generate a basic rhythm and pattern for stepping (Bear et al., 2016; Brown, 1914; Sherrington, 1910; Whelan, 1996). Later studies have shown that the circuitry mainly responsible for this resides in L1 and L2 lumbar cord in mice (Nishimaru et al., 2000) and later via electrical stimulation in L1 and L2 of the spinal cord in human paraplegic patients as well (Dimitrijevic et al., 1998; Guertin, 2009).

It has been previously shown that a large gray matter lesion in the rostral-lumbar enlargement resulted in gross locomotor deficits. These lesions were created with kainic acid (KA). KA is an excitotoxin normally found in seaweed and is an analogue to glutamate. It is 30 times more potent in neurotoxicity than glutamate and can cause neuronal death by excitotoxicity (McGeer & McGeer, 1978; Olney et al., 1974). The agonist kainate can activate both kainic acid receptors as well as α-amino-3-hydroxy-5-methyl-4-isoxazolepropionic acid (AMPA) receptors (Wang et al., 2005; Zhang & Zhu,

2011). After activation, a calcium influx leads to the disintegration of the endoplasmic reticulum membrane, generation of native oxygen species (NOS), and mitochondrial dysfunction ultimately causing neuron apoptosis and necrosis (Nicholls, 2004; Schinder et al., 1996; Zhang & Zhu, 2011). In culture, cerebellar granule cell death sharply increased 4 hours after KA exposure and peaked after 12 hours (Simonian et al., 1996). This toxin is most commonly used to mimic seizures in epileptic models however scientists have also injected KA into the lumbar spinal cord and found that it damages neurons in the gray matter (Hadi et al., 2000; Magnuson et al., 1998; Nothias & Peschanski, 1990). Density of excitatory amino acid receptors, including kainate receptors is higher on the dendrites of neurons rather than the soma, both of which are located within the gray matter (Arancio & MacDermott, 1991; Arancio et al., 1993). Previous studies have shown that following a gray matter lesion, gross hindlimb function was most severely affected when neuronal loss included spinal level L2; these deficits were not seen in a thoracic gray matter lesion highlighting the importance of neurons at this spinal level (Hadi et al., 2000; Magnuson et al., 1999). Furthermore, these deficits did not correlate with motoneuron loss or white matter damage. However, while it was suggested that the intermediate gray matter is responsible for these deficits, the most severe neuronal damage was seen in both the dorsal horns and intermediate gray matter (Hadi et al., 2000).

Within the lumbar spinal cord, researchers have tried to understand which cell populations play an important role in locomotion, where they reside and their connectivity (**Fig. 1)**. Genetic ablation experiments have examined the role of individual neurons responsible for locomotion. For example, studies examining the role of inhibitory V2b INs located in the ventral intermediate gray matter have shown their role in locomotion speed (Callahan et al., 2019). V1 INs can alter the speed of the step cycle and provide inhibitory signals for flexor muscles during the contraction phase of locomotion (Britz et al., 2015). Silencing ipsilateral and contralateral INs in L2-L5 of the rat spinal cord altered left-right hindlimb alternation while walking (Prokrastsky et al., 2017).

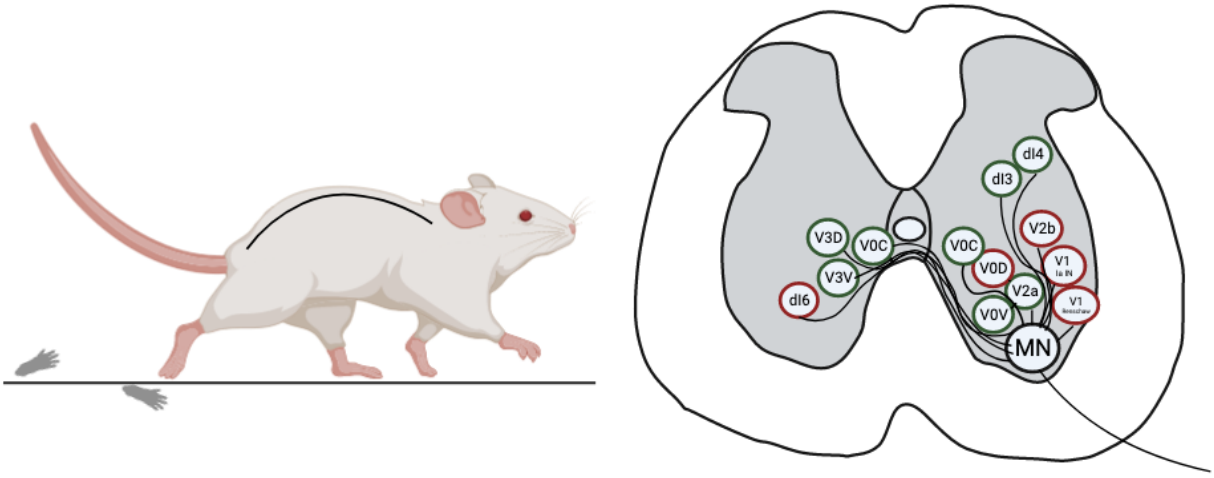

Figure 1. Simplified schematic of a subset of interneuronal pools that influence motoneuron activity during locomotion. Red circles indicate neuron pools are inhibitory, green circles indicate neuron pools are excitatory, black circles indicate motoneurons (MNs).

cFos experiments have analyzed neuronal activity in adult rats after treadmill walking. There were significantly more cFos positive neurons in laminae IV, V and VII in T13-L6 spinal cord in rats post-walking than those who did not (Ahn et al., 2006). More recent experiments have used sequencing techniques to identify neuronal subtypes involved in locomotion. Single nucleus RNA sequencing was used to identify 43 individual spinal cord neuron populations present in the mouse lumbar spinal cord. Furthermore, activity-induced Fos RNA expression was analyzed following formalin stimulation and rotarod training. The majority of neuronal populations specific to locomotor function were located in the intermediate gray matter and expressed genes including nuclear factor 1 B-type (*Nf1b*), special T-rich sequence-binding protein-1 (*Satb1*), forkhead box protein P2 (*Foxp2)*, and glutamate decarboxylase 2 (*Gad2*) (Sathyamurthy et al., 2018). Single nucleus RNA sequencing and spatial transcriptomic analysis on lumbar spinal cords in mice following a thoracic contusion injury have shown that one population in particular is responsible for locomotion after SCI. These neurons, $SC^{Vsx2:Hoxa10}$, were located in the intermediate gray matter and are derived from excitatory V2a INs. When activated, neurons that expressed variable charge x-linked 2 (*Vsx2*) and homeobox A10 (*Hoxa10*) elicited motor output comparable to that of epidural electrical stimulation (EES) stimulation. Ablation of these neurons prevented spontaneous recovery. Interestingly,

these neurons are not required for walking prior to injury however are essential after injury (Kathe et al., 2022). Together these experiments highlight the complex nature of individual neuronal subpopulations and networks involved in locomotion, particularly in rodents. (Adapted from (Kuehn et al., Manuscript in preparation) and was written by myself).

1.1.2 Spinal Cord Injury

Injury to the spinal cord, including the lumbar spinal cord, can be devastating and significantly change quality of life. Unlike the peripheral nervous system (PNS), the central nervous system (CNS) does not repair spontaneously resulting in often permanent damage. Spinal cord injury (SCI) can be caused by traumatic or non-traumatic injury. SCI is classified as non-traumatic when there is spinal cord damage due to an infection or tumor for example and usually takes time to develop. Damage to the spinal cord is classified as traumatic when the injury occurs suddenly, such as following a car accident or fall (Ahuja et al., 2017). Traumatic SCI prevalence is higher in more developed countries, the highest being in North America which has 39 cases per million individuals in comparison to western Europe 15 cases per million individuals (Ahuja et al., 2017; Cripps et al., 2011). Since 2015 in the US, the majority of SCI cases are caused by car accidents (38%) as well as falls (31%), followed by violence (15%), sports (8%) and medical/surgical causes (4%) (NSCISC, 2022; WHO, 2013). The average SCI patient is 43 years old (NSCISC, 2022). Younger individuals are more commonly affected by car accidents while older individuals are more commonly affected by falls (Ahuja et al., 2017; Alizadeh et al., 2019; DeVivo & Chen, 2011). Additionally, males are more commonly affected by SCI than females (78% & vs 22%) (Chen et al., 2016; NSCISC, 2022; WHO, 2013). Depending on the level and severity of the injury, patients are left with lifelong deficits to their quality of life as well as expensive healthcare bills (Alizadeh et al., 2019; NSCISC, 2022). Not only is SCI a major life change for the patient but the patient's loved ones as well.

1.1.3 SCI Pathology

On a biological level, traumatic SCI can be split into two main phases, primary and secondary injury (Quadri et al., 2020; Rowland et al., 2008). During the primary phase, the immediate injury impact can cause vertebral damage, compression and damage to the spinal cord. Primary injury causes the spinal cord to swell; damage to the blood-spinal cord barrier (BSCB) and hemorrhaging deprives cells of oxygen and glucose (Rowland et al., 2008; Tran et al., 2018). Extracellular glutamate reaches excitotoxic levels shortly after injury (Agrawal & Fehlings, 1996; Faden et al., 1989; Wrathall et al., 1996). Damaged neurons and glial cells release inflammatory cytokines such as tumor necrosis factor alpha (TNFα) and interleukin 1 beta (Il-1ß), initiating the secondary injury phase (Ahuja et al., 2017; Pineau & Lacroix, 2007). The secondary phase can be split into four phases of which the first, 2-48 hours after injury, is considered to be the acute phase in rodents (Rowland et al., 2008). During this time, damage to cell membranes increases membrane permeability and can lead to the release of glucose and calcium influx, causing mitochondrial disfunction and cytoskeleton destruction (Hayes et al., 1992; Weber, 2004; Young, 1992).The microtubules in the proximal part of the severed neuron destabilize allowing the neuron to die back while the distal part begins to undergo Wallerian degeneration where the severed axon and myelin sheath fragments begin to degenerate (Filous & Schwab, 2018). Further hemorrhaging particularly in the gray matter can lead to necrosis (Tator & Koyanagi, 1997). Continued compression of the spinal cord can lead to ischemia, increasing free radical production; high levels of highly reactive oxygen and nitrogen species lead to oxidative stress and can induce cell apoptosis (Borgens & Liu-Snyder, 2012; Oyinbo, 2011; Rowland et al., 2008). Additionally, there is an upregulation of inflammatory cytokines activating the immune response (Fleming et al., 2006; Popovich et al., 1997). Next, the subacute phase is considered 2 days to two weeks after injury (Rowland et al., 2008). Activated astrocytes, microglia and macrophages infiltrate the lesion site and further induce swelling and exacerbate the injury by releasing more inflammatory cytokines (Burda & Sofroniew, 2014; Kawaja & Gage, 1991; Tran et al., 2018; Wanner et al., 2013). During this time, astrocytes begin to fix the integrity of the blood spinal cord barrier. The fibroglial scar starts to form which prevents the injury from spreading further however also acts as a physical barrier for regenerating neurons. While

it may partially limit neuroregeneration, other studies have shown that attenuation of the astrocytic scar actually leads to a greater lesion size, more axonal dieback and more demyelination (Bush et al., 1999; Faulkner et al., 2004). Demyelination limits the conduction of nerve impulses. This highlights the complexity and double-sided nature of many of the SCI responses. Additionally during this subacute phase, while greater in PNS injury than CNS, the phagocytic response removes cellular and myelin debris (Donnelly & Popovich, 2008; Rowland et al., 2008). The following 2 week to 6 month period is considered the intermediate phase, where damaged neurons may start to regenerate or sprout (Hill et al., 2001). This occurrence and impact on function largely depends on the severity of the injury and several other confounding factors. Lastly, the chronic phase is the final phase (Rowland et al., 2008). Cyst formation in primates and rats (but not mice) may occur and damaged axons may continue to undergo Wallerian degeneration (Beattie et al., 2002; Coleman & Perry, 2002). The lesion is considered mature 1-2 years after injury and neurological function has likely stabilized (Rowland et al., 2008). Together, a combination of severed axons from the primary injury as well as strong inflammatory response, ecotoxicity, production of free radicals, demyelination and several other factors from the secondary response prevent the spinal cord from regenerating. These events highlight the complexity of SCI pathophysiology and why there still is no cure for SCI.

1.1.4 Current Treatment Approaches

Over the last decades, significant research has gone into finding potential treatment options for SCI. Many therapies are focused on neurostimulation, pharmacological treatment and cell transplantation or a combination of therapies. Advancements in neurostimulation to activate neuronal circuits in the forms of EES, transcutaneous spinal cord stimulation and brain-machine interface have shown promising results. Functional electrical stimulation has been shown to enhance neuroplasticity following SCI (Ho et al., 2014). EES of the cervical region aid forelimb grasping techniques in rats with a cervical SCI (Alam et al., 2017). In humans, EES of the dorsal roots in the lumbosacral region of the cord enabled SCI patients to walk again, though the movement was not natural (Kathe et al., 2022; Rowald et al., 2022).

Additionally, pharmacological treatments such as Riluzole, a glutamatergic modulator used to treat ALS patients, has been shown to aid motor function and decrease spasticity in rodent SCI models as well as human clinical trials (Kitzman, 2009; Martins et al., 2018; Srinivas et al., 2019). It attenuates secondary injury by blocking voltage gated sodium and potassium channels which prevents intracellular calcium influx and thereby limits neuronal death by glutamate excitotoxicity (Kretschmer et al., 1998; Nagoshi et al., 2015; Wang et al., 2004). While promising, the exact dosage and timing still needs to be further explored and there are adverse effects associated with rilozule such as pancreatitis, lung disease and neutropenia (Grossman et al., 2014; Srinivas et al., 2019).

Cell transplantation has also been more widely explored however the exact mechanisms to aid neuroregeneration remain unknown. The main goals for cell transplantation are to provide neuroprotection, aid angiogenesis, remyelination, form a bridge across the lesion site and support neuroregeneration (Assinck et al., 2017). Cells such as Schwann cells, olfactory enscheathing cells, neural stem cells (NSCs) and embryonic stem cells have been widely explored both in rodent and even human trials (Assinck et al., 2017; Chen et al., 2018; Cusimano et al., 2012; Davies et al., 2008; Fischer et al., 2020; Iwatsuki et al., 2008; Kjell & Olson, 2016; Watzlawick et al., 2016). Within human clinical trials, cell transplantation has been shown to be safe at least in the short term (18 months post-transplantation) (Al-Zoubi et al., 2014; Huang et al., 2006; Manley et al., 2017; Willison et al., 2020) however functional recovery remains limited (Willison et al., 2020). SCI leads to both white and gray matter damage and cellular replacement therapies are primarily focused on white matter regeneration. However loss of gray matter especially at spinal enlargements, is an obstacle to functional recovery. Therefore, while advancements in determining safety and feasibility have been made, additional research into treatment options and in particular cell transplantation remains crucial to better understanding the function and harnessing the potential cells have to aid functional recovery.

1.1.5 E14 Spinal Cells SCI Treatment Options

Traumatic injuries that lead to the loss of cellular tissue such as SCI require replacement options which have been recently explored with the use of embryonic stem and progenitor cell transplantation in rodent and nonhuman primate experimental models. After fertilization, the zygote develops into an 8-cell morula with totipotent capacity. Following, it becomes a blastocyst of which embryonic stem cells with pluripotent capacity develop into multipotent stem cells, and further multipotent neuronal progenitors. These cells become committed neuronal or glial-restricted progenitors before developing into fully differentiated neuron or glial cells (Sandner et al., 2012).

At rat embryonic day (E) E10.5, spinal cords are composed of neuroepithelial cells and multipotent NSCs (Mayer-Proschel et al., 1997). Within the developing spinal cord, there are 13 progenitor pools which post-mitosis leave the cell cycle: 8 dorsal domains (pd1-5, pdILA-B, pd6; four ventral domains: p0-4; and one motoneuron domain: pMN) (Alaynick et al., 2011). Gradients such as fibroblast growth factor (FGF) and retinoic acid (RA) are responsible for either caudalizing or rostralizing cells, respectively. In the dorso-ventral axis, bone morphogenetic protein (BMP) and wingless/integrated (Wnt) factors are responsible for dorsalizing signals while Sonic hedgehog (Shh) is responsible for ventralizing signals (Lu et al., 2015) (**Fig. 2**). By embryonic day 12.5 in mice (Francius et al., 2013), which corresponds to E14 in rats (Zholudeva & Lane, 2019), the developing spinal cord contains neuronal restricted precursors (60%) and glial restricted precursors (30%) and neuroepithelial cells (10%) (Reier et al., 1983). The above-mentioned gradients activate transcriptional responses responsible for the differentiation of neuronal progenitors into over 23 classes of neurons in the spinal cord (Lu et al., 2015; Muroyama et al., 2002; Timmer et al., 2002). These classes can be split up into dorsal (DI1- DI6) and ventral (V0-V3) classes and be further differentiated depending on their location, length, function and transcription factor expression (Sweeney et al., 2018; Zavvarian, Hong and Fehlings, 2020; Gosgnach et al., 2017).

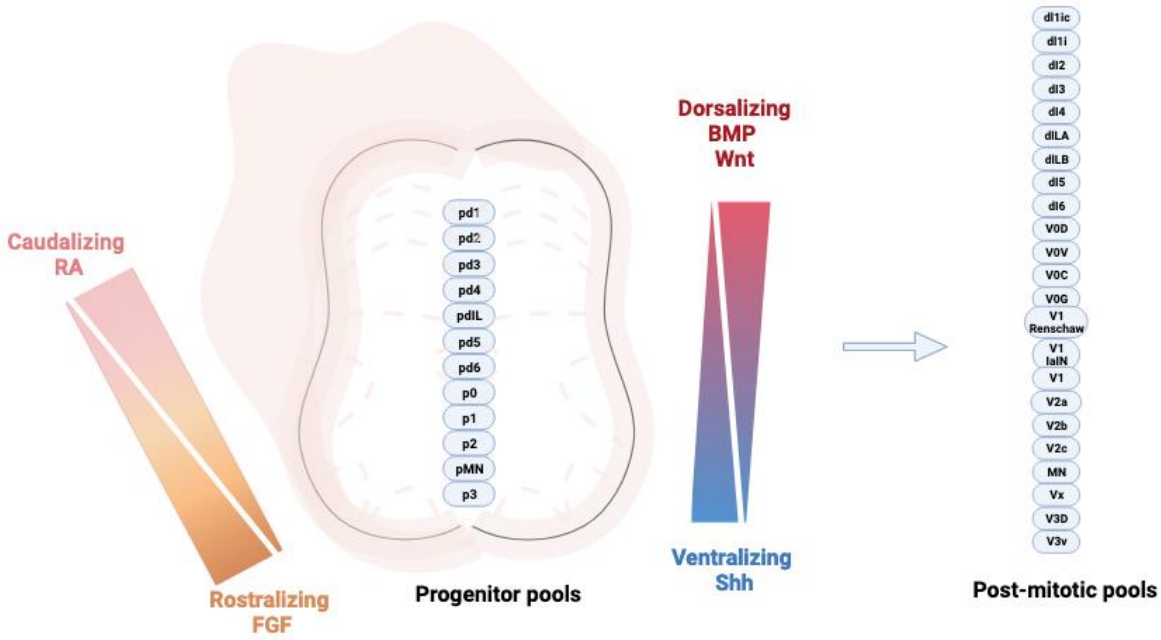

Figure 2. Cell differentiation in the developing spinal cord. Thirteen progenitor pools in the developing spinal cord are driven by dorsalizing BMP/ Wnt and ventralizing Shh as well as rostralizing FGF and caudalizing RA signaling to differentiate into over 23 different post-mitotic neuron pools.

Cells harvested from rat E14 spinal cords have shown promising results. Unlike cell transplantation studies that transplant a single cell type, transplanting E14 spinal cells allows for both the replacement of several different types of damaged neurons as well as helping provide an environment conducive to neuroregeneration. An early study showed that cultured rat E14 spinal neuronal and glial restricted precursors cells survived and integrated into a SCI lesion site, while neuroepithelial cells did not (Lepore et al., 2004). Following studies have supported these findings and have shown that rat E14 spinal cord cells that have been transplanted with or without supporting growth factors can fill the lesion site and differentiate into neuronal and glial cells (Kumamaru et al, 2019 and Dulin et al, 2018 and Kumamaru et al, 2018 and Kadoya et al, 2016 and Bonner et al, 2011). Graft neuronal axons extended from the lesion site, formed functional relays and synapses with host motor neurons, functionally improving hindlimb motion following a thoracic level 3 full transection injury (Lu et al, 2012). In contrast to a relay capacity, a study published by Dulin and colleagues showed that E14 spinal grafts transplanted into a white matter dorsal column lesion at C4 are able to differentiate into INs and form multiple mini gray matter lamina-specific layers in rats. They adopted cell fates such as calretinin+ and Tlx3+ neurons found in laminae I-II even when cultured or transplanted

without additional growth factors *in vitro* and *in vivo* after SCI. Host nociceptive neurons (staining positive for Calcitonin gene-related peptide, CGRP) made functional connections into these ectopic superficial laminae while host corticospinal axons specifically avoided these sections (Dulin et al, 2018). A follow-up study published by Kumamaru and colleagues supported these findings and showed that corticospinal axons regenerate into motor domains of neural progenitor cell grafts transplanted in both rodents and nonhuman primates and avoid sensory graft targets indicating their ability to integrate into gray matter structures in the injured white matter of the spinal cord. Early after transplantation, E14 spinal cells differentiated into V1 inhibitory and V2a INs, as well as somatosensory INs dI1-3, dILb, dI5. 6 months after transplantation, E14 grafts had matured and differentiated into several other premotor and sensory INs (Kumamaru et al, 2019). This differentiation occurred even when transplanted into a white matter lesion. While the full scope of connectivity with the host neurons remains unexplored, these studies have shown that grafted cells survived in a SCI lesion, differentiated into gray matter neuronal subtypes both *in vitro* and *in vivo* and allowed for the formation of neuronal relays believed to reconnect lost circuitry. However, functional recovery still remained limited. This may be due to the lesion extent and/or the placement of the graft into the white matter instead of the gray matter it is intended to replace.

1.2 Aim of Thesis

Vertebrate locomotion is a highly complex task made up of intricate neuronal networks. SpIN ensembles in the intermediate gray matter receive and gate descending motor and ascending sensory input and elicit signals to other INs and motoneurons. Elegant cFos and genetic knockout/silencing experiments have revealed the functions of IN populations in laminae V-VII in the lumbar cord during locomotion in both mice and rats (Ahn et al., 2006; Flynn et al., 2011; Hayashi et al., 2018; Koch et al., 2017; Ruder et al., 2016; Sathyamurthy et al., 2018). While these experiments highlight the roles of individual SpIN subtypes, these studies have not shown the phenotype of combined SpIN loss. Previous studies have shown that changes to the ratio of excitatory to inhibitory INs can influence the speed and pattern of the motor output as well (Sternfeld et al., 2017). For example, inhibitory V1 INs have been shown to be necessary for fast motor bursting. Ablation of V1 INs lengthened the step cycle and slowed motoneuron burst frequency (Gosgnach et al., 2006), while ablation of both V1 and V2b affects flexor-extensor alternation (Zhang et al., 2014). Furthermore, *in vitro* studies reconstructing SpIN circuits have shown that changing the ratio of excitatory and inhibitory neurons such as by adding more inhibitory V1 INs or excitatory V3 can influence rhythmic activity (Sternfeld et al., 2017). Therefore, changes to the regulatory SpIN network located in the intermediate gray matter, such as from a SCI, can affect motor output in an unpredictable manner. Previous studies have shown that a large gray matter lesion in the lumbar cord results in significant gross hindlimb deficits (Magnuson et al., 1999). However, this lesion included severe neuronal loss to the dorsal horn. Although injury to the dorsal horn is more commonly associated with sensory deficits, it is unclear whether this also played a role in locomotor deficits. Damage to the dorsal horn can evoke pain (Yezierski et al., 1998) and animals with pain in their hindlimbs can show altered gait patterns (Deshpande et al., 2021; Pitzer et al., 2016). Therefore, loss of afferent or other information due to the severity of the lesion may have impacted motor output. To our knowledge, it has not been shown what locomotor deficits are created after collective damage to the lumbar intermediate gray matter alone. With this study, I aim to create a targeted gray matter lesion to examine the roles of SpIN and propriospinal IN in the lumbar cord. Furthermore,

I aim to thoroughly investigate the behavioral deficits of lumbar gray matter SpIN loss to examine the contribution of these neurons to locomotion. (This paragraph was modified from (Kuehn et al., Manuscript in preparation) and was written by myself).

With this model, I also aim to test E14 spinal cell survival in an intermediate gray matter lesion in a proof of principle, discrete lesion. E14 spinal cells have been shown to survive, differentiate into gray matter INs both *in vitro* and *in vivo* and make connections with host neurons. However, they have been more commonly used to bridge the gap in white matter tract relays following injury and functional recovery remains limited. Their potential to replace damaged cells particularly in the lumbar gray matter remains unknown. This work lays the groundwork for future experiments to evaluate E14 spinal cell potential to replace damaged gray matter and aid functional recovery (**Fig. 3)**.

1.2.1 Hypothesis

Damage to SpIN and propriospinal INs in laminae V-VII in the rostral lumbar region significantly affects locomotion. These deficits remain stable and cannot be compensated. Additionally, unaided E14 spinal cells grafted into a lumbar gray matter KA lesion survive and fill the lesion site.

1.2.2 Aims

1) Establish a gray matter lesion in the lumbar spinal cord targeting SpIN and propriospinal INs laminae V-VII of the intermediate gray matter.
2) Establish appropriate behavioral tests to characterize functional deficits following a discrete lumbar gray matter lesion.
3) Define contribution of SpIN and propriospinal INs in the lumbar intermediate gray matter to motor and sensory function.
4) Analyze factors such as lesion length and spinal level that contribute to functional deficits.
5) Determine whether the behavioral deficits remain stable in the long-term.

6) Determine whether E14 spinal grafts can survive and fill a lumbar gray matter KA lesion unaided and if a high cell transplantation number is necessary.

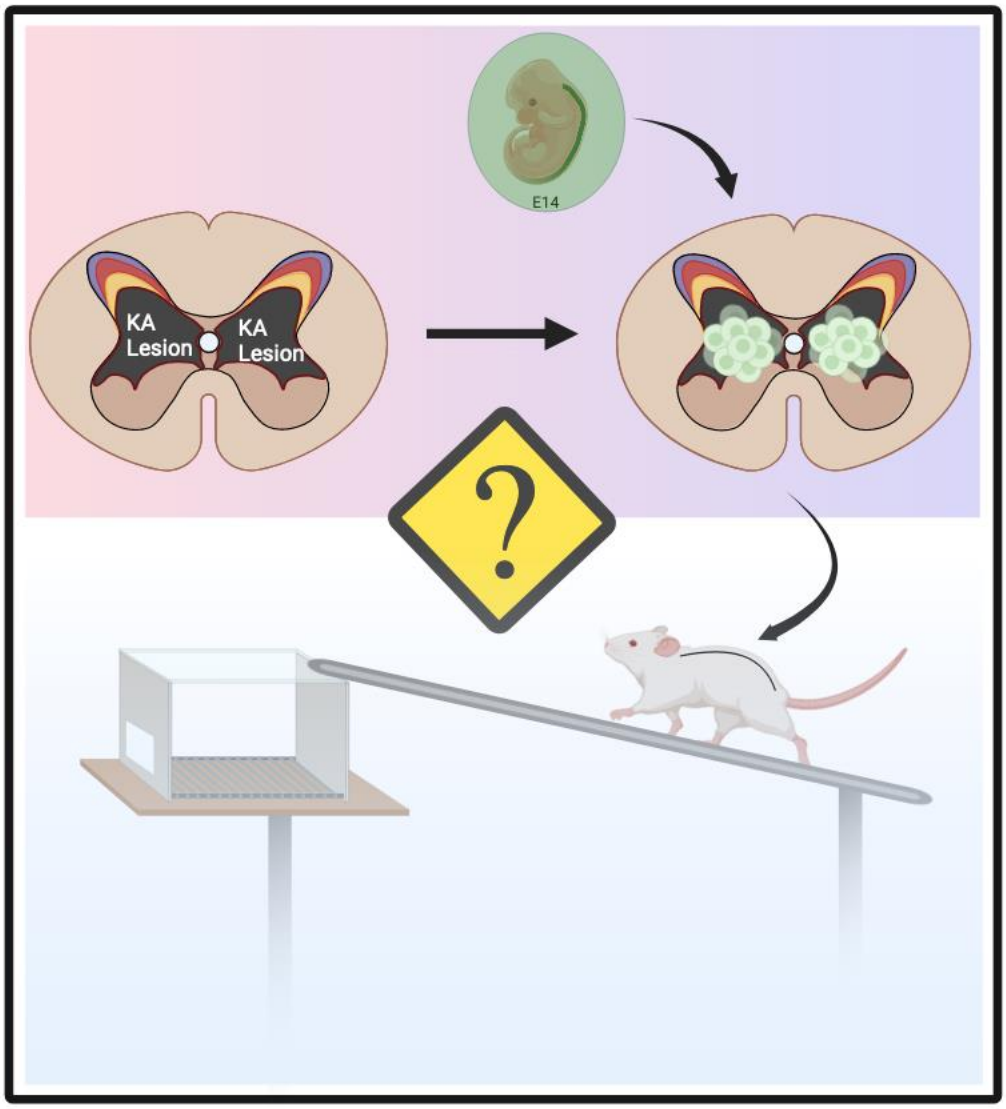

Figure 3. Proof of principle: Does transplanting E14 cells into a KA lesion restore behavioral deficits? The overall goal of developing the KA model is to investigate the potential transplanted E14 spinal cells have to replace damaged gray matter and recover lost function after injury.

2 Materials and Methods

2.1 Materials

2.1.1 Animals

Table 1: List of Animals

Short Name	Full Name	Type	Description	Provider
Fischer F344 Rat		Inbred	WT Females	Janvier
GFP Fischer F344 Rat		Inbred	GFP+ Males	Janvier and in-house breeding

2.1.2 Equipment and instruments

Table 2: Equipment and instruments

Equipment/Instrument	Usage	Manufacturer
Pipette Puller PC-100 Puller Narishige	KA and cell injections	Biosurplus Inc., SD, USA
Shaker	Immunohistochemistry	Neolab Migge GmbH Heidelberg, Germany

Table 3: Equipment and instruments for surgical procedures

Equipment/Instrument	Usage	Manufacturer
Borosilicate Glass Capillaries	KA and cell injections	World Precision Instruments, Friedberg, Germany
Bepanthen® Augen und Nasensalbe	KA and cell injection surgery	Bayer Vital GmbH Leverkusen, Germany
Braunol®	Disinfection	Braun Meslungen, AG, Meslungen, Germany
Dental punch pliers	Surgery preparation	Aesculup AG, Tuttlingen, Germany
Disposable scalpel (No.11 and No.15)	KA and cell injection surgery	FEATHER Safety Razor Co. Ltd, Osaka, Japan

Dumont #2Forceps	KA and cell injection surgery	Fine Science Tools, Foster City, CA, USA
Dumont #5 Forceps	KA and cell injection surgery	Fine Science Tools, Foster City, CA, USA
Eppendorf centrifuge	Cell injection surgery	VWR International GmbH Darmstadt, Germany
Fine Scissors	KA and cell injection surgery	Fine Science Tools, Foster City, CA, USA
Friedman Pearson Rongeurs (gebogen)	Laminectomy	Fine Science Tools, Foster City, CA, USA
Hasley needle holder	KA and cell injection surgery	Fine Science Tools, Foster City, CA, USA
Hamilton blunt, 24G	KA and cell injection surgery	Sigma Aldrich, Merck Group, St. Louis, MI, USA
Kopf R-Stereotact	KA and cell injection surgery	David Kopf Instruments Tujunga, CA, USA
Octagon Forceps	KA and cell injection surgery	Fine Science Tools, Foster City, CA, USA
Picospritzer II Intracellular microinjection system	KA and cell injection surgery	Parker Hannifin, New Hampshire, USA
Remington Razor	Surgery preparation	Spectrum Brands, Inc. DeForest, WI 53532
Stainless steel wound clips 9mm	KA and cell injection surgery	MikRon Precision Inc. Gardena, CA, USA
Steri250 surgical tool sterilizer	Surgery preparation	Simon Keller AG, Switzerland
Sugi Sponge points	KA and cell injection surgery	Kettenbach GmbH & Co. AG, Eschenburg, Germany
Surgical Microscope	KA and cell injection surgery	Olympus Deutschland, GmbH, Deutschland
Suture string 4/0, 75cm	KA and cell injection surgery	Silkam, Aesculap AG, Tuttlingen, Germany
T/Pump Professional	Heating pad	Gaymar/Stryker, Portage, MI, USA

Table 4: Equipment and instruments for E14 cell isolations

Equipment/Instrument	Usage	Manufacturer
Bonn Microforceps	Tissue Dissection	Fine Science Tools, Foster City, CA, USA
Braunol®	Disinfection	Braun Meslungen, AG, Meslungen, Germany
Cell strainer 40µm, Nylon	E14 cell isolation	Greiner-Bio One GmbH Frickenhausen, Germany
Dissector Scissors	Tissue Dissection	Fine Science Tools, Foster City, CA, USA
Dumont #5 Forceps	Tissue Dissection	Fine Science Tools, Foster City, CA, USA
Dumont #55 Forceps	Tissue Dissection	Fine Science Tools, Foster City, CA, USA
Ice pack	Tissue Dissection	Custom
Large Forceps	Tissue Dissection	Hammacher Instruments, Solingen, Germany
Octagon Forceps	KA and cell injection surgery	Fine Science Tools, Foster City, USA
Remington Razor	Surgery preparation	Spectrum Brands, Inc. DeForest, WI 53532
Stainless steel measuring spoon	Tissue Dissection	Amazon
Surgical Microscope	KA and cell injection surgery	Olympus Deutschland, GmbH, Deutschland
Tungston Carbide Standard Pattern Scissors	Tissue Dissection	Fine Science Tools, Foster City, CA, USA
Vannas scissors, bent	Tissue Dissection	Fine Science Tools, Foster City, CA, USA
Vannas Spring Scissors	Tissue Dissection	Fine Science Tools, Foster City, CA, USA

Table 5: Equipment and instruments for behavioral tests

Equipment/Instrument	Usage	Manufacturer
CatWalk	Catwalk	Noldus, Wageningen, the Netherlands
Hargreaves Apparatus	Hargreaves	Ugo Basile Srl, Gemonio, VA, Italy
Horizontal ladder	Horizontal Ladder	Custom-made
Modular animal enclosure	Von Frey and Hargreaves chambers	Ugo Basile Srl, Gemonio, VA, Italy
Open field (round)	BBB	Custom-made
Perforated metal platform	Von Frey testing	Ugo Basile Srl, Gemonio, VA, Italy
Rotarod	Rotarod	Ugo Basile Srl, Gemonio, VA, Italy
Von Frey hair filaments 1.4g, 4g, 8, 16g, 60g	Von Frey testing	Stoelting Europe Terenure, Dublin, Ireland
Wooden rods 1.3 and 1.9cm	Inclined Beam	Custom-made

Table 6: Equipment and instruments for tissue processing

Equipment/Instrument	Usage	Manufacturer
Bonn Microforceps	Transcardial perfusion, Tissue dissection	Fine Science Tools, Foster City, CA, USA
Cryostat Blades	Cryo-sectioning	C.L. Sturkey Inc., Lebanon, PA, USA
Cryostat Hyrax C60	Cryo-sectioning	Microm GmbH, Walldorf, Germany
Dumont #5 Forceps	Tissue dissection	Fine Science Tools, Foster City, CA, USA
Dumont #55 Forceps	Tissue dissection	Fine Science Tools, Foster City, CA, USA
Friedman-Pearson Rongeurs	Tissue dissection	Fine Science Tools, Foster City, CA, USA
Hasley needle holder	Transcardial perfusion	Fine Science Tools, Foster City, USA

ISMATEC REGLO Digital MS-4/8	Transcardial perfusion	IDEX Health & Science Oak Harbor, WA, USA
Large forceps	Transcardial perfusion	Hammacher Instruments, Solingen, Germany
Large Scissors	Transcardial perfusion	Hammacher Instruments, Solingen, Germany
Paint brushes	Cryo-sectioning	Faber-Castell Stein, Germany

Table 7: Equipment for microscopy and imaging

Equipment/Instrument	Usage	Manufacturer
CCD digital color camera XC30	Image Acquisition	Olympus Deutschland GmbH, Hamburg, Germany
Fluoview FV1000 confocal laser scanning microscope	Image Acquisition	Olympus Deutschland GmbH, Hamburg, Germany
System Microscope BX53	Image Acquisition	Olympus Deutschland GmbH, Hamburg, Germany
Plate microscope	Image Acquisition	Olympus Deutschland GmbH, Hamburg, Germany

Table 8: List of software used

Software	Usage	Manufacturer
Cell^F Imaging Software for Life Science Microscopy	Imaging for bright field microscope	Olympus Deutschland GmbH, Hamburg, Germany
Image J	Image Processing	NIH
FIJI	Image Processing	NIH
Prism 6	Graphing and Statistical analysis	GraphPad Software Inc., La Jolla, CA, USA
Microsoft Excel	Behavioral data processing	Microsoft, Redmond, WA, USA

Confocal software	Confocal imaging	Olympus Deutschland GmbH, Hamburg, Germany
Photos	Behavioral video analysis	Apple
CatWalk XT	CatWalk parameter analysis	Noldus, Wageningen, the Netherlands

2.1.3 Chemicals

Table 9. List of chemicals

Chemicals	Usage	Company
4', 6-diamidino-2-phnylindole (DAPI)	Immunostaining	Sigma Aldrich Co., St. Louis, MO, USA
Acetobromazine (ventraquil® 1%)	Analgesics	Ceva Tiergesundheit GmbH, Düsseldorf Germany
Acetone (ROTIPURAN®)	EC Staining	Carl Roth GmbH & Co. KG, Karlsruhe, Germany
Ammonium iron (III) sulfate dedecahydrate ($NH_4Fe(SO_4)_2$)	EC Staining	Carl Roth GmbH & Co. KG, Karlsruhe, Germany
Ampicillin (Ampi-Dry® 5.0g)	Post-surgery treatment	Ratiopharm GmbH, Ulm, Germany
B27™ supplement, serum-free 50x	E14 spinal cultures	ThermoFischer Scientific Waltham, MA, USA
Buprenorphine HCl (Temgesic®)	Post-surgery treatment	Reckitt Benckiser, Slough, UK
CTB	Surgery	List Biological Laboratories Inc. Campbell, CA, USA
D(+)-Saccharose (sucrose)	Tissue Processing	Carl Roth GmbH & Co. KG, Karlsruhe, Germany
Distilled water (ultra-pure type 1 water)	Solutions preparation	ELGA LabWater, UK
Disodium hydrogen phosphate (Na_2HPO_4)	EC Staining	Carl Roth GmbH & Co. KG, Karlsruhe, Germany

Disodium tetraborate decahydrate ($Na_2[B_4O_5(OH)_4]x8H_2O$; Borax)	EC Staining	Carl Roth GmbH & Co. KG, Karlsruhe, Germany
Dulbecco's Modified Eagle Medium (DMEM) /F12 (with HEPES, L-Glutamine, phenol red)	E14 spinal cultures	ThermoFischer Scientific, Waltham, MA, USA
Eriochrome cyanine® (EC)	EC Staining	Merck KGaA, Darmstadt, Germany
Fast Green FCF	Surgeries	Sigma Aldrich, St. Louis, MO, USA
Fetal bovine serum (FBS), heat inactivated, sterile filtered	E14 spinal cultures	Merck KGaA, Darmstadt, Germany
Gentamycin (10mg/ml)	E14 spinal cultures	Life Technologies, Carlsbad, CA, USA
Hanks' balanced salt solution (HBSS), without Ca2+ and Mg2+	E14 spinal cultures	Merck KGaA, Darmstadt, Germany
Kainic Acid, 1mg	Kainic Acid	BioTechne Tocris Minneapolis, MN, USA
Ketamine 10%	Analgesics	Bremer Pharma GmbH, Warburg, Germany
Luteinizing hormone follicle-stimulating hormone (LHRH)	E14 Breedings	Sigma Aldrich, St. Louis, MO, USA
Liquid blocker PAP PEN Immunostaining pen, 5mm	Immunohistochemistry	Kisker Biotech GmbH & Co., Steinfurt, Germany
Neo-clear®	EC Staining	Merck KGaA, Darmstadt, Germany
Neo-Mount®	EC Staining	Merck KGaA, Darmstadt, Germany
Neuralbasal Media (NBM)	E14 spinal cultures	Life Technologies, Carlsbad, CA, USA
Paraformaldehyde (PFA)	Perfusions, solution preparation	Carl Roth GmbH & Co. KG, Karlsruhe, Germany
Penicillin-streptomycin (Pen/Strep) (10,000U/ml)	E14 spinal cultures	ThermoFischer Scientific, Waltham, MA, USA
Poly-D-Lysine (PDL)	E14 spinal cultures	Sigma Aldrich Co., St. Louis, MO, USA
Potassium hexacyanoferrate(III) ($C_6N_6FeK_3$)	EC Staining	neoLab Migge Laborbedarf-Vertriebs GmbH, Heidelberg, Germany
Ringer's solution	Surgery	Braun Melsungen AG, Melsungen, Germany

Sodium Chloride (NaCl)	Solution preparation	VWR, Leuven, Belgium
Sodium dihydrogen phosphate (NaH_2PO_4)	Solution preparation	Carl Roth GmbH & Co. KG, Karlsruhe, Germany
Sodium hydroxide solution 40% (10M, NaOH)	Perfusions, solution preparation	Carl Roth GmbH & Co. KG, Karlsruhe, Germany
Sterile filtered donkey serum	Immunohistochemistry	Equitech-Bio Inc., Kerrville, TX, USA
Sterile Saline Solution	Surgery	Braun Melsungen AG, Melsungen, Germany
Sulfuric acid (H_2SO_4)	EC Staining	neoLab Migge Laborbedarf-Vertriebs GmbH, Heidelberg, Germany
Tissue Tek® O.C.T.™ compound	Cryosectioning	Sakura Finetek Germany GmbH, Staufen, Germany
Tris (hydroxymethyl)aminomethane; ($C_4H_{11}NO_3$) – Tris	Solution preparation	neoLab Migge Laborbedarf-Vertriebs GmbH, Heidelberg, Germany
Tris-Hydrochloride (Tris-HCl)	Solution preparation	neoLab Migge Laborbedarf-Vertriebs GmbH, Heidelberg, Germany
Triton X-100		neoLab Migge Laborbedarf-Vertriebs GmbH, Heidelberg, Germany
0.25% Trypsin-EDTA (1x), phenol red	E14 spinal cultures	Life Technologies, Carlsbad, CA, USA
Xylazine 20mg (XYLARIEM®)	Analgesics	Ecuphar N.V., Oostkamp, Belgium

2.1.4 Antibodies

Table 10. List of primary antibodies

Antibody	Host	Isotype	Clonality	Dilution	Company	Cat. No.
ßIII-Tubulin	Mouse	IgG	monoclonal	1:1000 ICC	Promega Madison, WI, USA	G7121
Calbindin	Rabbit	Serum IgG	-	1:1000 IHC	Swant, Marly, Switzerland	CB-38a
CTB	Goat	Serum IgG	-	1:10,000 IHC	List Labs, Campbell, California	703
Foxp2	Rabbit	IgG	polyclonal	1:1000 ICC, IHC	Abcam, Cambridge, UK	Ab16046
Gata2/3	Rabbit	IgG	polyclonal	1:500 IHC	Abcam, Cambridge, UK	Ab106625
GFAP	Mouse	IgG	monoclonal	1:1000 ICC, IHC	Merck Millipore	IF03L
GFAP	Rabbit	IgG	polyclonal	1:1000 ICC, IHC	Dako, Santa Clara, USA	Z0334
GFP	Goat	IgG	polyclonal	1:1500 IHC	Rockland Inc. Philadelphia, PA, USA	600-101-215
GFP	Rabbit	IgG	polyclonal	1:1000 IHC	Invitrogen, Thermofischer	A-11122
Iba1	Rabbit	IgG	polyclonal	1:1000 IHC	Wako Chemicals GmbH, Neuss, Germany	019-19741
NeuN	Guinea pig	Serum IgG	polyclonal	1:1000 IHC	Millipore, Merck KGaA, Darmstadt, Germany	ABN90
Olig2	Goat	IgG	polyclonal	1:500 ICC	Santa Cruz Biotechnology, Dallas, USA	SC-19969
Pax 6	Mouse	IgG1	monoclonal	1:200 ICC	DSHB, Iowa City, USA	AB_528427
Pax 7	Mouse	IgG	monoclonal	1:200	DSHB, Iowa City, USA	AB_528428
Sox 2	Goat	IgG	polyclonal	1:200 ICC, IHC	Santa Cruz Biotechnology, Dallas, USA	SC-17320

Table 11. List of secondary antibodies used for immunofluorescence staining

Antibody	Host	Isotype	Dilution	Company	Cat. No.
AlexaFluor®488 anti-gt	donkey	IgG (H+L)	1:300 (ICC, IHC)	Life Technologies Carlsbad, CA, USA	A11055
Alexa Fluor®594 anti-gt	donkey	IgG (H+L)	1:300 (ICC, IHC)	Life Technologies Carlsbad, CA, USA	A11058
AlexaFluor® 488 anti-rb	donkey	IgG (H+L)	1:300 (ICC, IHC)	Life Technologies Carlsbad, CA, USA	A21206
AlexaFluor® 594 anti-rb	donkey	IgG (H+L)	1:300 (ICC, IHC)	Life Technologies Carlsbad, CA, USA	A21207
AffiniPure® Cy™5 anti-rb	donkey	IgG (H+L)	1:300 (ICC, IHC)	Jackson Immuno Research West Grove, PA, USA	711-175-172
AlexaFluor®594 anti-gp	donkey	IgG (H+L)	1:300 (ICC, IHC)	Dianova Hamburg, Germany	706-585-148
AlexaFluor®488 anti-gp	donkey	IgG (H+L)	1:300 (ICC, IHC)	Dianova Hamburg, Germany	706-545-148
AlexaFluor®488 anti-ms	donkey	IgG (H+L)	1:300 (ICC, IHC)	Life Technologies Carlsbad, CA, USA	A21202
AlexaFluor® 594 anti-ms	donkey	IgG (H+L)	1:300 (ICC, IHC)	Life Technologies Carlsbad, CA, USA	A21203
AffiniPure® Cy™5 anti-ms	donkey	IgG (H+L)	1:300 (ICC, IHC)	Jackson Immuno Research West Grove, PA, USA	715-175-150

2.1.5 Buffer and solutions

Table 12: Kainic Acid

Buffer/solution	Reagents	Added
Kainic Acid Stock (12.5 mM)	Kainic Acid (1 mg) Sterile, filtered dH2O	1 mg 380 µl Stored in 10µl aliquots
Kainic Acid Injection (1 mM)	Kainic Acid (12.5 mM) Saline	4 µl 46 µl Total volume: 50 µl
Saline Injection	Saline	50µl Total volume: 50 µl

Table 13: Coating 48-well plate with PDL

Buffer/solution	Reagents	Added
PDL in dH_2O	dH_2O PDL (50µg)	15mL 75µl Add 125µl/well

Table 14: E14 spinal culture media

Buffer/solution	Reagents	Added
10% FBS in DMEM	FBS DMEM	1 mL 9 mL Total volume: 10 mL
2% B27 in NBM	B27 NBM	100 µl 4.9 mL Total volume: 5 mL
E14 spinal culture medium	PenStrep 2% B27 in NBM	50 µl 4.95 mL Total volume: 5 mL

Table 15: Animal anesthesia

Drug	Concentration	Added
Acepromacine	0.625 mg/kg	0.75 mL
Ketamine	62.5 mg/kg	7.5 mL
Xylacine	3.175 mg/kg	1.9 mL
NaCl 0.9%	-	9.85 mL
		Total volume: 20 mL

Table 16: Rat post-operative care (ABR)

Drug	Agent	Dosage
Ampi-Dry®	Ampicillin	50 mg/kg
Burpenovet®	Buprenorphine	0.03 mg/kg
Saline	-	-

Table 17: Buffer and solutions for animal perfusions

Buffer/solution	Reagents	Added
0.2M Sodium Phosphate Monobasic solution	NaH_2PO_4	27.6 g
	ddH_2O	Fill up to 1L
		Total volume: 1 L
0.2M Sodium Phosphate dibasic solution	Na_2HPO_4	28.6g
	ddH_2O	Fill up to 1 L
		Total volume: 1 L
0.2M Phosphate Buffer	Sodium phosphate monobasic solution (0.2M)	230 mL
	Sodium phosphate dibasic solution (0.2M)	770 mL
		Total volume: 1 L
Perfusion Saline (0.9%)	NaCl	18.0 g
	0.2M Phosphate Buffer	1 L
	ddH_2O	1 L
		Total Volume: 2 L
PFA solution (4% w/v)	Paraformaldehyde	80 g
	10 M NaOH	8 drops
	Phosphate buffer (0.2M)	1 L
	ddH_2O	1 L
		Total Volume: 2 L
Sucrose solution (30% w/v)	D(+)-sucrose	300 g
	Phosphate buffer (0.2M)	350 mL

	ddH_2O	350 mL Total volume: 1 L

Table 18: Buffer and Solutions for Histology

Buffer/solution	Reagents	Added
Borax-Ferricyanide Solution	Sodium tetraborate decahydrate ($Na_2B_4O_7$ x 10 H_2O, Borax) Potassium Ferricyanide ($K_3Fe(CN)_6$) ddH_2O	2 g 2.5 g 200 mL Total volume: 200 mL
Ferric Ammonium Sulfate Solution (10%)	Ammonium iron (III) sulfate dodecahydrate ($NH_4Fe(SO_4)_2$ 12 H_2O ddH_2O	10 g 100 mL Total Volume: 100 mL
Ferric Ammonium Sulfate Solution (5%)	Ammonium iron (III) sulfate dodecahydrate ($NH_4Fe(SO_4)_2$ 12 H_2O ddH_2O	5 g 100 mL Total volume: 100 mL
Eriochrome Cyanine Solution	Eriochrome Cyanine R Concentrated H_2SO_4 10 % Ferric Ammonium Sulfate Solution ddH_2O	0.4 g 1.0 mL 8 mL 192 mL Total volume: 200 mL

Table 19: Buffer and Solutions for Immunocytochemistry (ICC)

Buffer/solution	Reagents	Added
10% Triton X-100	Tris-buffered saline (TBS) Triton X-100 (10 % v/v)	9 mL 1 mL Total volume: 10 mL
Blocking and permeabilization Buffer for ICC	TBS Triton X-100 (10 % v/v) Donkey serum	9.8 mL 100 µl (0.1 % v/v) 100 µl (1 % v/v) Total Volume: 10 mL
Staining buffer for ICC (primary and secondary antibody)	TBS Triton X-100 (10 % v/v) Donkey serum	9,250 µl 250 µl (0.25 % v/v) 500 µl (1 % v/v) Total volume: 100 mL

Table 20: Buffer and Solutions for Immunohistochemistry (IHC)

Buffer/solution	Reagents	Added
10% Triton X-100	TBS Triton X-100 (10 % v/v)	9 mL 1 mL Total volume: 10 mL
Blocking buffer for IHC	TBS 10 % Triton X-100 Donkey serum	9,250 µl 250 µl (0.25 % v/v) 500 µl (5 % v/v) Total volume: 10 mL
Staining buffer for IHC (primary antibody)	TBS 10 % Triton X-100 Donkey serum	9,650 µl 250 µl (0.25 % v/v) 100 µl mL (1 % v/v) Total volume: 10 mL
Staining buffer for IHC (secondary antibody)	TBS Donkey serum	9,9000 µl 100 µL (1 % v/v) Total volume: 10 mL

2.2 Methods

2.2.1 Animals

Rats were housed in accordance with the European Union Directive and institutional guidelines. Female Fischer 344 rats (Janvier Labs, Saint-Berthevin Cedex, France) weighing 180-200g (10-12 weeks old at the time of luteinizing hormone releasing hormone (LHRH) injection or 10 weeks old at the time of surgery) and male GFP+ rats were used for these experiments. Rats were maintained in a 12-hour light-dark cycle at 22°C. Rats were group housed in Type IV cages, with a maximum of 6 rats per cage. Animals had ad libitum access to water and food throughout the experiment. All experiments were planned and conducted according to the PREPARE and ARRIVE guidelines (Percie du Sert et al., 2020; Smith, 2020). Sections have been adapted from (Kuehn et al., Manuscript in preparation) and were written by myself unless otherwise noted.

2.2.2 LHRH Preparation

To begin, LHRH (Sigma, cat # L-4513, 5mg) is diluted in 25mL of filtered, sterile saline under the cell culture hood to a final concentration of 200µg/ml. Following, 800µl of the solution was drawn up into 1ml syringes and stored in the -80°C freezer until further use. Each syringe could be used to inject 2 females.

2.2.3 LHRH Injection and E14 Pairing

On the day of injection, a female Fischer rat (typically 10-12 weeks old) was injected interperitoneally (IP) with 300µl (60µg) of LHRH at 10am. The pairing followed for one night four days post-injection. For example, if the female was injected with LHRH on a Thursday morning, then the pairing occurred from Monday evening to early Tuesday morning. It was important to place the females into the male cage for pairing and to remove the females from the cages as early as possible the next morning. We found that

it was best to have a maximum of 1 male: 2 females per pairing. The following morning, female rats are first weighed and then placed into a new cage. A vaginal plug could be checked for but was not necessary. Following, female rats were weighed at the same time in the morning every 2-3 days.
If E14 embryos were required for consecutive days, it was best to use a different male for each pairing.

2.2.4 E14 Spinal Cord Isolation

Two weeks after separation, pregnant females were weighed in the morning. If they had gained at least 40g within two weeks, it was a good indication that they were pregnant. Pregnant females were injected IM (intramuscularly) with previously prepared anesthesia mix in the animal facility (this was more effective than newly prepared anesthesia mix). Following, the stomach fur was shaved off and they were carefully wrapped in paper towels to keep them warm during transport.

Once in the lab, animals were placed under the hood and further administered an overdose of anesthesia mix until reflexes and breathing had stopped. This could take some time as pregnant female rats are not as sensitive to ketamine. Once breathing had stopped, the stomach and lower abdomen were disinfected with 80% ethanol.

To harvest the embryos, first two petri dishes (60mm) with ice cold HBSS were prepared and placed on ice. Two large forceps and large scissors were sterilized and prepared. The first set were used to make the primary skin and muscle incisions at the most rostral part of the abdomen, about 0.5cm from the base of the tail. Then in a U shape, an incision was made on both the right and left side. It was very important that these tools did not touch any organs and that any fur did not touch any organs. Using the next set of tools, the uteri with embryos were lifted out of the abdomen and any connective tissue was removed using the second pair of sterilized scissors. It was very important that uteri did not touch any skin or organs to eliminate any risk of contamination. Both were placed into ice cold HBSS until further use.

To isolate the embryos, first, the uteri with embryos were gently shaken in the HBSS to remove any blood and transferred into a new petri dish with ice cold HBSS. Using a pair of bent forceps and scissors, the uteri tube was cut at one end and the first embryo was allowed to slip out. The placenta should be kept intact. This process was repeated for each embryo. Following, they were transferred to a new petri dish with ice-cold HBSS where the placenta was removed.

Under the stereoscope and on a flat ice pack, one embryo was scooped into the custom-made teaspoon and any surrounding HBSS was removed. The embryo was placed into a small petri dish with fresh ice-cold HBSS. The sac was removed with two sharp forceps (Dumont #5), freeing the embryo. Following, the head and tail were pinched off: the head should be removed below the ventricle in a downward angle. Next, the embryo was placed on its stomach with the neck facing towards the experimenter. The limbs were stabilized using a new set of forceps. A pair of bent scissors were used to carefully cut the skin upwards from the rostral to the most caudal end of the spinal cord. A new pair of Dumont #5 forceps were used to pinch away any tissue first on the right side of the spinal cord and then on the left side. Finally, any remaining connective tissue below the spinal cord was removed to free the spinal cord from the embryo. Once the cord was removed, one pair of forceps were used to stabilize the cord and another pair was used to remove the dura, dorsal root ganglia (DRG) or vertebrae in one swift manner. While recommended, it was not completely necessary to keep the cord intact. Only fully cleaned cords were used for further culturing or transplantation to ensure pure spinal cord samples.
The spinal cord was placed into a 2ml falcon tube with 1ml of ice-cold HBSS on ice. One falcon tube can contain 8-10 cords.
All isolation work with E14 embryos must be performed on ice. This protocol is based upon the Dulin Laboratory E14 isolation protocol.

2.2.5 Preparation of PDL-coated 48 well plates

Prior to isolation, 48-well plates needed to be coated with PDL (Sigma Aldrich, USA) the day before. Under the sterile cell culture hood, a solution with 50µg/ml PDL in sterile dH_2O was prepared, with 125µl solution fully covering the bottom of each well. The well plate was then wrapped in aluminum foil and stored at room temperature overnight in the cell culture hood. The next day, each well was washed three times with sterile dH2O, 10 minutes each wash. The final wash was carefully aspirated and the plates were allowed to dry for 30-60 minutes without the lid on under the hood. Once completely dried, 48-well plates were sealed using parafilm and wrapped in foil for storage at 4°C until use.

2.2.6 Cell Culture: E14 spinal cord digestion into single cells

Once all spinal cords were isolated, they were transferred to the cell culture room. 1 mL of 0.25% trypsin (Life Technologies) was added to each falcon tube and placed into a 37°C water bath for 8-10 minutes until the cords looked “cloudy”. They were then transferred to a 15ml falcon tube with 10mL of 10% FBS and DMEM (ThermoFischer Scientific, USA). The falcon tubes were inverted twice and spun down at 2500rpm for 2 minutes. Following, the supernatant was aspirated and 2mL of NBM/B27 was added. Cords were triturated with P1000 pipette until no tissue chunks were visible. They were again spun down at 2500rpm for two minutes and the supernatant was removed. 2mL of NBM/B27 was added and cells were gently resuspended and filtered through a 40µm cell strainer into a 50mL falcon tube. This was again spun down at 2500rpm for 2 minutes. The supernatant was removed and 1ml of NBM/B27 was added and used to resuspend cells. Cells were transferred into a 2mL eppendorf tube. To count cells, 10µl of cell suspension was added to 90µl of DPBS and counted using a hemocytometer.

Cells were then prepared for either cell transplantation or prepared for cell culture.

For cell culture, cells were resuspended in NBM medium with 1% Pen/Strep such that there were 1 million cells/well, 125µl per well. Each well already contained 125µl of fresh media, final volume of 250µl. Gently pipette up and down in each well without creating

bubbles while plating to ensure proper cell dispersion. Cells attached very quickly to the plates. This protocol is based upon the Dulin Laboratory E14 cell culture protocol.

Half media changes with E14 spinal culture media were performed once the media turned yellow. The interval between media changes depended on the number and concentration of cells per well. Media was prepared fresh for each half-media exchange.

To analyze cell maturity and identity, cells were either fixed after 24 hours or after 10 days. For the 10-day experiment, cells were monitored daily to observe maturation and ensure that there was no contamination. After 10 days, media was removed and cells were first washed with DPBS. To ensure that cells were not disturbed from the plate, it was important to remove any media or solution with a pipette and not an aspirator. 500µl of 2% PFA in 0.1M phosphate buffer was added to each well and cells were fixed for 30 minutes. It was important not to over fix cells since this can cause difficulties for transcription factor antibody binding. After fixing, cells were gently washed three times in TBS and stored in 0.05% sodium azide/0.1M phosphate buffer in 4°C until further use.

2.2.7 Immunocytochemistry

To stain fixed E14 spinal cells, cells were first washed three times with TBS for ten minutes each. A blocking and permeabilization solution was prepared using 1% donkey serum and 0.1% Tx-100 in TBS and applied to cells for 30 minutes at room temperature. Following, primary antibodies were diluted in blocking buffer and added to the wells. Cell plates were sealed using parafilm and stored at 4°C in the fridge overnight. The following day, cells were washed three times with TBS for ten minutes each. Then, the secondary antibody solution with DAPI (Sigma Aldrich, USA) was diluted again in blocking buffer and applied to wells for 2 hours at room temperature. Finally, cells were gently washed again three times with TBS before imaging.

2.2.8 *In Vitro* Analysis

All stained well plates were imaged using a fluorescence microscope (Olympus IX81, Olympus Life Sciences) using Cell^F software. Five random spots in each well were imaged at 20x. Cell differentiation analysis was done in ImageJ and Fiji.

2.2.9 Animal Surgery and Behavioral Tests

Surgery. Experiments were conducted in accordance with the European Union Directive (Directive 2010/63/EU amended by Regulation (EU) 2019/1010) and institutional guidelines. Animals were split into the control and test group by an unblinded colleague based on their baseline von Frey 1.4g hair filament performance. Female Fischer 344 rats were injected intramuscularly with an anesthesia mix of xylazine, ketamine and acepromazine. After tail, paw and eye reflexes subsided, animals were weighed and the backs of the animals were shaved and disinfected with Braunol® (Braun Meslungen, Germany). Additionally, Bepanthen® (Bayer Vital Gmbh, Leverkusen, Germany) was applied to prevent their eyes from drying out. Using the feather scalpel #11, a 3cm skin incision was performed laterally along the thoracolumbar vertebrate. After the surrounding muscles were cleared from the vertebrae using the feather scalpel #15, animals received a laminectomy at vertebrate T13 spanning 6mm with a rongeur. Following, animals were brought to a stereotactic frame where three sets of bilateral 0.5µl injections of KA (1mM; Tocris) were applied 0.4mm deep, 0.5mm laterally from the midline using a PicoSpritzer II (General Valve, Fairfield, NJ, USA) and a pulled glass capillary. The KA solution was resuspended before each injection and drawn up into a Hamilton syringe before being transferred into the glass capillary. Each set of injections was 3mm apart along the rostral-caudal axis. Control animals received saline injections. Animal reflexes were continuously monitored throughout the surgery. Following, the overlaying muscles were sutured using 4/0 prolene thread and the skin was stapled using 9mm suture clips (MikKron Precision Inc, Gardena, USA). Animals received 1mL of saline subcutaneously and Bepanthen® (Bayer Vital Gmbh, Leverkusen, Germany) was reapplied to the eyes. Animals were transferred to a warm heating pad until all reflexes had returned. All surgeries were performed by a blinded experimenter. Two days postoperatively, rats were given

buprenorphine (analgesic) (0.03mg/kg; Reckitt Benckiser) and ampicillin (167 mg/kg; Ratiopharm) subcutaneously three times daily. Bladder function was also assessed during this time however rats did not display bladder dysfunction.

Behavioral testing. Behavioral testing was performed throughout the experiment to assess sensorimotor deficits or recovery. Only animals with weight support on both hindlimbs (BBB score ≥ 9) were tested on the horizontal ladder, inclined beam, CatWalk, with von Frey hair filaments, and Hargreaves method. All behavior tests were performed by blinded experimenters and were performed during the same time of day, in the morning, to maintain consistency. Additionally, all behavioral analysis was performed by a blinded experimenter.

Basso, Beattie, Bresnahan (BBB) Score and Subscore. At baseline, 1, 3, 14 days post-SCI, and another cohort additionally 30, 60, 90 days post-SCI, animals were placed into an open field where two blinded experimenters assessed gross hindlimb function according to the previously established BBB protocol (Basso et al., 1995). The score ranges from 0-21. The score depends on the degree of mobility in the ankle, knee and hip joints (0-7), whether or not they have weight support (8-13) and have coordination while walking on a flat surface (14-21). This is not a linear score and only once animals have passed these specific thresholds (weight support and consistent coordination) can a higher score be awarded. An additional subscore with a total of 13 points looked at hindlimb function dependent on coordination (including toe clearance, paw position, trunk stability and whether the tail was up or down).

Even and Uneven Horizontal Ladder. The horizontal ladder consisted of a custom, 1 meter set up with plexiglass and metal rungs. Rats were allowed to cross an elevated, unevenly spaced horizontal ladder (rungs spaced 2-3cm apart) five times to their home cage. After an hour break, animals were then allowed to cross an evenly spaced, elevated horizontal (rungs 3cm apart) ladder five times. Prior to baseline testing, animals were habituated on the evenly spaced ladder by allowing them to cross five times. No food reward was given at the end of the task. Following, animals were tested at baseline, 2

weeks post-SCI and another cohort additionally 4, 8, 12 weeks after injury. A Canon Legria HFR806 camera was placed perpendicular to the ladder set up and used to record performance. Animal fore-and-hindlimb placement on the rungs were evaluated in slow motion using 25 frames per second and scored based on a previously established protocol (Metz & Whishaw, 2009). A new uneven rung pattern was tested at each time point to prevent a learning effect. Percent hindlimb slips and overall hindlimb performance scores were calculated and averaged. Animals that did not have weight support received 100% slips and a score of performance score of 0. The following uneven ladder patterns were used:

Habituation and even ladder: x _ _ x _ _ x _ _ x

Uneven ladder baseline: x_x_x_ _ x _ _ x_ x _ _

Uneven ladder 2 weeks post-injury: x _ x _ _ x _ _ x _ _ x _ x _

Uneven ladder 4 weeks post-injury: x _ x _ x _ _ x _ _ x _ x _ _

Uneven ladder 8 weeks post-injury: x _ _ x _ x _ _ x _ _ x _ x _

Uneven ladder 12 weeks post-injury: x _ x _ _ x _ _ x _ _ x _ x _

Pawprint Analysis. Rat pawprints were analyzed manually. The rat hindpaws were painted two different colors of non-toxic, edible paint. Following, rats were allowed to walk through a 1 meter narrow path to aid walking in one direction. This was repeated three times. After the paint had dried, stride length and step width were measured and averaged. This test was performed at baseline, 7 and 14 days post-injury.

Backwards Rotating Rod. A rotarod (Ugo Basile) was modified such that the diameter increased to 12.75cm and was covered in a gray rubber mat with edges to aid grip. Animals were placed onto the rotating rotarod backwards and latency to fall was recoded. The rotating rod started at 4 rotation per minute (r.p.m) and increased to 40 r.p.m. over a period of 60 seconds. A cutoff of 150 seconds was set. Three trials were recorded per time point and latency to fall was averaged. This test was performed at baseline, 7, 13 and 14 days post-injury. This protocol was taken from (van Gorp et al., 2014).

Inclined Beam. Rats were tested on the inclined beam at baseline, 2 weeks post-SCI, and another cohort additionally 4, 8, 12 weeks after injury. For this test, rats were placed onto an elevated and angled (10 degrees) 1.9cm narrow wooden, circular 1 meter rod and trained to cross to reach their home cage. A green sheet was placed 0.3 meters below to gently catch rats who fell. Prior to baseline testing, animals were habituated by allowing them to cross five times or until they could cross without hesitation. For testing, rats were given the opportunity to cross the beam three times. A Canon Legria HFR806 camera was placed posterior to the beam and used to record inclined beam performance. Ability to complete the full task unassisted, time to cross and hindlimb slips were evaluated and scored. Each hindlimb step was given a maximum of 5 points, -1 point if foot placement was unstable; -2 points if the foot slipped off the beam but continued walking without stopping; -3 points the foot slipped off the beam and walking was interrupted; -4 points if the rat fell but was able to pull itself back up and complete the task; -5 points if the animal fell and did not complete the task. A completion time cut-off of 75 seconds was set. The total number of points was summed and normalized by the total possible number of points (total number of footsteps x 5). Scores for both hindlimbs over the three trials were averaged to calculate the average performance. Animals that did not complete the task received a 0.

Von Frey Hair Filament Mechanical Sensitivity Testing. During habituation, animals were placed in a small box on a metal grid (Ugo Basile) for one hour for three consecutive days. Following, mechanical sensitivity was tested at baseline, 1, 2 weeks post-SCI, and another cohort additionally 4, 8, 12 weeks after injury. Von Frey hair filaments 1.4g, 4g,

8g, 16g, 60g were used to cover the spectrum of light touch to nociceptive stimuli. Positive responses on each hindpaw were recorded after five applications. There were 4 minutes between each consecutive stimulation to prevent desensitization. Von Frey hair filament testing was only performed with animals that had weight support and full plantar steps for both hindlimbs (a BBB score of at least 9).

Hargreaves Thermal Testing. During habituation, animals were placed in a small box on a plastic floor (Ugo Basile) for one hour for three consecutive days. Following, baseline testing was performed in which a laser machine (50 units, maximum 30 seconds) was placed beneath each hindpaw and response time was recorded. Each hindpaw was tested four times and there were 8 minutes between each stimulation to prevent desensitization and damage. If there was urine or feces in the box, two minutes passed post-removal before testing resumed. This test was performed at baseline, 1, 2 weeks post-SCI, and another cohort additionally 4, 8, 12 weeks post-injury. Hargreaves testing was only preformed with animals that had weight support and full plantar steps for both hindlimbs (a BBB score of at least 9).

CatWalk Gait Analysis. All animals were transported to the Interdisciplinary Neurobehavioral Core (INBC) in Heidelberg three days prior to testing for acclimatization. Following, a CatWalk Noldus XT was used to perform the gait experiments. The following settings were used: camera height (48 cm); walkway width (7cm); green intensity threshold (0.1); camera gain dB (18.10); red ceiling light v (17.7); green ceiling light (16.0). For this test, animals were trained to traverse the walkway without stopping. Habituation was performed one day prior to testing until animals could successfully complete the task. On the day of the experiment, the first 5 runs where the maximum speed variation was under 50 and had speed variation less than ten were taken. All analysis was performed using the CatWalk Noldus XT software. The parameter linear discriminant analysis (pLDA) score was calculated according to the previously established protocol (Timotius et al., 2021). Animals without weight support were not included in the CatWalk analysis. Following gait analysis, animals were transported back to the ZOUP Animal Facility Heidelberg for completion of the experiment.

2.2.10 Transplanting E14 spinal cells into a KA Lesion

Two weeks post-KA-injection, half of the lesioned animals underwent E14 spinal cell transplantation. Animals were split into the KA and KA+cells group by an unblinded colleague based on their BBB and von Frey hair 1.4g filament performance. Using the E14 cell isolation protocol mentioned above, E14 spinal cells were harvested the morning of cell transplantation. After digestion and preparation into single cells, cells were resuspended in ice-cold DPBS prior to transplantation.

In the surgery room, animals were anesthetized and prepared in the same manner as previously described for the KA-injections. Due to increased anesthesia tolerance, I found that it was best to first intermuscularly inject animals with 200µl anesthesia mix and place them back into their covered cage until they stopped walking. Following, rats received another 200µl of anesthesia mix right after preparation to ensure that all reflexes subsided and breathing was steady. Reflexes were continuously checked throughout the surgery. After the initial skin incision with a feather scalpel #11, scar tissue over the previously exposed spinal cord was carefully removed with a feather scalpel #15. This was difficult to perform due to excessive vasculature and bleeding from the surrounding scar tissue. If there was bleeding, ice cold saline was placed over the exposed site and allowed to sit for two minutes before removal to speed up coagulation. Additionally, triangle cotton pads were placed over ruptured vessels to help reduce bleeding.

Once the cord was exposed again, cells were spun down and resuspended. One microliter containing 500,000 E14 cells were taken up by the Hamilton and placed into the prepared pulled pipette. Like the KA injections, three sets of bilateral injections with 500,000 cells/injection each were spaced 3mm apart, 0.4mm deep into the lesioned spinal cord. A total of 3 million cells were injected per animal. Post-transplantation, the overlaying muscles were sutured with 4/0 prolene and the skin stapled with 9mm suture clips (MikKron Precision Inc, Gardena, USA). Animals received an additional injection of 1 mL saline and extra Bepanthen® (Bayer Vital Gmbh, Leverkusen, Germany) over their eyes before being placed onto the warmed heating mat for post-surgery recovery. Once

reflexes had returned and animals were moving again, they received one subcutaneous injection of 1 mL ABR and were placed into their cage on the heating pad for post-operative care.

2.2.11 Tissue Processing

Transcardial Perfusion. For perfusions, all animals were transcardially perfused with saline and fixed with 4% PFA in 0.1M phosphate buffer. To begin, animals were interperitoneally injected with an overdose of anesthesia mix. After all reflexes and breathing were gone, animals were placed onto a perfusion grid under a chemical hood. A skin incision was made over the midline to expose the sternum. Two incisions were made laterally exposing the diaphragm. The diaphragm was opened and two incisions across the ribs on both sides exposed the thoracic cavity and heart. After the pericardium was removed, a 21G butterfly needle was inserted into the left ventricle and immediately after an incision was made into the upper right atrium. First ice cold saline was pumped through for ten minutes (approximately 200ml). Following, fresh, ice cold 4% PFA was pumped through for 15 minutes (approximately 250ml). After perfusion, the brain and spinal cord were exposed, the dura was carefully removed and after isolation, were placed into 4% PFA overnight for post-fixation at 4°C. All cords were dehydrated and cryoprotected in 30% sucrose in 0.1M phosphate buffer for one week at 4°C or until the brains sunk to the bottom of the falcon tube.

Sectioning. All thoracolumbar cord sections were first embedded in Tissue-Tek® O.C.T (Sakura Finetek, Germany) and sectioned into 25µm coronal sections in a 1:7 series. A cryostat with object temperature -25°C and blade temperature -22°C were used to section cords. All sections were placed onto super frosted, positively charged glass slides (Microscope Slides Superfrost® Plus, ThermoFischer) and stored at -20°C until further use. All cords were typically sectioned within 3 weeks following perfusion.

I*mmunohistochemistry.* Slides were first dried for 15 minutes at room temperature. Slides were washed 3x with TBS and sections were permeabilized with a blocking solution of 5% donkey serum (Equitech-Bio Inc), 0.25% Tx-100 (neoLab Migge GmbH) in TBS for

two hours at room temperature. Primary antibodies for either KA lesion analysis (Merck guinea pig anti-NeuN 1:1000, Cat # ABN90; Wako rabbit anti-Iba-1 1:1000, Cat # 019-19741; Merck mouse anti-GFAP 1:1000, Cat # IF03L) or graft analysis (Merck guinea pig anti-NeuN 1:1000, Cat # ABN90; Invitrogen goat anti-GFP 1:1000, Cat # 111-22; Wako rabbit anti-Iba-1 1:1000) was added in 0.1% TX-100 and 1% donkey serum and incubated overnight at 4C. The next day, slices were washed three times with 1% serum in TBS and incubated in secondary antibody (Dianova Alexa-Fluor® 594 donkey anti-guinea pig 1:300, Cat # 706295148; AlexaFluor® 488 donkey anti-rabbit 1:300 Cat #A21206; AffiniPure Cy^{TM}5 donkey anti-mouse 1:300 Cat # 715-175-150) or (AlexaFluor® 488 donkey anti-goat 1:300, AlexaFluor® 594 donkey anti-guinea pig 1:300, AffiniPure Cy^{TM}5 donkey anti-rabbit 1:300) with DAPI (1:2000) for four hours at room temperature. Slides were washed again in TBS before being mounted on a cover-slip with Fluoromount G (Biozol, Cat # SBA-0100-01).

2.2.12 Histological Analysis

Lesion Length and Exclusion Criteria. To determine the lesion length in the rostral to caudal axis, neuronal loss was identified in coronal sections stained with NeuN using an Olympus BX53 microscope. The number of slices with neuronal loss in a complete series were quantified and then multiplied by 25 microns x 7 to determine the length of the lesion. All histological analysis was performed by a blinded experimenter.
To determine if animals were appropriately lesioned and to ensure that the observed behavior is due to the desired lesion, we applied specific exclusion criteria based on the histological results. If control animals had a lesion length greater than 2800µm, they were excluded from the experiment. If KA animals had a lesion length smaller than 6000µm, they were excluded from the experiment.

NeuN Quantification in Laminae V-VII. *"*This section was written with collaborator Dr. Carlo Beretta who helped develop this workflow. To quantify NeuN in laminas V-VII, a new workflow was developed with Dr. Carlo Beretta of the Department of Functional Neuroanatomy, Heidelberg University. Spinal cord sections were imaged using the Olympus XT1000 confocal microscope. Z-Stacks of 1.5 micron step size were acquired of each epicenter with the 10x magnification objective (UPlanSApo, 10x/0.40, infinity/0.17/FN26.5). Tiles were stitched in ImageJ/Fiji using the Grid/Collection stitching plugin with the following settings: Unknown Position; Linear Blending fusion method; 0.30 regression threshold; 2.5 Max/avg displacement threshold; 3.5 absolute displacement threshold; and with subpixel accuracy (Preibisch et al., 2009). N= 1 coronal section per lesion epicenter, 3 epicenters per spinal cord.

To determine the correct spinal level, the maximum intensity projection (MIP) of each injection epicenter was computed and registered with the matching spinal cord atlas section (Watson et al., 2009). A customized ImageJ/Fiji script was developed to semi-automate the registration process (https://github.com/cberri/2D_Registration_BrainAtlas_ImageJ-Fiji). The ImageJ/Fiji script uses the BUnwarpJ plugin (https://imagej.net/plugins/bunwarpj/) to register the MIP

images with the corresponding selected atlas map (T13-L4). Indeed, the atlas section that best correspond to the spinal cord gray matter was selected and registered to the appropriate spinal section using land markers. The laminas V-VII (region of interest, ROI) were cropped with ImageJ/Fiji polygon selection tool and saved (Schindelin et al., 2012). N= 1 coronal section per lesion epicenter, 3 epicenters per spinal cord, 6 ROIs per spinal cord.

To enhance signal to noise ratio and normalize the background across images, all the individual Z-stack tiles were processed using the ilastik pixel classification workflow (Berg et al., 2019). Two label classes (foreground NeuN and background) were used to differentiate NeuN positive pixels from background pixels and the resulting foreground probability maps stitched in ImageJ/Fiji with the Grid/Collection stitching plugin. Ilastik pixel classification training was performed prior on 10 sample images. The 2D ROIs generated as described above were over-imposed on the 3D probability map and the pixels outside filled with zero values using the ImageJ/Fiji Clear Outside plugin.

3D automated image segmentation was performed on the processed ROI probability maps using cellpose *Nuclei* pretrained model in a customized Jupyter Notebook (cellpose version 0.6.2; (Stringer et al., 2021)). The labeled images were imported in arivis Vision4D (arivis AG) for visualization. Minor mistakes in the segmentation were manually corrected using arivis Vision4D 3D magic wand tool. The NeuN counts were exported in an excel table and normalized by the selected ROI image volume (counts divided by (ROI area x 25microns)). Normalized NeuN counts for the respective left and right sides were summed to get the total NeuN count per volume at a specific spinal level. Total NeuN in L2-L4 was calculated by summing the total NeuN in each individual spinal level. To determine if there were differences between groups, the total averages per group were compared." (This section was taken from (Kuehn et al., Manuscript in preparation) and was written by Dr. Carlo Beretta and myself).

$$Normalized\ NeuN\ Counts = \frac{Total\ NeuN\ Counts}{ROI\ Area\ * Z\ Height}$$

Workstation Hardware Specification. All image analysis was performed on a workstation equipped with a Nvidia RTX 2070 Super GPU, 128 GBs RAM and 10 Cores Intel i7 processor.

Software Accessibility. All custom code written for this project can be found under the following link: https://github.com/naemikuehn/lumbarcordanalysis.git

Motoneuron Analysis. To determine the number of remaining motoneurons at each lesion epicenter, NeuN+ soma in laminas IX were quantified using a similar method as previously published (Wen et al., 2015). The correct lamina was determined using the Spinal Cord Atlas (Watson et al., 2009). All NeuN+ cells with a soma area larger than 919.632µm^3 in lamina IX were counted and then analyzed in Graphpad Prism 6 to determine if there was a correlation between remaining motoneurons and behavioral performance. N = 1 image per lesion epicenter, 3 epicenters per spinal cord. All analysis was performed by a blinded investigator.

White Matter Analysis. To determine if white matter was damaged, the area of white matter and percent white matter of the spinal cord cross-sectional area (CSA) at each given epicenter were calculated. A protocol previously published (Sliwinski et al., 2018) was used. To begin, slides were taken out of the freezer and allowed to dry for a minimum of 2 hours at 37°C. Following, they were transferred into fresh acetone for 5 minutes and then dried for 20 minutes. Next, they were placed into the Eriochrome Cyanine Solution for 30 minutes. This solution is usually reusable and can be filtered if needed; if not prepared fresh, it's recommended to add 1mL of fresh H_2SO_4 into the solution before use. Afterwards, slides were placed into ddH_2O for 5 minutes and into 5% Iron Alum for 5-20 minutes (usually 20 minutes). This solution is made fresh each time. Then slides were rinsed in tap water for 10 minutes. The differentiation is completed once slides have been placed into the borax-ferricyanide solution for 10 minutes. This solution is reusable. Again, slides were placed into ddH_2O for five minutes and dehydrated with the following graded ethanol solutions: 70%, 95%, 100% each two times; each wash was two minutes long. Lastly, slides were placed into histoclear (Merck, Darmstadt, Germany) three times for

two minutes each. They were cover slipped with Neo-mount (Neomount; Merck) and stored in a dark box until imaging.

Slides were imaged using a XC30 camera and an Olympus Bx53 microscope (Olympus, Hamburg, Germany). White matter area of the spinal cord was calculated in Image J compared between the control and KA groups. Additionally, percent white matter of the spinal cord CSA was calculated in Image J by dividing the tissue sparing (total CSA of the slice – lesion size) and dividing it by the total CSA. One coronal section was analyzed per bilateral injection site (lesion epicenter) and a total of three epicenters per spinal cord were analyzed. Sections from the first cohort of the two-week experiment were analyzed. All analysis was performed by a blinded investigator.

Heatmap Analysis. Behavioral tests and neuronal quantification at spinal levels L2-L4 were compared between individual KA-lesioned animals and the average controls. All values were normalized to the average of the controls and reported as a percentage of the average controls except for lesion length. For lesion length, all values were normalized to the largest lesion length, 15,925µm.

2.2.13 Statistical Analysis

All data is shown as mean ± the standard error of the mean unless otherwise reported. A repeated measures 2-way ANOVA with Sidak's post hoc multiple comparisons test was calculated to evaluate differences between the two groups in tests that were repeatedly performed over a period of time (BBB score, BBB subscore, pilot experiment sensory and additional motor tests, as well as additional motor tests from the cell transplantation experiment). Unless otherwise noted, all reported p-values are group differences p-values. All other tests underwent Shaprio-Wilk's normality test. If normally distributed, a Welch's unpaired t-test to determine differences between the two groups, if not normally distributed, a Mann-Whitney test was used (inclined beam, horizontal ladder, von Frey hair filament testing, Hargreaves, CatWalk, motoneuron, white matter sparing and area, NeuN counts). Linear regression analysis was performed to compare lesion length, motoneuron counts and white matter sparing with behavior. Shapiro-Wilk's normality test

was performed prior to Pearson's (normally distributed) or Spearman's (not normally distributed) correlation analysis to analyze the relationship between the two variables. All statistical tests were performed with Prism 6 and Prism 9 software (Graphpad, San Diego, CA, USA).

2.2.14 Schematics

Schematics were created with BioRender.com (BioRender, 2021), powerpoint and Google images.

3 Results

3.1 Establishing a KA lesion model with correct behavioral tests

The aim of this project was to develop a spinal cord injury (SCI) model to evaluate the potential of E14 spinal cells to replace damaged gray matter and restore lost function in the lumbar spinal cord. A previously established large KA lesion model was uniquely modified to create a discrete gray matter lesion targeting laminae V-VII in lumbar spinal levels which elicits a strong behavioral readout. Select behavioral evaluations were tested to measure sensorimotor functions affected by this specific injury. This work lays the groundwork to test the functional potential of cell replacement therapies after a lumbar gray matter SCI.

3.2 Section I

3.2.1 Kainic acid injections of 0.5µl at 0.4mm depth create damage in laminae V-VII

As most experimental SCI models damage both the white and the gray matter, I turned to the neurotoxin kainic acid (KA) to create selective gray matter damage. As the majority of glutamate receptors are on the cell dendrites and soma in the gray matter, kainate injections create primarily gray matter and not white matter damage. With advice from the Magnuson laboratory which had previously worked with KA spinal injections, I tested various KA concentrations, volumes, injection depths as well as spinal levels in the lumbar cord to create targeted intermediate gray matter lesions (**Table 21**). Bilateral injections of 1µl of 1mM KA at a depth of 0.8mm were tested. Post-histological analysis, I found that this created more severe damage in the dorsal-ventral axis than desired; the dorsal horn as well as motoneurons were severely damaged and accompanied by a strong inflammatory response (**Fig. 4*A,B***). These coordinates were refined to 0.5µl of 1mM KA injected at a depth of 0.4mm. While injection coordinates still needed to be refined to create more consistent injections on the left and right sides, these injection coordinates created a less severe gray matter injury located primarily in the intermediate gray matter (**Fig. 4*C,D***).

Table 21. Overview of pilot experiments to determine the correct KA injection coordinates.

Pilot	Location (vertebral level)	Number of Injections	Concentration	Volume	Depth	Animal #s (veh/KA)	Behavioral Tests
#1	Caudal T12	1 x bilateral	0.5mM KA 1mM KA	1µl	1.0mm	N=6 (2/2)	BBB
#2	Mid/caudal T12	2 x bilateral	1mM KA	1µl	1.0mm	N =3 (1/2)	BBB
#3	Caudal T12	2 x bilateral	1mM KA	1µl	0.8mm	N = 2 (1/1)	BBB
#4	Caudal T12	2 x bilateral	1mM KA	1µl	0.8mm	n = 3 (1/2)	n/a
#5	mid T12	2 x bilateral	1mM KA	1µl	0.5mm	n = 6 (2/4)	BBB Ladder
#6	Rostral T12	1 x bilateral	1mM KA	1µl	0.4mm	n = 6 (2/4)	BBB Ladder Paw print test Rotarod Von Frey, Hargreaves
#7	Caudal T12 Mid T13	2 x bilateral	1mM KA	0.5µl	0.4mm	n = 8 (3/5)	BBB Ladder Von Frey Rotarod Pawprint
#8	Mid T13 Rostral T13	2 x bilateral	1mM KA	0.5µl	0.4mm	n = 7 (1 died) (3/4)	BBB Ladder, Inclined Beam Von Frey, Hargreaves CatWalk

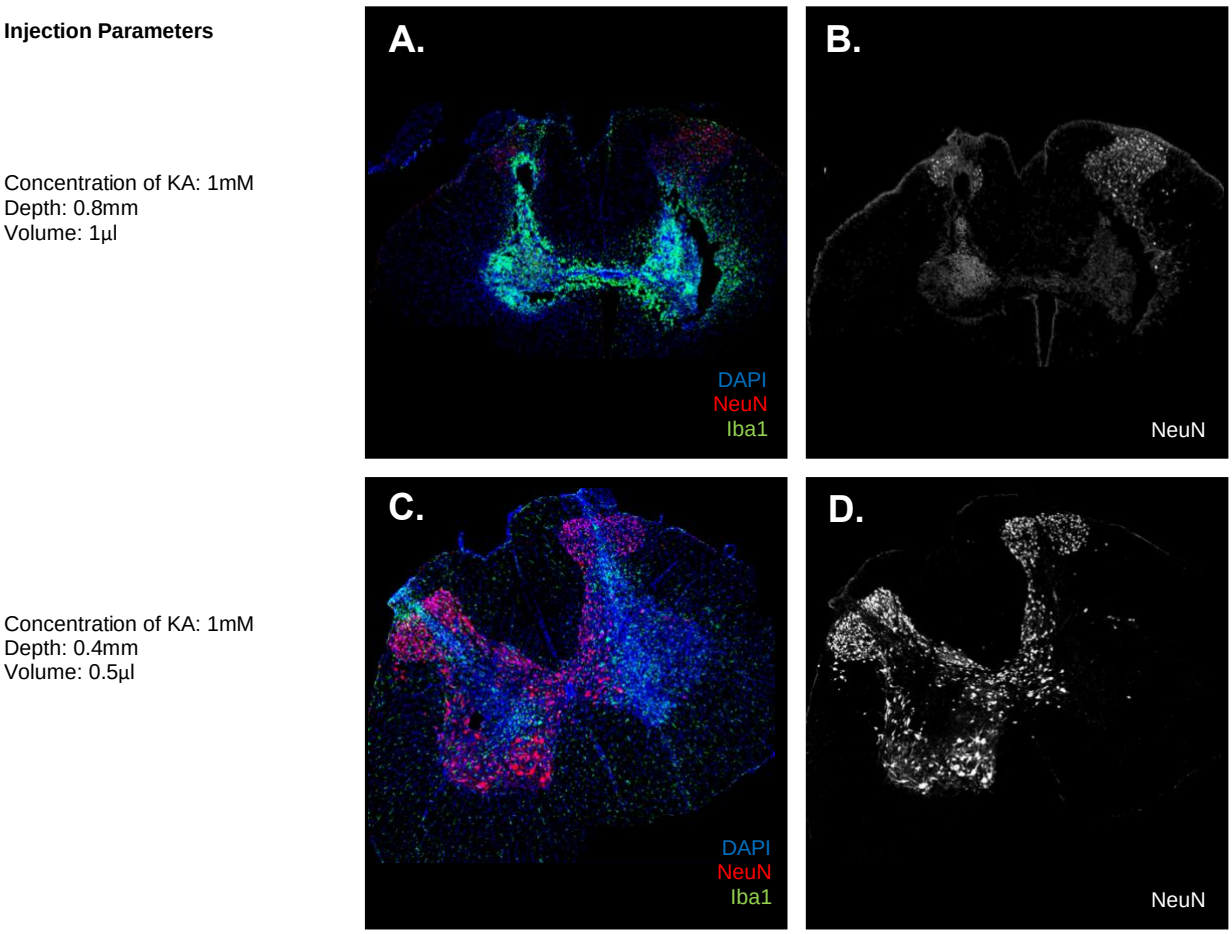

Figure 4. Determining correct depth and volume for KA injections. ***A,B*** Representative pictures show initial KA injections of 1µl, 1mM KA at a depth of 0.8mm which created severe tissue damage including motoneuron damage. ***C,D*** Reducing the volume and depth to 0.5µl and 0.4mm created less severe gray matter damage. Neurons were visualized in red, microglia and macrophages in green and cell nuclei in blue.

3.2.2 Establishing behavioral tests following spinal levels L1-L4 KA injections

While testing the injection volume and depth, I also aimed to find the correct spinal levels and number of injections that elicited a quantifiable behavioral readout. I aimed to target the upper lumbar cord where circuitry responsible for locomotion resides. Previously, the Magnuson laboratory had injected 1.5µl of 2.5mM or 5mM KA into vertebra T12 to target the L2 spinal cord and created large gray matter damage (Magnuson et al., 1998). Another paper performed a T12-T13 or T13 laminectomy and

injected 1µl of 1mM KA, 0.5-0.8mm from the midline and 1.2mm deep into the spinal cord to target the dorsal and intermediate gray matter in T11-12 to L5 spinal cord (Hadi et al., 2000). I aimed to modify the KA-injection paradigm the Magnuson laboratory had established in Sprague Dawley rats to evaluate what works in Fischer rats. In pilot experiment #7, two sets of bilateral injections at caudal vertebra T12 and rostral vertebra T13 were tested in Fischer rats to target spinal levels L1 and L2 (**Fig. 5*A***). After injury, gross hindlimb function was evaluated using the Basso-Beattie-Bresnahan (BBB) score, which is an open field test performed 1, 3, 7 and 14 days post-injury. There were no significant differences sustained after injury that lasted two weeks (**Fig. 5*B,C*:** BBB score: controls = 17.1 ± 1.71, KA group = 19.83 ± 0.44, group, p = 0.1181; BBB subscore: controls = 12.07 ± 0.27, KA = 9.94 ± 1.20, group p = 0.1940, 2-way ANOVA, n = 3 controls, n = 5 KA animals). Although the BBB score is useful in classifying SCI animals, it is not as sensitive for tasks we believe are affected by our lesion model. Therefore, tasks specific to this lesion paradigm such as rhythmic and skilled-walking were tested including on the even horizontal ladder and uneven horizontal ladder (Martins et al., 2022). There were no differences in rhythmic walking or skilled-walking using the above-mentioned injection paradigm two weeks post-injections (**Fig. 5*E,F*:** even horizontal ladder % slips: control = 0.42 ± 0.42%, KA = 2.47 ± 2.13%, p = 0.7778; uneven horizontal ladder % slips: control = 2.25 ± 0.43%; KA = 52 ± 0.98%, p = 0.3798, 2-way ANOVAs, n = 3 control, n = 5 KA animals).

During the BBB test, I observed a slight hindpaw rotation and therefore performed a standard pawprint test of the hindpaws. To measure paw rotation, one must know the trunk position, which was difficult due to the animal's lack of calm and motivation preventing them from walking in a straight line even in a modified narrow tunnel. Therefore due to walking variability, the paw angle could not be calculated. However, while stride length and step width measurements were obtainable, there were no significant differences two weeks post-injury (**Fig. 5*G,H****:*** step width: control = 2.86 ± 0.22cm, KA = 2.86 ± 0.22cm, group p = 0.97; stride length: control = 15.42 ± 0.85cm, KA = 16.14 ± 0.56cm, p = 0.1491, 2-way ANOVA, n = 3 control and n = 5 KA animals). As the standard pawprint test resulted in high variability with less parameters analyzed, I planned to test animals on the automated CatWalk (Noldus) apparatus for future experiments.

In an attempt to find more appropriate behavioral tests, I tested KA animals on the backwards rotating rod. Single nucleus transcription sequencing and cFos experiments revealed that neurons in the lumbar intermediate gray matter were active in mice following rotarod training (Sathyamurthy et al., 2018). Furthermore, a previous study had published that the backwards rotating rod was able to better discriminate between sham and mildly injured animals than the forwards rotating rod, myogenic motor evoked potential and inclined ladder during the acute, subacute and chronic phases of SCI following a lower thoracic contusion injury (van Gorp et al., 2014). Therefore, a student, Nicolas Rodemer, and I replicated their model by increasing the diameter of the rod to 12.5cm and placing a rubber surface around the rod to help with grip. The paper mentioned that the test was performed without additional training. However, we found that training was highly necessary for animals to walk backwards properly and even with training, animals lacked motivation and jumped off the rod, skewing results. It was evident already from baseline testing that animal performance was highly variable and rather a readout of motivation than ability to complete the task and coordination. There were no significant differences two weeks after injury **(Fig. 5*D:*** latency to fall: control = 8.22 $\pm$ 2.53 sec, KA = 13.73 $\pm$ 4.80 sec, group p = 0.4106, 2-way ANOVA, n = 3 control and n = 5 KA animals). Given these difficulties, this test may not be the best assessment tool for this lesion model.

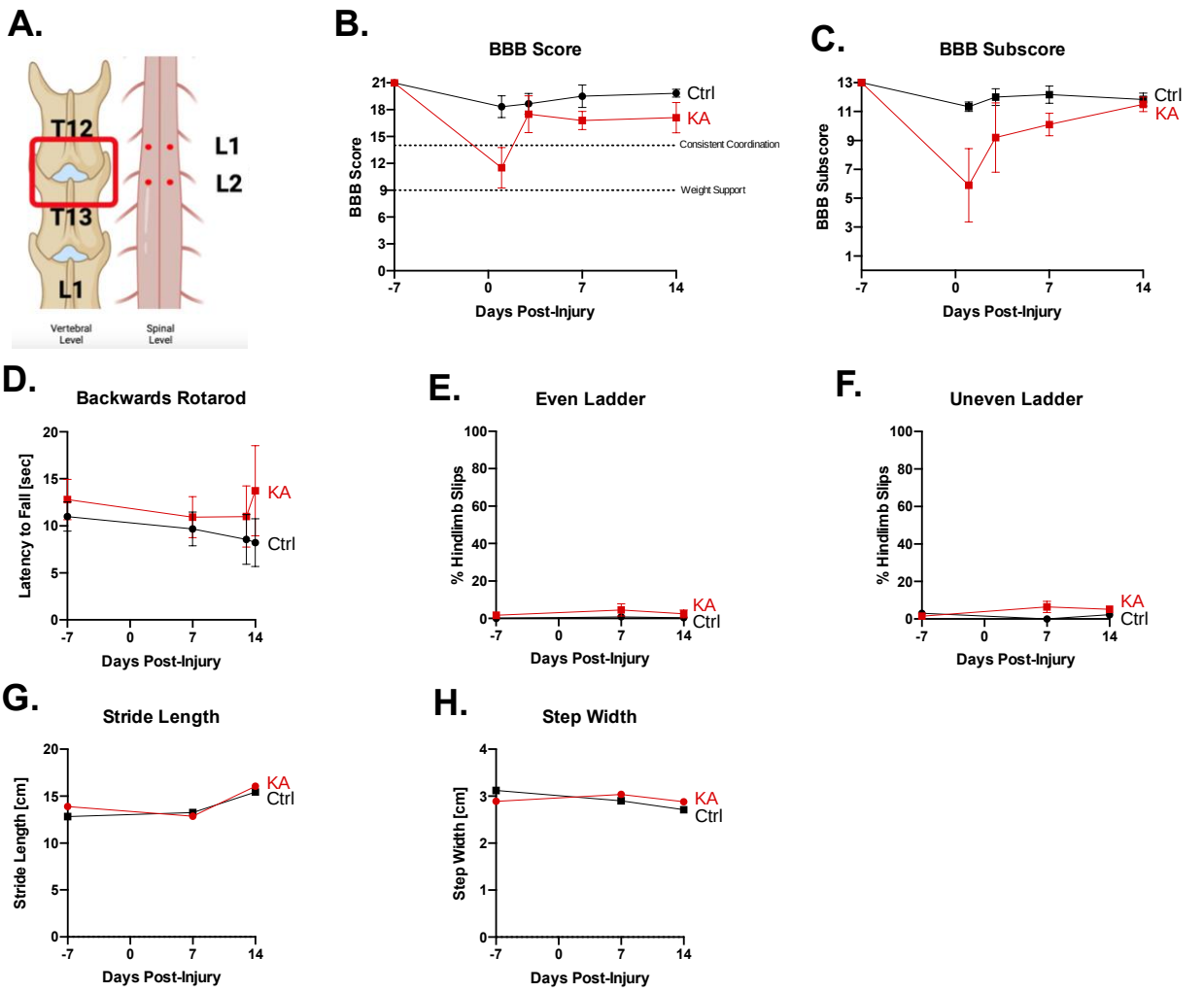

Figure 5. Two sets of bilateral KA injections caudal vertebra T12 and mid vertebra T13 did not elicit behavioral deficits after two weeks. ***A***, Schematic of KA injection parameters**.** ***B,C*** BBB score and subscore after two weeks did not show significant differences. BBB score group p = 0.1181, BBB subscore group p = 0.1940, 2-way ANOVA. ***D,*** Performance on the backwards rotating rotarod had high variability within the two groups and did not show differences after two weeks. ***E,F*** Coordination and balance measured by the even and uneven ladder hindlimb slips was not significantly differ. ***G,H*** Finally, step width and length was not significantly different after two weeks. 2-way ANOVA, n = 3 control and n = 5 KA animals.

To determine if this lesion affected mechanical sensory function, I used the von Frey hair filament test. There were no significant differences in mechanical sensitivity however I observed a trend towards increased sensitivity (mechanical allodynia) with the 1.4g von Frey hair filament two weeks after injury (**Fig. 6*A,B*:** 1.4g response rate: control = 23.33 ± 6.67%, KA = 54 ± 13.64%, group p = 0.1633; 60g response rate: control = 80.00

± 11.54%, KA = 90.00 ± 3.16%, group p = 0.6907, 2-way ANOVA, n = 3 control and n = 5 KA animals).

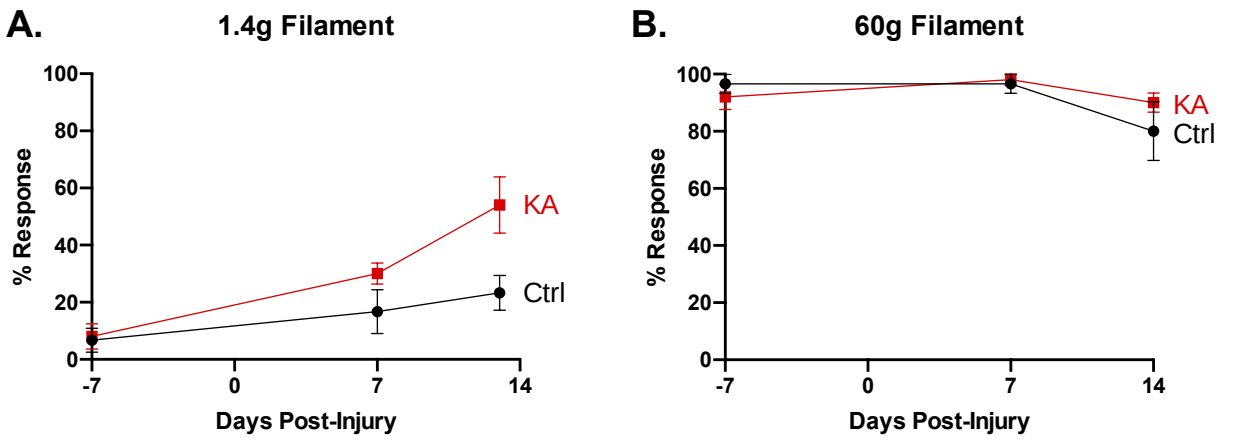

Figure 6. Two sets of bilateral KA injections caudal vertebra T12 and mid vertebra T13 did not elicit mechanical alterations after two weeks. ***A,B*** von Frey hair filament testing with 1.4g (light touch) and 60g (nociception) did not show group differences after two weeks. 1.4g group p = 0.1633, 60g group p = 0.6907, 2-way ANOVA, n = 3 control and n = 5 KA animals.

As there were no significant behavioral differences two weeks post-injury, I adjusted the location of the injections and applied two sets of bilateral KA injections more caudally in the spinal cord, at mid and caudal vertebra T13, corresponding to spinal levels L3 and L4 (**Fig. 7*A***). Evaluation of gross hindlimb function revealed a dip in performance shortly after injury, which I believe is due to the surgery itself as this is seen in both the control and KA groups (**Fig. 7*B*)**. There were no significant differences two weeks post-injury (**Fig. 7*B:*** BBB score: control = 18.17 ± 0.44, KA = 19.38 ± 0.75, group p = 0.7703, 2-way ANOVA, n = 3 control, n = 4 KA animals). Evaluation of the BBB subscore revealed a significant difference in coordination one day after surgery, however animals recovered and there were no significant differences after two weeks (**Fig. 7*C:*** BBB subscore: control = 11.33 ± 0.44, KA = 12.25 ± 0.32, group p = 0.2940, 2-Way ANOVA, n = 3 control and n = 4 KA animals).

As paw angle and other more sensitive temporal parameters could not be reliably measured with the paper pawprint test, I performed CatWalk (Noldus) gait analysis, allowing for static and dynamic parameters of each forelimb and hindlimb as well as the whole-body automated gait analysis. Analysis of commonly reported parameters including base of support, stride length, and body speed revealed a significant difference between the latter two (**Fig. 7*D-F:*** base of support: control = 2.47 ± 0.11cm, KA = 2.71 ± 0.05cm, group p = 0.0975; stride length: control = 16.39 ± 0.56cm, KA = 14.41 ± 0.34cm, p = 0.0206; body speed: control = 50.53 ± 2.05 cm/sec, KA = 41.06 ± 1.69 cm/sec, p = 0.0078, unpaired Welch's t-test, n = 3 control and n = 4 KA animals). As KA animals did not leave full pawprints, it was not possible to accurately calculate paw angles. An algorithm (parameter-combined linear discriminant analysis, pLDA) that combines 9 SCI-related gait parameters found to be predictive of injured vs uninjured thoracic SCI rat models was applied to these results. While there was a decrease in pLDA score, there were no significant differences between the two groups (**Fig. 7*G:*** control = 0.14 ± 0.01, KA = 0.12 ± 0.00, p = 0.1922, unpaired Welch's t-test, n = 3 control and n = 4 KA animals).

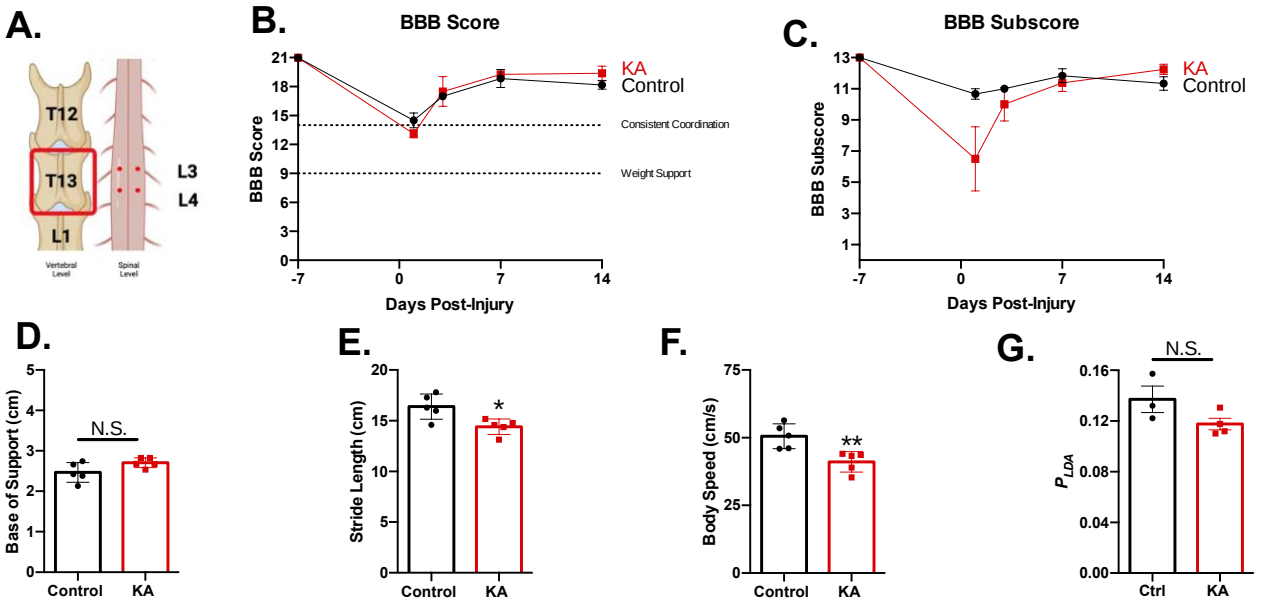

Figure 7. Two sets of bilateral KA injections mid and caudal vertebra T13 did not elicit significant gross hindlimb deficits and only minor gait deficits after two weeks. ***A****,* Schematic of KA injection parameters. ***B,C*** BBB score and subscore after two weeks did not show significant differences in gross hindlimb function and coordination after two weeks, BBB score group p = 0.7703, BBB subscore group p = 0.2940, 2-way ANOVA. ***D****,* CatWalk parameter base of support did not reveal significant differences, p = 0.0905, unpaired Welch's t-test. ***E,*** Stride length was significantly smaller in comparison to the controls, p = 0.0206, unpaired Welch's t-test. ***F,*** KA animals were significantly slower than the controls, p = 0.0078, unpaired Welch's t-test. ***G,*** pLDA score does not reveal significant differences in gait between the two groups, p = 0.1922, Welch's t-test. N = 3 control and n = 4 KA animals,* $p \leq 0.05$, ** $p \leq 0.01$. N.S. stands for not significant.

In an attempt to further quantify discrete deficits, I also applied a more discriminant test, the inclined beam. It combines principles from the inclined ladder and balance beam to test coordination and balance. A wooden rod is placed between two cages at a 10-degree angle where the ability to cross and hindlimb function is evaluated. I tested two wooden rods with a diameter of 1.9cm and 1.3cm beams and developed a novel scoring method to evaluate hindlimb function and coordination. All animals were able to complete the 1.9cm and 1.3cm beam both before and after injury (**Fig. 8*A,B****:*** 1.9cm and 1.3cm beam average completion control = 100 $\pm$ 0.00%, KA = 100 $\pm$ 0.00%, n = 3 control and n = 4 KA animals). As expected, animals had more difficulty traversing the narrower 1.3cm beam, as the latency for KA animals to cross is over 1.6x longer than the 1.9cm beam two weeks after injury (**Fig. 8*G,H****:*** KA latency to cross 1.9cm beam 14dpi = 7.66 $\pm$ 1.73 sec, KA latency to cross 1.3cm beam 14dpi = 12.52 $\pm$ 0.64 sec, n = 3 control and n = 4 KA animals). However unfortunately, there were no significant group differences in beam score, number of steps and latency to cross for both beams two weeks post-injury (**Fig. 8*C-H:*** beam score: 1.9cm beam group p = 0.4344, 1.3cm beam group p = 0.7277; number of steps: 1.9cm group p = 0.3539, 1.3cm group p = 0.0.3848; latency to cross: 1.9cm group p = 0.7203, 1.3cm group p = 0.1900, 2-way ANOVA, n = 3 control and n = 4 KA animals)**.**

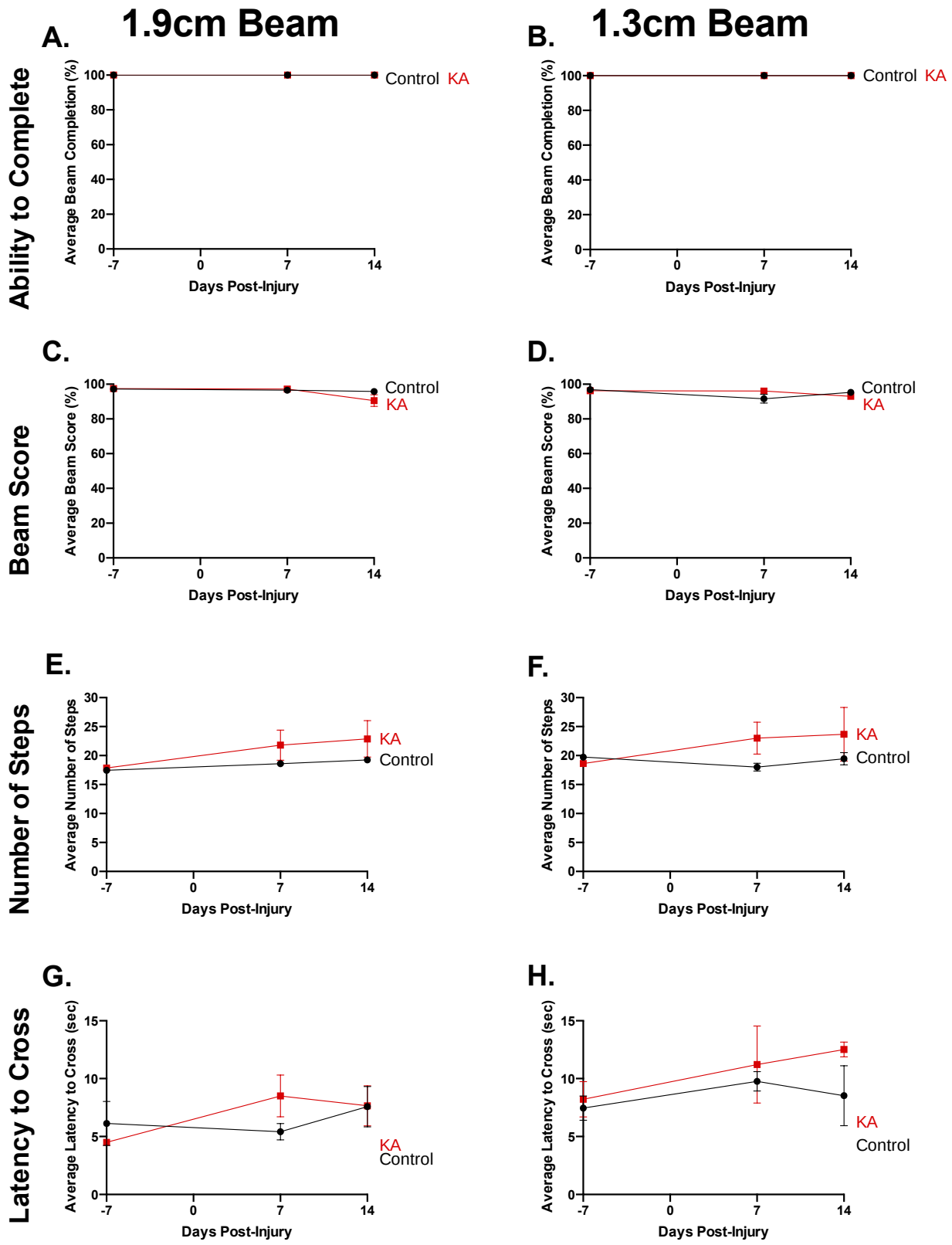
A.
1.9cm Beam
B.
1.3cm Beam
Ability to Complete
Average Beam Completion (%)
Control
KA
Days Post-Injury
C.
D.
Beam Score
Average Beam Score (%)
E.
F.
Number of Steps
Average Number of Steps
G.
H.
Latency to Cross
Average Latency to Cross (sec)

Figure 8. Inclined beam performance indicates there were no significant balance and coordination behavioral deficits. ***A,B*** All animals were able to successfully traverse the 1.9cm and 1.3cm beams both before and after injury ***C-H*** There were no significant group differences in beam score, number of steps and latency to cross on both the 1.9cm and 1.3cm beams after two weeks. For the 1.9cm beam: beam score group p = 0.4344, number of steps group p = 0.3539, latency to cross group p = 0.97203. For the 1.3cm beam: average beam score group p = 0.7277, number of steps group p = 0.3848, latency to cross group p = 0.1900; 2-way ANOVA, n = 3 control and n = 4 KA animals.

Lastly, to evaluate sensory function, I also tested animals for mechanical and thermal sensitivity. There were no significant differences in mechanical sensitivity to the 1.4g and 60g von Frey hair filaments after two weeks (**Fig. 9*A,B****:*** von Frey hair filament response rate1.4g: control 13.33 ± 6.68%, KA: 23.25 ± 9.78%, group p = 0.4706; von Frey hair filament response rate 60g: control 86.68 ± 3.33%, KA = 97.50 ± 2.50%, group p = 0.4261, 2-way ANOVA, n = 3 controls and n = 4 KA animals). No differences in thermal sensitivity after two weeks were found either (**Fig. 9*C:*** latency of withdrawal: control = 9.33 ± 1.17 sec, KA = 9.73 ± 1.20 sec, group p = 0.2082, n = 3 control and n = 4 KA animals). Together, while the CatWalk revealed some significant gait parameter differences after two weeks, overall, animals do not show significant gross motor, coordination, balance, pLDA and sensory behavioral differences with the above-mentioned injection coordinates. Therefore, it appeared the ideal target region of vital intermediate gray matter to induce quantifiable behavioral deficits was not yet achieved.

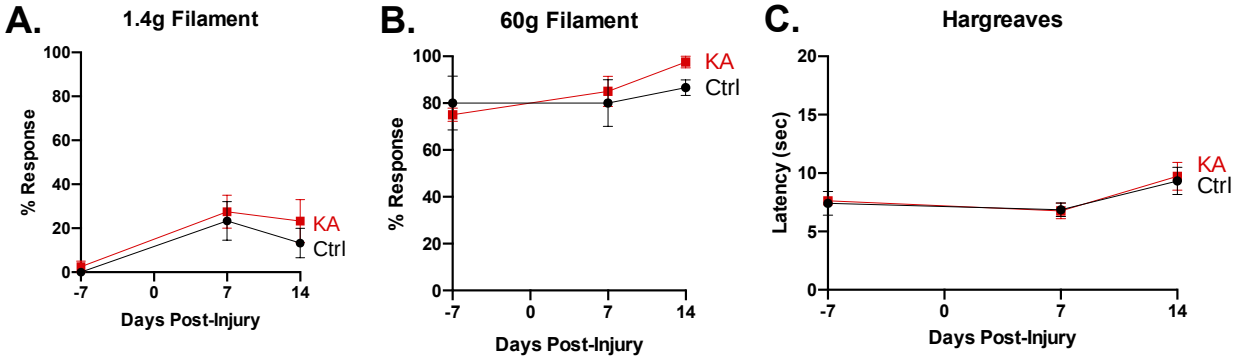

Figure 9. Two sets of bilateral KA injections mid and rostral vertebra T13 did not elicit changes in sensitivity after two weeks. ***A,B*** von Frey hair filament testing with 1.4g and 60g did not show group differences in light touch or nociception after two weeks (1.4g 2-way ANOVA group p = 0.4706, 60g 2-way ANOVA group p = 0.4261). ***C,*** Hargreaves testing did not show changes in thermal sensitivity after two weeks (2-way ANOVA group p = 0.2082). N = 3 control and n = 4 KA animals.

3.2.3 Targeting intermediate gray matter for neuronal loss in lumbar spinal levels L2-L4 with three sets of bilateral KA injections

In the final attempt to create a lesion that targeted various SpINs contributing to locomotion, KA injection parameters were again refined to create selective intermediate gray matter damage in the lumbar cord with a behavioral readout. (The remainder of this section has been adapted from (Kuehn et al., Manuscript in preparation) and was written by myself.) This was achieved by combining the injection paradigms of the two previously mentioned pilot experiments and using three bilateral KA injections performed at vertebral level T13 in female Fischer rats. Each injection consisted of 0.5µl of 1mM KA injected 0.5mm from the midline at a depth of 0.4mm (**Fig. 10*A*-*C***). To confirm which spinal levels and laminae were targeted, all gray matter neurons were visualized with NeuN with a custom workflow to confirm damage in the target region set up in collaboration with Dr. Carlo Beretta of the Department of or Anatomy and Cell Biology and Institute of Pharmacology at Heidelberg University. The ImageJ/FIJI plugin "registration of pairs" was used to align the spinal atlas over 3D confocal coronal section Z-stacks for determination of the spinal level and target laminae (**Fig. 10*D***). To quantify the number of NeuN positive neurons in laminae V-VII from spinal levels L2-L4 in a consistent and unbiased fashion, the newly developed combined image analysis workflow was used: ilastik pixel classification, 3D segmentation using cellpose and arivis Vision4D for visualization and segmentation correction (**Fig. 11**). This KA lesion significantly reduced the number of NeuN positive neurons in laminae V-VII to 14.39 $\pm$ 1.92 neurons/µm^3*10^{-5} in comparison to 24.91 $\pm$ 1.89 neurons/µm^3*10^{-5} in the control group ($p = 0.002$, unpaired Welch's t-test, **Fig. 10*E*)**. With this experiment, I have confirmed that injecting KA with these defined parameters creates intermediate gray matter damage in the spinal levels L2-L4 of the spinal cord.

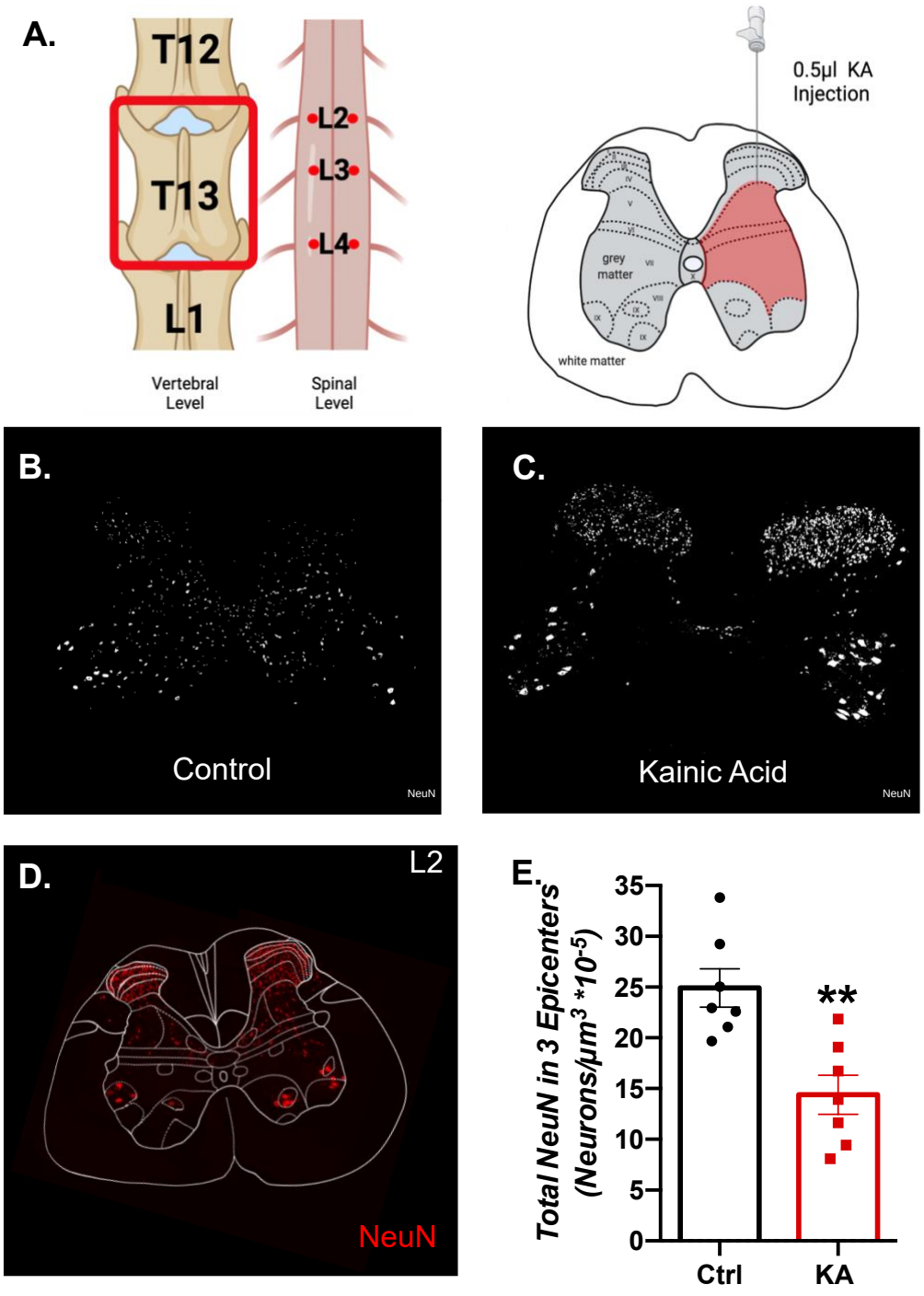

Figure 10. Defined KA injection parameters create selective intermediate gray matter damage in the lumbar spinal cord. ***A,*** Schematic shows vertebral and spinal injection levels in the rostral and caudal axis as well as in the dorsal-ventral axis. ***B,*** Representative images of lesion epicenters stained with NeuN to visualize neuronal loss in the control and KA-lesioned spinal cord. ***C*****,** Representative images of atlas overlays on coronal spinal cord sections confirms that spinal levels L1-L4 were targeted. ***D*****,** Visualization of neuronal loss in the SC ***E,*** Total NeuN in laminas V-VII at lesion epicenters were quantified and compared, (Unpaired Welch's t-test, **p = 0.0021), n = 7/group. Adapted from (Kuehn et al., Manuscript in preparation).

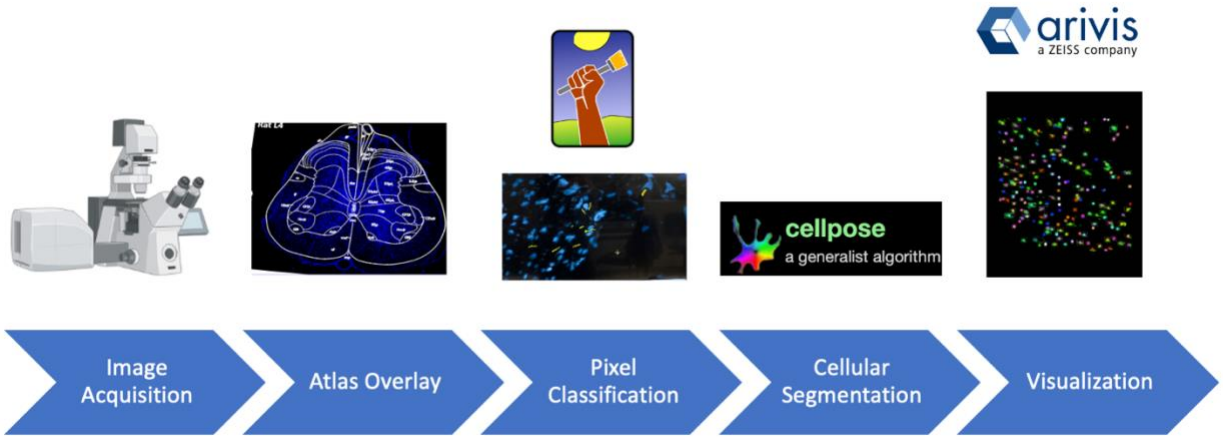

Figure 11. Image acquisition and analysis workflow designed for neuronal quantification. First, Z-stack tiles of coronal slices stained with the NeuN antibody were acquired using a confocal XT1000 microscope with the 10x magnification objective. The tiles were stitched in ImageJ/Fiji and a spinal cord atlas overlay was registered over the maximum intensity projection using the BunwarpJ ImageJ/Fiji plugin. Once the correct spinal levels and ROIs were determined (laminas V-VII), the ilastik pixel classification workflow was trained, and the output foreground probability map used as an input in cellpose to 3D segment the nuclei (cellpose, nuclei pretrained model). The 3D labeled images were visualized in arivis Vision4D and segmentation mistakes were manually corrected. The neuronal counts were normalized by ROI volume. Adapted from (Kuehn et al., Manuscript in preparation).

3.2.4 KA rats show deficits in gross hindlimb function, rhythmic and skilled walking, coordination, balance and gait after two weeks

To assess the behavioral deficits induced by a discrete KA gray matter SCI, I performed a series of behavioral tests two weeks post-injury previously established in the pilot experiments (**Fig. 12**). Animals with a KA lesion were observed to have significant deficits in gross hindlimb function 1 day after injury and have a stabilized significantly lower BBB score two weeks post-SCI (**Fig. 13*B*:** Mean BBB scores after 14 dpi: control = 17.57 $\pm$ 0.69, KA = 11.21 $\pm$ 2.25, group $p<0.0001$, 2-way ANOVA, n = 7/group) as well significant deficits in hindlimb function dependent upon coordination (**Fig. 13*C*:** mean BBB subscore after 14 dpi: control = 11.29 $\pm$ 0.18, KA = 4.57 $\pm$ 1.67, group $p<0.0001$, 2-way ANOVA, n = 7/group). These deficits correlate to lesion length in the rostro-caudal axis (**Fig. 13*D,E:*** BBB score r = -0.8254 and p= 0.0004, BBB subscore r = -0.7138 and p = 0.0041, Spearman's correlation, n = 7/group). Two animals did not have weight support. The animal with the greatest lesion length had the lowest BBB score, however the second animal without weight support had the same lesion length as another animal who did have

weight support (**Fig. 13*D***), indicating that lesion length is not the only determining factor for behavioral performance.

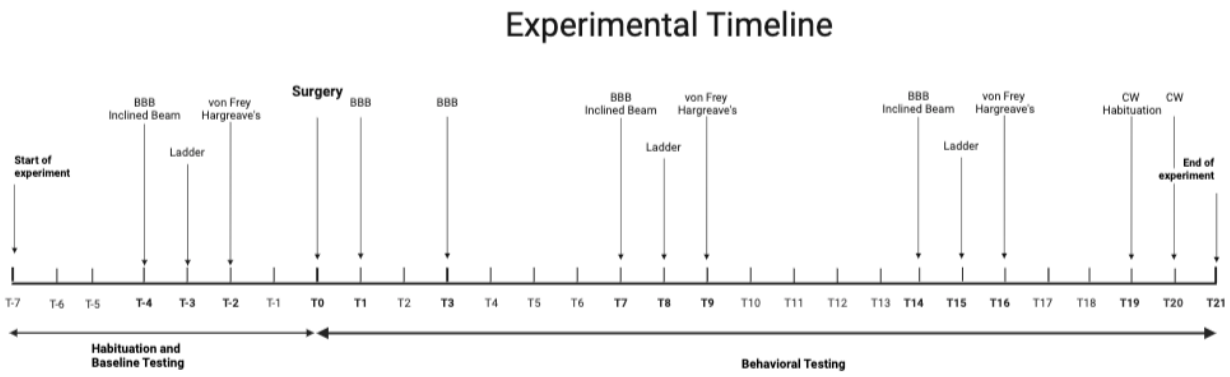

Figure 12. Experimental timeline of KA injections and behavioral testing. Animals underwent baseline testing prior to KA injections. Post-injections, animal gross hindlimb function, coordination, balance, gait, and sensory functions were evaluated prior to being sacrificed three weeks after injections.

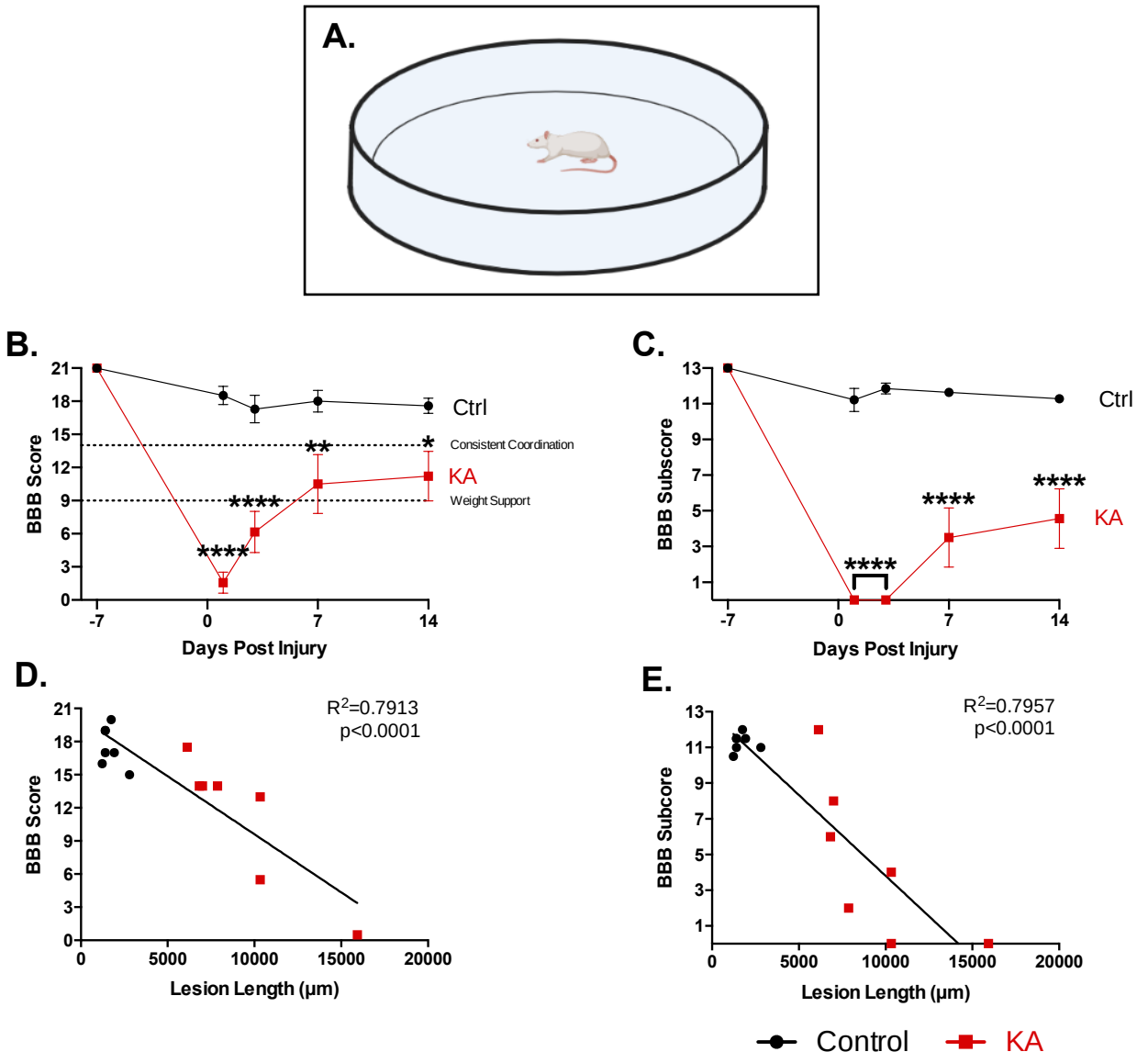

Figure 13. Three sets of KA injections into vertebra T13 create significant gross hindlimb deficits two weeks post-injury. ***A*,** Schematic of open field BBB scoring platform. ***B,C*** KA-injected animals have a stabilized significantly lower BBB score and subscore after two weeks in comparison to the control (BBB score: group $p<0.0001$; BBB subscore: group $p<0.0001$; 2-way ANOVA). ***D,E*** There were significant correlations between lesion size in the rostral-caudal axis and BBB score and subscore 14 dpi (BBB score $p<0.0001$, $R^2 = 0.7913$; BBB subscore $p<0.0001$, $R^2 = 0.7957$, Linear Regression Analysis). For all data, n = 7 animals per group; * $p \leq 0.05$, ** $p \leq 0.01$, **** $p \leq 0.0001$. Adapted from (Kuehn et al., Manuscript in preparation).

Next, I evaluated rhythmic and skilled walking, coordination and balance. (**Fig. 14*A,D,G***). KA rats show significantly higher number of hindlimb slips on both the even and uneven horizontal ladders indicating deficits in rhythmic walking (**Fig. 14*B*:** even ladder: controls = 0.70 ± 0.34%, KA = 39.91 ± 15.81%, p = 0.0006, Mann-Whitney test, n

= 7/group) and coordination (**Fig. 14*E*:** uneven ladder: controls = 1.71 ± 0.91%, KA = 48.68 ± 15.12%, p = 0.0023, Mann-Whitney test, n = 7/group). Only 3 of the 7 KA rats were able to complete the inclined beam test (**Fig. 14*H*:** controls = 100 ± 0% completion, KA = 23.81 ± 14.02%, p = 0.0047, Mann-Whitney test, n = 7/group). Those KA rats which did complete the beam had a lower performance score (controls: 95.66 ± 1.25%, KA: 21.19 ± 13.32%, group p = 0.0002, 2-way ANOVA, n = 7/group) further indicating deficiencies in coordination and balance (**Supplementary Video:** https://heibox.uni-heidelberg.de/d/71d56830564d42799aa6/). These behavioral tests significantly correlated to lesion length in the rostro-caudal axis (**Fig. 14*C*,*F*,*I***: even horizontal ladder r = 0.8490 and p = 0.0003, uneven horizontal ladder r = 0.8401 and p = 0.0004, inclined beam r = -0.8944 and p < 0.0001, Spearman's correlation analysis).

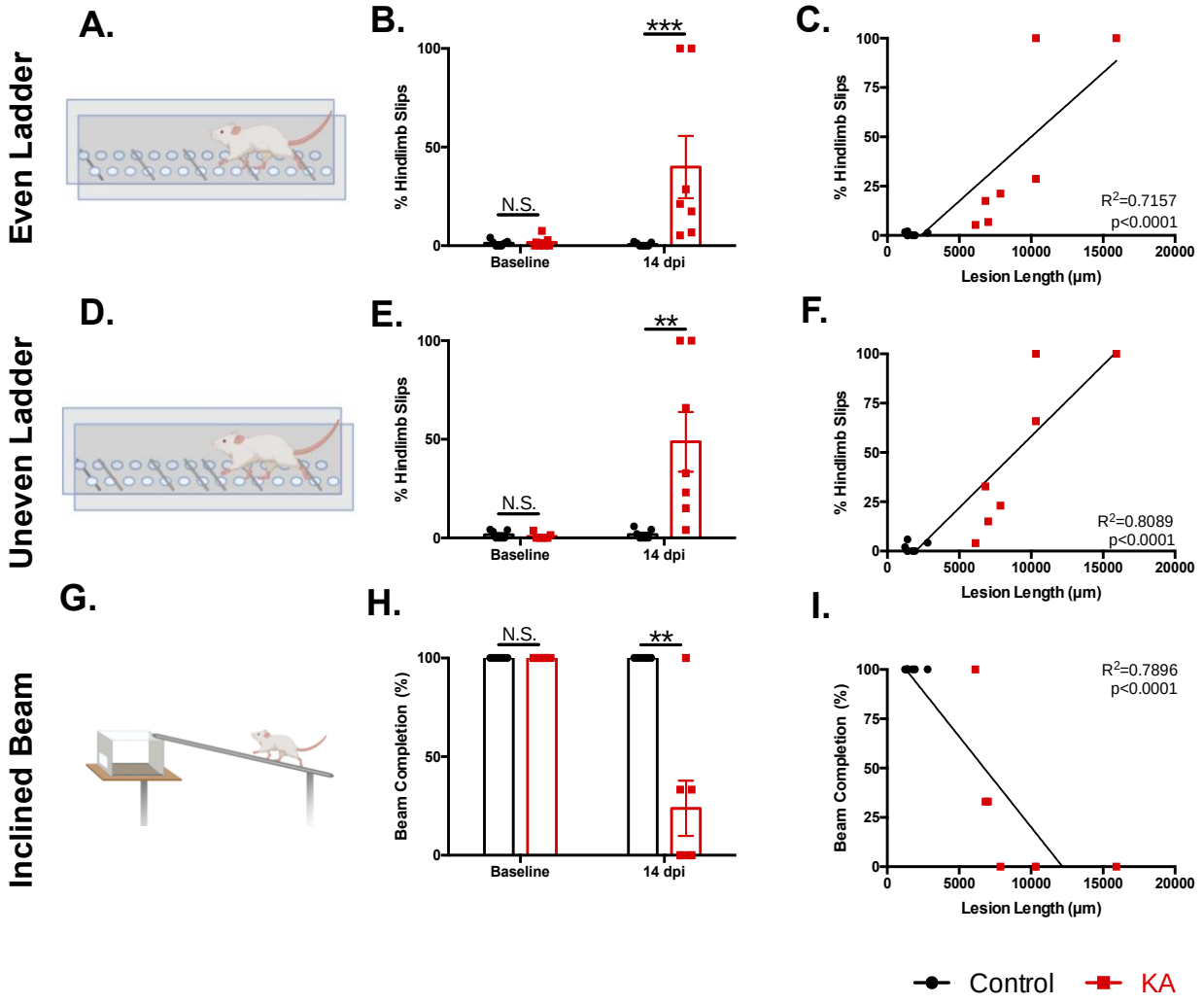

Figure 14. Three sets of KA injections into vertebra T13 elicit significant rhythmic and skilled-walking, coordination and balance deficits, correlating to lesion size. ***A,*** Schematic of the evenly-spaced rungs of the horizontal ladder. ***B*****,** Percent hindlimb slips were compared two weeks post-KA SCI (At baseline p = 0.9184, at 14 dpi p = 0.0006, Mann-Whitney test). ***C*****,** Correlation analysis is significant between hindlimb slips and lesion size in the rostro-caudal axis ($p < 0.0001$, $R^2 = 0.7157$, Linear Regression Analysis). ***D*****,** Schematic of the unevenly spaced rungs of the horizontal ladder. ***E*****,** Percent hindlimb slips were compared two weeks post-KA SCI (at baseline p = 0.4126, at 14 dpi p = 0.0023, Mann-Whitney test). ***F*****,** Correlation analysis is significant between hindlimb slips and lesion size in the rostro-caudal axis ($p < 0.0001$, $R^2 = 0.8089$, Linear Regression Analysis). ***G*****,** Schematic of the inclined beam behavioral test. ***H*****,** Ability to complete the inclined beam task was significantly impaired in KA SCI rats (at 14dpi p = 0.0047, Mann-Whitney test). ***I*****,** Correlation analysis is significant between ability to complete the inclined beam and lesion size in the rostro-caudal axis ($p < 0.0001$, $R^2 = 0.7896$, Linear Regression Analysis). For all data, n = 7 animals per group; N.S. stands for not significant, ** $p \leq 0.01$, *** $p \leq 0.001$. Adapted from (Kuehn et al., Manuscript in preparation).

As mentioned earlier, the CatWalk test further measures gait-specific parameters and also allowed us to further investigate the role of propriospinal INs connecting the cervical and lumbar enlargements (Brustein & Rossignol, 1998; Laliberte et al., 2019; Pocratsky et al., 2017; Pocratsky et al., 2020). In comparison to the controls, KA rats have a significantly lower pLDA score two weeks after SCI (**Fig. 15*B*:** controls = 0.13 ± 0.01, KA = 0.076 ± 0.01, p = 0.0006, unpaired Welch's t-test). Separation into the nine individual parameters indicated significant differences in all except for hindlimb base of support and alternate B (AB) step sequence (**Fig. 15*D***). Additionally, KA-lesioned rats had a significantly higher cruciate A (CA) step sequence in comparison to the controls (**Fig. 15*A,C**:* controls = 10.48 ± 4.50%, KA = 27.41 ± 5.46%, p = 0.0415, unpaired Welch's t-test). A closer analysis of the rhythmic components of gait showed significant differences in forelimb swing time, stand time and duty cycle **(Fig. 16*A,C,E*:** p = 0.022; p = 0.0441; p = 0.0031, unpaired Welch's t-test, respectively). However**,** the hindlimb parameters were not significantly different (**Fig. 16*B,D,F**).*

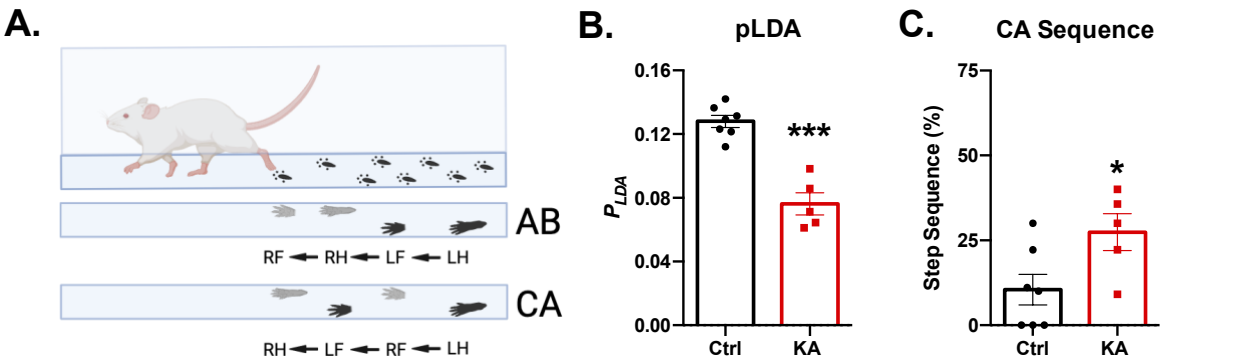

D.

pLDA Parameter	Control ± SEM	KA ± SEM	P-value	
AB Sequence	61.67±8.582	44.07±7.695	P = 0.158	
Body Speed	55.22±3.203	38.77±3.479	P = 0.0067	**
Forelimb Duty Cycle	53.15±2.509	62.87±1.745	P = 0.0101	*
Forelimb Max Contact At	39.56±0.590	51.76±1.762	P = 0.0013	**
Forelimb Stride Length	17.30±0.626	12.48±0.951	P = 0.0035	**
Forelimb Swing Time	0.138 ± 0.00252	0.110 ± 0.00494	P = 0.0022	**
Hindlimb Base of Support	2.550±0.143	2.325±0.543	P = 0.7065	
Hindlimb Stride Length	16.99±0.608	11.32±0.951	P = 0.0014	**
Regularity Index	98.99±0.488	94.53±1.328	P = 0.0248	*

Figure 15. CatWalk gait analysis highlights deficits in SCI-related gait parameters two weeks post-injury. *A*, Schematic of the CatWalk behavioral test with AB (alternate) vs CA (cruciate) step sequences. The AB step sequence requires a shift from hind-to forelimb (or fore-to hindlimb) on the ipsilateral side of the body while the CA step sequence requires a shift from fore-to-forelimb (or hind-to-hindlimb) on the contralateral side. ***B*,** Comparison of the pLDA gait score (parameter linear discriminant analysis) shows significant differences ($p = 0.0006$, Welch's unpaired t-test). ***C*,** Comparison of CA sequence shows significant differences ($p = 0.0415$, Welch's unpaired t-test). ***D*,** Analysis of individual pLDA CatWalk parameters. Significance determined using Welch's unpaired t-test. For all data n = 7 control and n = 5 KA animals; * $p \leq 0.05$, ** $p \leq 0.01$, *** $p \leq 0.001$. Adapted from (Kuehn et al., Manuscript in preparation).

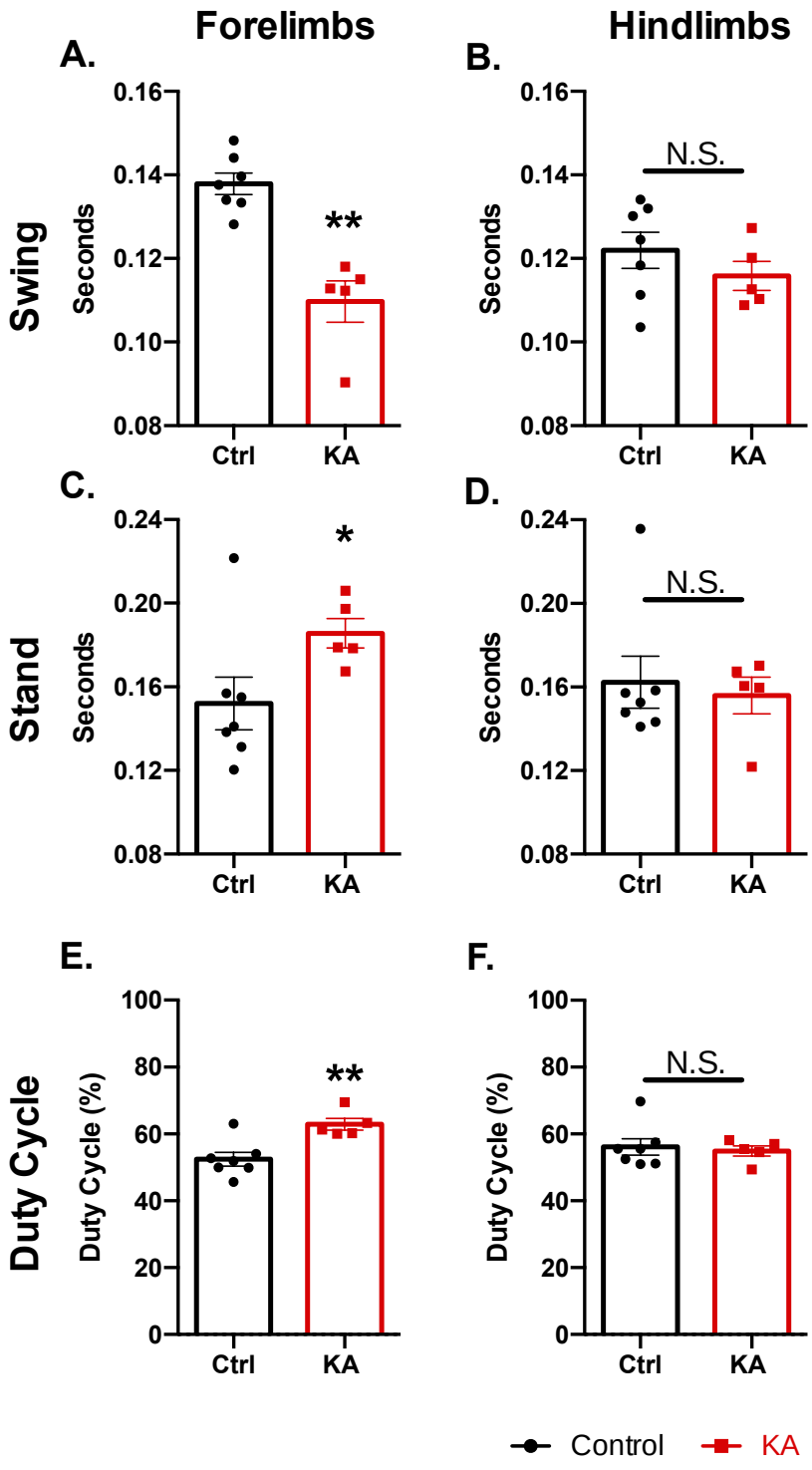

Figure 16. Rhythmic component in gait is significantly affected in KA-injured animals two weeks post-injury. ***A-F*** Average swing time, stand time and duty cycle in the forelimbs were significantly different but not in the hindlimbs (***A***, p = 0.022 ***B,*** p =0.2939 ***C,*** p = 0.0441 ***D,*** p = 0.6858 ***E,*** p = 0.0031 ***F,*** = 0.6807, Welch's unpaired t-test). N = 7 control and n = 5 KA animals. * $p \leq 0.05$, ** $p \leq 0.01$. N.S. stands for not significant. Adapted from (Kuehn et al., Manuscript in preparation).

To further investigate the specificity of this lesion and ensure it did not disrupt the dorsal horn circuitry that may lead to sensory deficits (Vierck et al., 2013; Yezierski et al., 1998), I performed several sensory tests. There were no significant differences in mechanical and thermal sensitivity in animals two weeks post-KA SCI (**Fig. 17*A-C*:** von Frey hair filament 1.4g response rate: control = 35.71 ± 4.81%, KA = 26.00 ± 9.27%; von Frey hair filament 60g response rate: control = 78.57 ± 4.04, KA = 86.00 ± 4.00%; Hargreaves latency of withdrawal: control = 15.88 ± 2.12 sec, KA = 13.72 ± 0.71 sec, n = 7 control and n = 5 KA animals). These results suggest that KA did not damage the dorsal horn as there were no significant sensory differences after two weeks.

Together, this battery of behavioral assessments of rats with a lumbar (L2-L4) intermediate gray matter SCI shows gross hindlimb deficits, impaired rhythmic walking, coordination, balance and gait but no differences in sensory function two weeks post-injury. Lesions rostral to vertebra T13 and/or smaller did not show significant differences after two weeks (pilot experiments mentioned above). Furthermore, KA animals with three bilateral injections in L2-L4 but with a lesion size smaller than 6000µm did not consistently show significant behavioral deficits and were excluded from the analysis. These results indicate that the observed deficits are specific to this lesion.

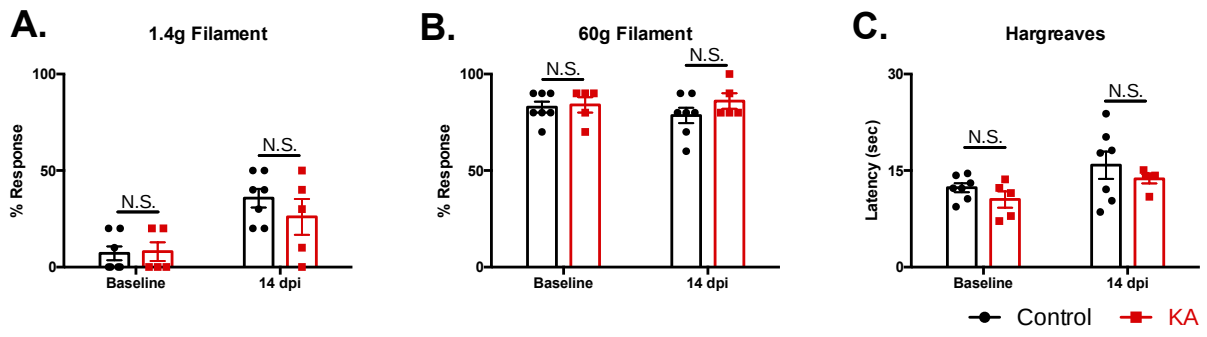

Figure 17. Three sets of bilateral KA injections into vertebra T13 do not elicit changes in mechanical or thermal sensitivity after two weeks. ***A,B*** Hindpaw stimulation with 1.4g innocuous and 60g noxious von Frey hair filaments did not show significant differences at baseline or after two weeks (1.4g at baseline $p > 0.9999$, Mann-Whitney test; 1.4g at 14 dpi $p = 0.3875$; 60g at baseline $p = 0.8222$, 60g 14 dpi at $p = 0.2217$, Welch's unpaired t-test). ***C,*** Hargreaves hindpaw stimulation did not show differences in thermal sensitivity between the two groups (at baseline $p = 0.2496$, at 14 dpi $p = 0.3727$, Welch's unpaired t-test). For all data, n = 7 control and n = 5 KA animals. N.S. stands for not significant. Adapted from (Kuehn et al., Manuscript in preparation).

3.2.5 Neuronal quantification highlights role of spinal level L2-L4 SpINs in coordination and balance

I next wanted to determine whether neuronal loss in a specific spinal level significantly contributes to behavioral deficits. Using the above mentioned NeuN quantification method in Figures 7 and 8, the number of NeuN+ neurons in laminae V-VII in spinal L2-L4 epicenters in KA animals were analyzed and compared them to the average controls. In comparison to the average controls, there is a reduction of NeuN in all three spinal levels for all KA animals except for KA #1 in spinal level L2 (**Fig. 18*A***). The number of NeuN+ neurons in all three spinal levels L2-L4 epicenters significantly but moderately correlates to the inclined beam performance (**Fig. 18*B-D***: L2 $p = 0.0187$ and $r = 0.6325$; L3: $p = 0.0219$ and $r = 0.6371$; L4: $p = 0.0021$ and $r = 0.8029$, Spearman's correlation, respectively). This data indicates that intermediate gray matter IN loss in all three spinal level (L2-L4) epicenters plays a significant role in coordination and balance **(Fig. 19)** and that together they are required for the overall effect.

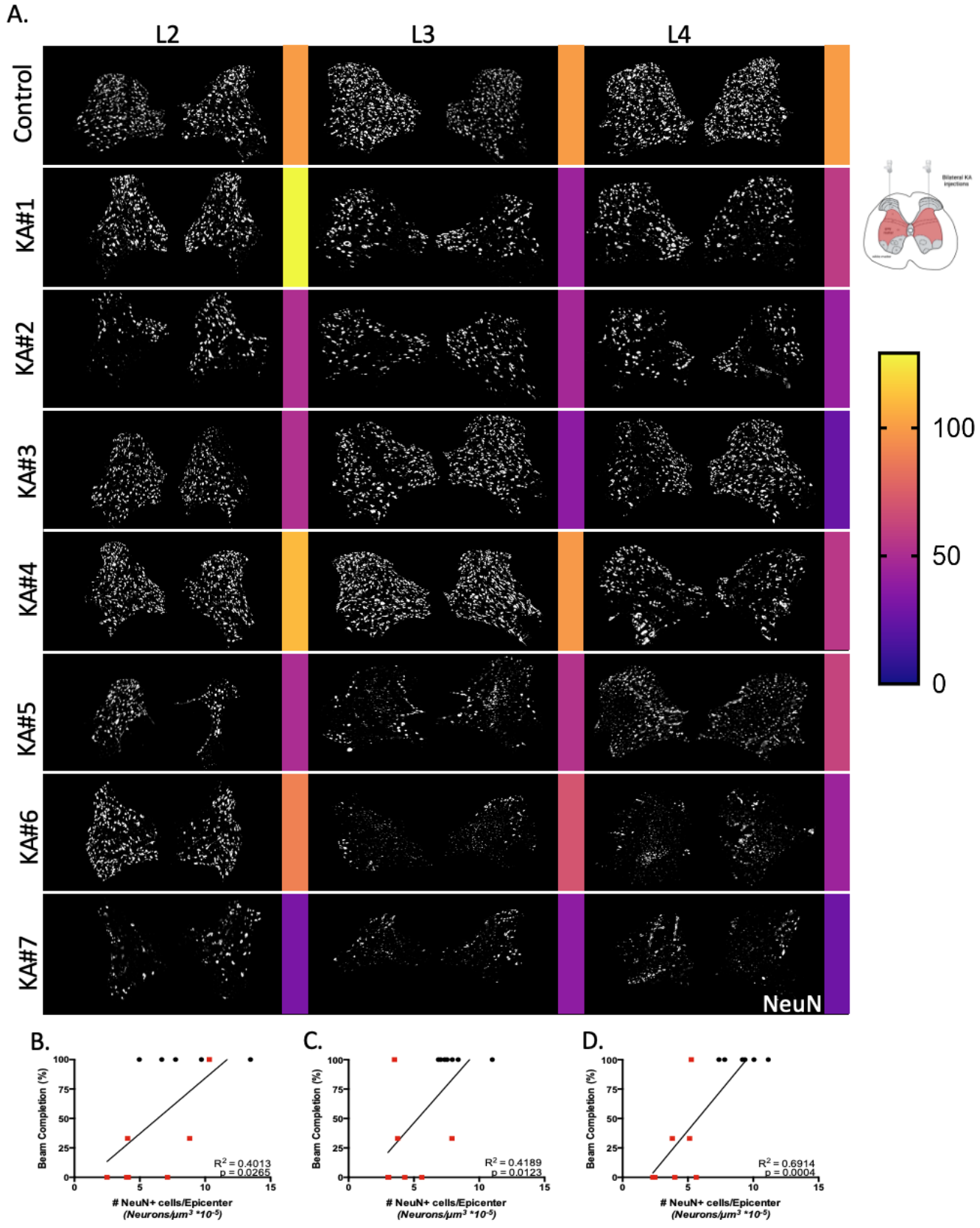

Correlation with inclined beam

Figure 18. Laminae V-VII neuronal loss in spinal level L2-L4 epicenters correlates with deficits in balance and coordination deficits. *A,* Visualization of NeuN of only laminae V-VII in spinal level L2-L4 epicenters using ilastik MIPs. Single images of the KA epicenters in comparison to a control representative epicenter. ***B-D,*** Correlation of laminae V-VII NeuN in spinal level L2-L4 in comparison to inclined beam performance (L2 inclined beam p = 0.0265, R^2 = 0.4013; L3 inclined beam p = 0.0123, R^2 = 0.4189; L4 inclined beam p = 0.0004, R^2 = 0.6914; Linear Regression Analysis, n = 5-7 animals per group). Adapted from (Kuehn et al., Manuscript in preparation).

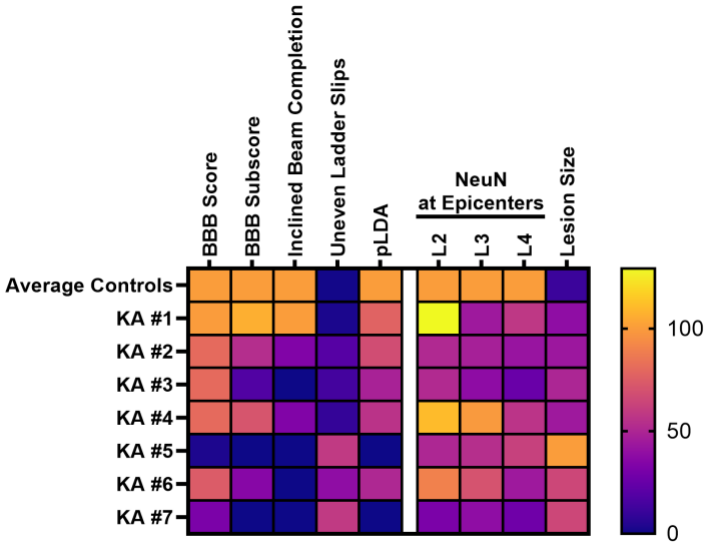

Figure 19. Representative heatmap comparing control and KA NeuN-positive cells in laminae V-VII in spinal level L2-L4 epicenters to behavioral performance. All neuronal values and behavioral performances are normalized to the average of the controls; the lesion size is normalized to the largest lesion extent (KA #5). All values are shown as a percentage (0% in violet, 100% in orange, above 100% in yellow). Adapted from (Kuehn et al., Manuscript in preparation).

3.2.6 Lower motoneurons and white matter area at the L2-L4 lesion epicenters do not significantly contribute to behavioral performance

Having shown that intermediate gray matter SpIN loss correlates with the observed deficits, I wanted to investigate if there was any correlation between motoneuron or white matter loss and behavior. The number of lower motoneurons at the injection epicenters were counted and correlated to the BBB score and inclined beam, and found not to be significant (**Fig. 20*A*,*B*:** BBB r = -0.2327 and p = 0.388, inclined beam r = -0.2338 and p = 0.226, Spearman's correlation).

Although KA targets gray matter primarily, I wanted to ensure there was no secondary damage to the white matter tracts, the area and percent white matter of the spinal cord cross-sectional area by eriochrome cyanine staining were examined. Unlike classical contusion model analysis, there are three sites of damage and therefore examined each individual injection epicenter to confirm there was no white matter damage. There were no significant differences in white matter area at any given epicenter between the two groups (**Fig. 20*E:*** p = 0.3896, Welch's unpaired t-test) nor were significant correlations between percent white matter of the cord and BBB score or inclined beam found (**Fig. 20*C,D:*** BBB r = -0.1333 and p = 0.664; inclined beam r = -0.4221 and p = 0.103, Spearman's correlation). Taken together, these results show that motoneuron and white matter were not significantly altered to contribute to the observed behavioral deficits.

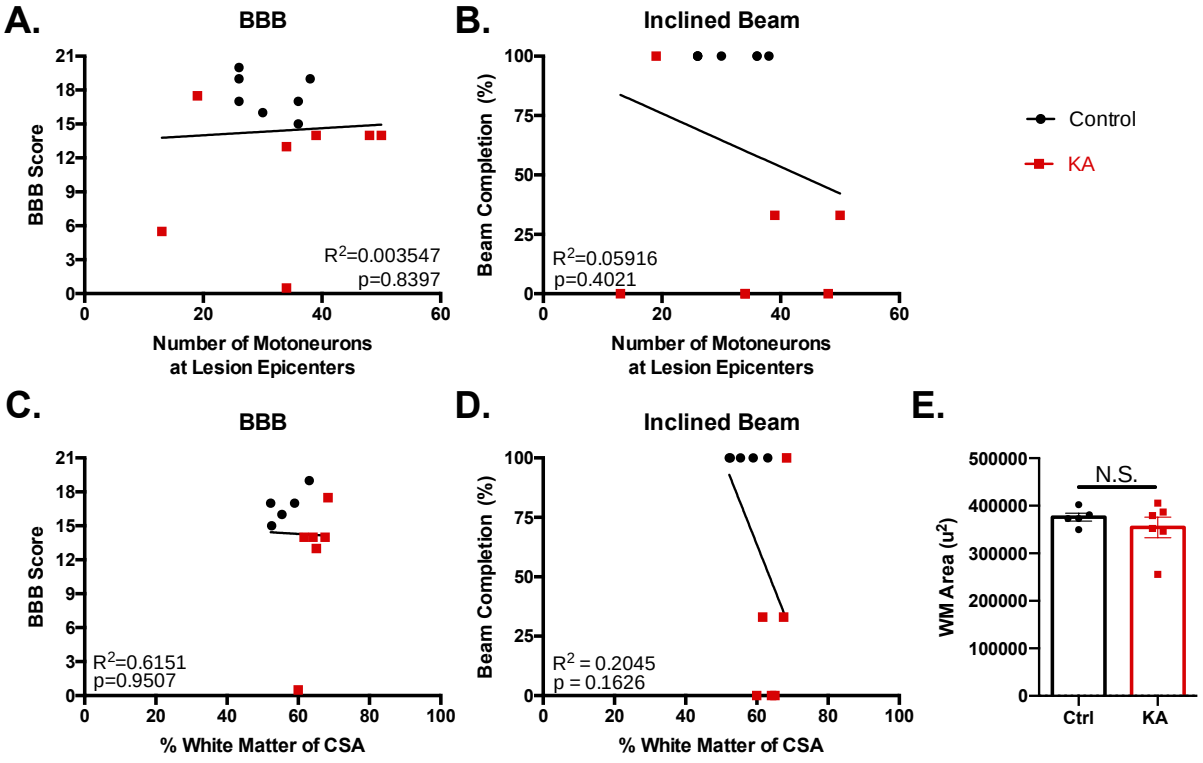

Figure 20. Motoneuron counts and white matter area at spinal L2-L4 lesion epicenters do not significantly affect behavioral deficits. ***A,B*** Motoneuron counts at lesion epicenters does not correlate with BBB score nor inclined beam completion (BBB score p = 0.8397, R^2 = 0.003547; Beam Completion p = 0.4021, R^2 = 0.05916, Linear Regression Analysis, n = 7 animals per group). ***C,D*** White matter sparing does not correlate with behavioral tests (BBB score p = 0.9507, R^2 = 0.6151; beam completion p = 0.1626, R^2 = 0.2045, Linear Regression Analysis, n = 5 control animals, n = 6 KA animals). ***E,*** Average white matter area at the three lesion epicenters is not significantly different between the control and KA groups (p = 0.3869, Welch's unpaired t-test, n = 5 control, n = 6 KA animals). N.S. stands for not significant. Adapted from (Kuehn et al., Manuscript in preparation).

3.2.7 KA lesioned animals do not recover over time

Endogenous plasticity is thought to help regain function after thoracic SCI and should be evaluated over time. KA-lesioned rat behavioral performance three months post-injury reveal that deficits in gross hindlimb function and coordination remain (**Fig. 21**). A closer look at the BBB score and subscore show that KA-injured rats have significant deficits in hindlimb function (**Fig. 21*A,B*:** BBB score controls = 19.83 $\pm$ 0.60, KA = 10 $\pm$ 2.5, p = 0.0062, 2-way ANOVA; BBB subscore controls = 12 $\pm$ 0.58, KA = 2.33 $\pm$ 2.33, p = 0.0096, 2-way ANOVA). Two of the three animals did not regain weight support and were not able to participate in the ladder and beam tasks which doesn't allow for sufficient statistical comparisons (**data not shown**). However, from the BBB score and subscore it appears that the KA group is injured and remains injured. I found that while lesion length did correlate with the gross hindlimb function (**Fig. 21*C,D:*** BBB score r = -0.8971, p = 0.0110, BBB subscore r = -0.8971, p = 0.0111, Spearman's correlation), the motoneuron number at the injection epicenters did not (**Fig. 21*E,F:*** BBB score r = -0.1160, p = 0.7778; BBB subscore r = -0.1160, p = 0.7778, Spearman's correlation). This suggests that the targeting of the intermediate gray matter of the L2-L4 spinal cord leads to permanent locomotor deficits that cannot be overcome by plasticity or natural measures alone.

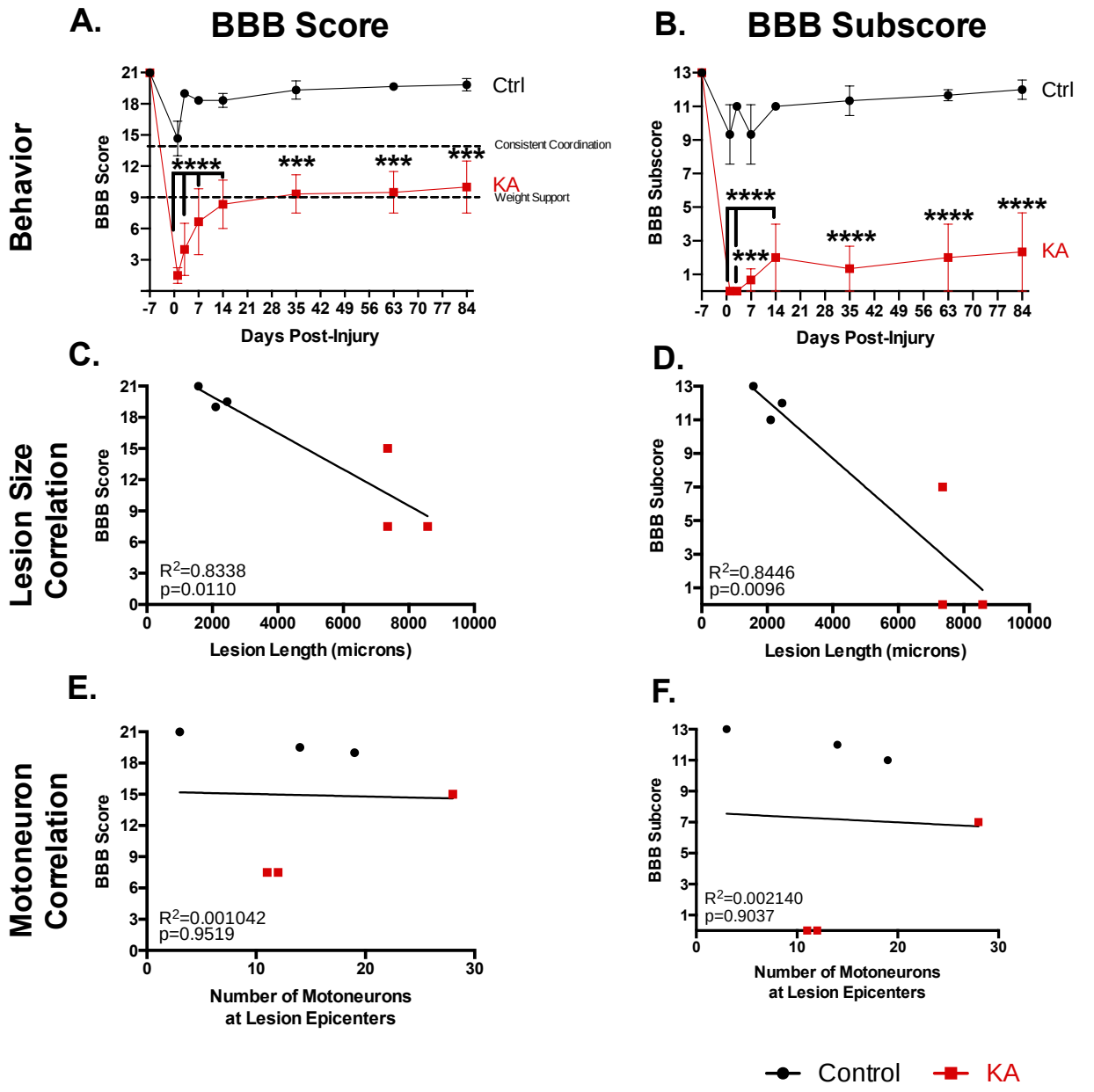

Figure 21. Analyzing the behavioral stability of the lesion after three months shows gross hindlimb and coordination deficits remain. ***A,B*** BBB score and subscore over a three-month period shows that gross hindlimb functional deficits remain (BBB group p = 0.0062; BBB subscore group p = 0.0013, 2-way ANOVA with Sidak's post-hoc test). ***C, D*** BBB score and subscore correlate significantly to lesion size after three months (BBB score p = 0.0110, R^2 = 0.8338; BBB subscore p = 0.0096, R^2 = 0.8446, Linear Regression Analysis). ***E, F*** Remaining motoneurons at lesion epicenters do not correlate to behavioral performance after three months (BBB score p = 0.9516, R^2 = 0.001042, Linear Regression Analysis). For all data, n = 3 animals per group; *** p ≤ 0.001, **** p ≤ 0.0001. Adapted from (Kuehn et al., Manuscript in preparation).

3.3 Section II

3.3.1 Developing an E14 timed-mating breeding scheme

With the now-established KA-model with thoroughly characterized behavioral deficits, I could next investigate E14 cell transplantation to replace lost intermediate gray matter. I tested several timed-mating breeding schemes to ensure that harvested embryos are exactly 14 days old. Harvesting spinal cords from younger embryos would result in grafts with multipotent neural stem cells which are not differentiated enough and harvesting spinal cords from older embryos would result in more glial restricted progenitor cells (Delaunay et al., 2008; Mayer-Proschel et al., 1997). Therefore, to get a highly neuronal cell population, it was important to establish that embryos were exactly 14 days old. An interperitoneal (IP) injection of LHRH (60µg) at 10am followed by pairing for one night, 105 hours afterwards resulted in E14 embryos (**Fig. 22**). I observed that animals with a weight gain of at least 40g were highly likely to be pregnant and could be sacrificed.

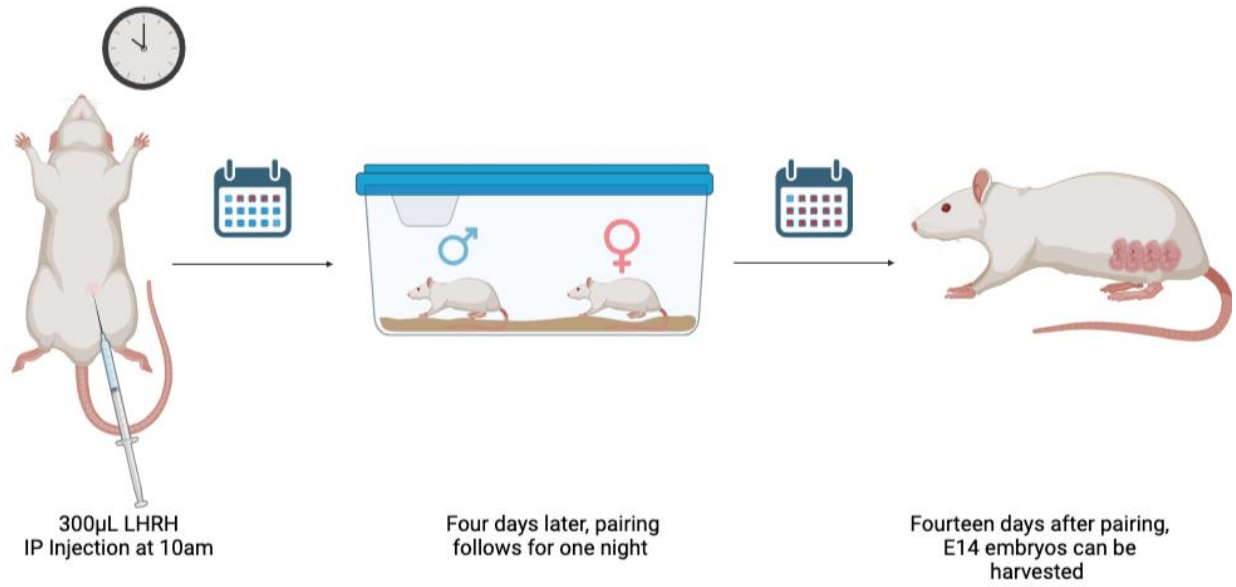

Figure 22. Timeline of LHRH injection and paired timing for E14 embryos. Female Fischer rats are intraperitoneally injected with 300µl (200µg/ml) LHRH diluted in saline at 10am to induce ovulation. Four days (or 105 hours) later, females are placed into the male cage overnight and removed early the next morning. During the following two weeks, female weight gain is monitored at the same time of day every other day. Fourteen days after separation, females with a weight gain of over 40g are sacrificed to harvest E14 embryos.

To confirm E14 embryos were at the same maturity level as previously published, I performed preliminary *in vitro* quantification of maturation and differentiation markers. Cells were cultured for either 1 or 10 days *in vitro* (DIV) and following fixation (**Fig. 23**), stained for neural stem/neural progenitor cells (NSCs/NPCs) Sox 2 and neuronal NeuN markers to evaluate graft maturity. These time points were chosen so that cell maturity could be compared to previously published work (Dulin et al., 2018). I found that cells were around 20% Sox2+ after 1 DIV and decreased to 17% after 10 DIV (**Fig. 24*B***), similar to what had been previously published (Dulin et al., 2018). After 10 DIV, I found that cells were on average 80% NeuN+ (**Fig. 24*B***), however this is likely an underestimation since cells form large, overlapping clusters making it very difficult to quantify single cells. After 10 DIV, cultures were on average 2.8% GFAP+, 0.0% Olig2+ and 0.5% Iba1+, indicating that there very few astrocytes, oligodendrocytes and microglia/macrophages, respectively (data not shown). These results indicate that these E14 embryos are indeed at maturity level typical of E14 and spinal cultures are highly neuronal.

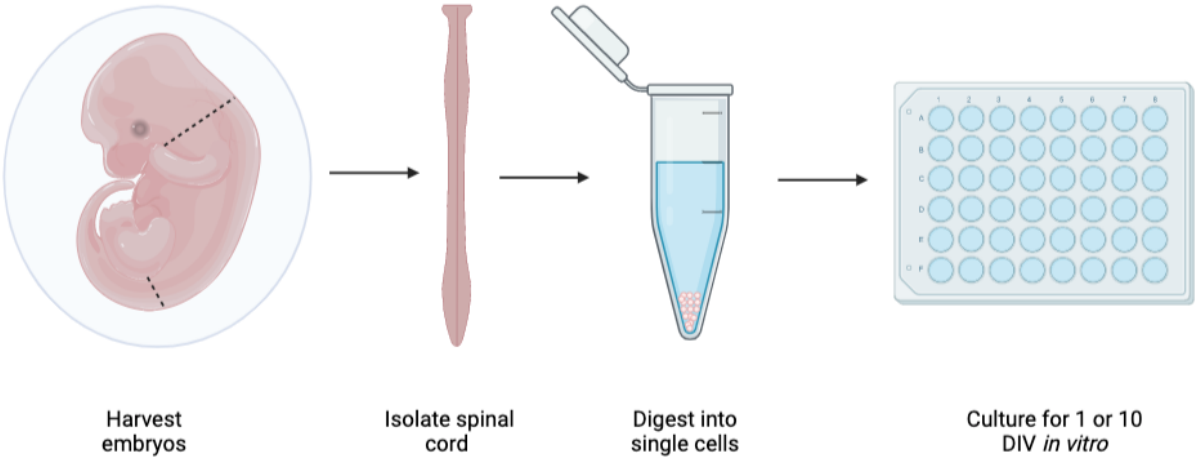

Figure 23. Schematic for E14 fetal cell extraction. Spinal cords are dissected from E14 rat embryos on ice. The dura and any connective tissue are removed to ensure a pure culture. Cells are trypsinized into single cells, plated into a 48 well-plate and cultured for 1 or 10 days *in vitro* or directly transplanted directly into the spinal cord.

A.

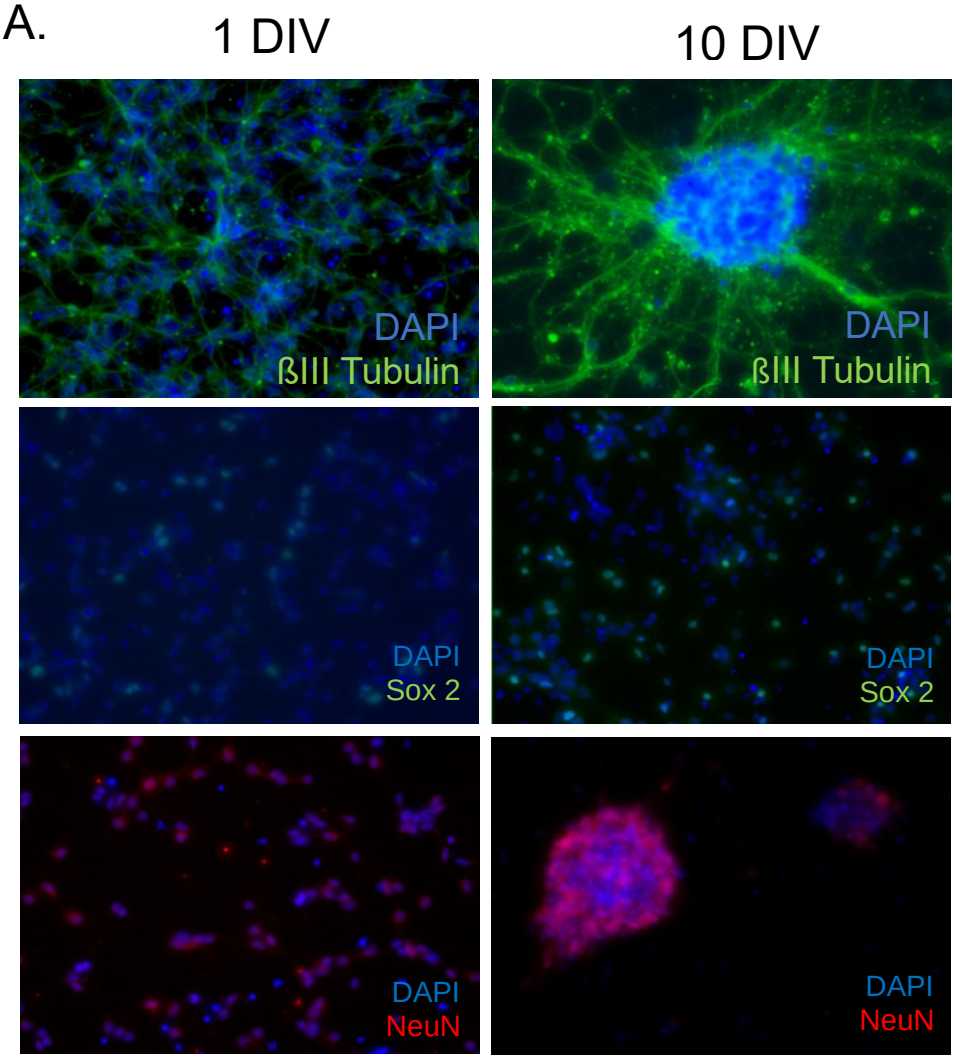
1 DIV
10 DIV
DAPI
ßIII Tubulin
DAPI
ßIII Tubulin
DAPI
Sox 2
DAPI
Sox 2
DAPI
NeuN
DAPI
NeuN

B.

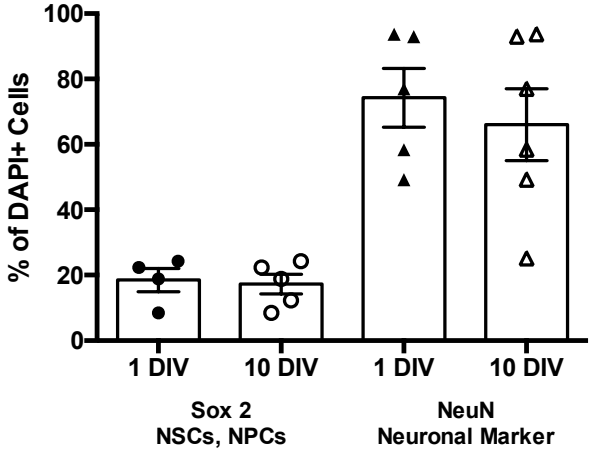
% of DAPI+ Cells
100
80
60
40
20
0
1 DIV
10 DIV
1 DIV
10 DIV
Sox 2
NSCs, NPCs
NeuN
Neuronal Marker

Figure 24. E14 spinal graft maturity after 1 and 10 DIV. ***A****,* Representative images of ßIII-Tubulin (green), Sox2+ (green) and NeuN+ (red) E14 spinal cells after 1 and 10 DIV. ***B,*** While not significant, percentage of NSCs/NPCs Sox 2+ cells slightly decreases from 1 DIV to 10 DIV. Percentage of neuronal NeuN+ cells is not significantly different after 10 DIV, however percent NeuN is likely higher due to the difficulty of quantifying clustered cells.

3.3.2 Grafted E14 spinal cells survive and differentiate into NeuN+ cells in the unlesioned lumbar spinal cord

In one of the early pilot grafting experiments, E14 spinal cells were grafted into the unlesioned spinal cord to test cell survival as well as injection coordinates. 100,000 cells (1µL) were injected 0.8mm deep into caudal vertebral level T12 at spinal level L1 spinal cord. Cells were allowed to survive for 2 and 4 weeks. Following, fixed spinal cord sections were stained with GFP, Sox 2 and NeuN to visualize graft maturity. Histological analysis revealed that E14 spinal grafts survived and there were GFP+/Sox2+ after two weeks as well as GFP+/NeuN+ cells after four weeks indicating grafts did differentiate into neurons **(Fig. 25)**. GFP+ cells were located both in the gray and white matter. As these pilot grafting experiments were performed prior to the KA experiments, cell injection coordinates, including injection depth, still needed to be optimized.

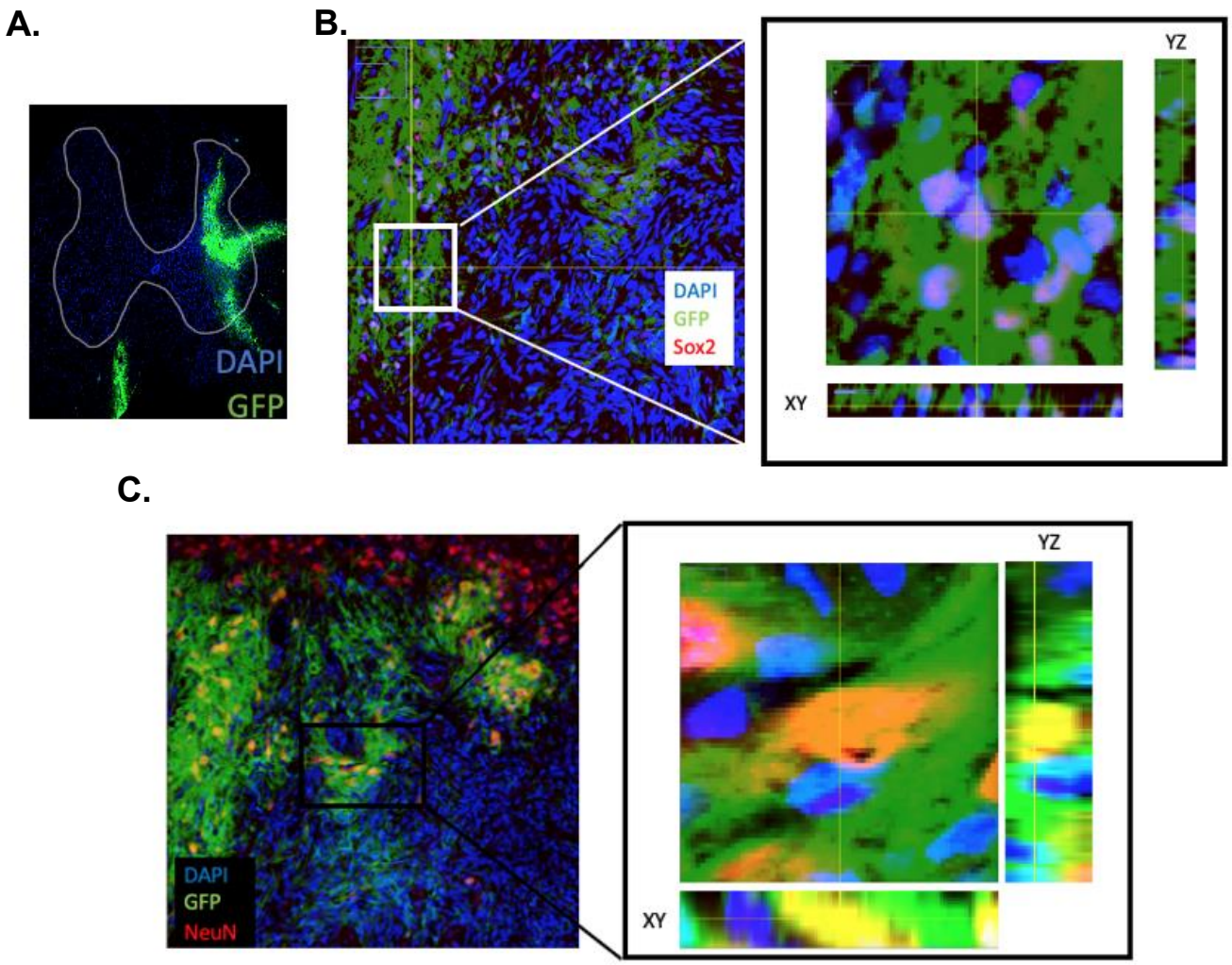

Figure 25. E14 spinal cells differentiate into NeuN+ cells in the unlesioned spinal cord. E14 spinal cells were injected into L1 of the lumbar spinal cord and allowed to survive for 2 and 4 weeks respectively. Immunofluorescence staining indicates that E14 spinal cells survived. ***A,*** Representative image of E14 spinal grafts (green) in the unlesioned spinal cord, the white line outlines the gray matter. ***B,*** Representative image of GFP+ (green), Sox2+ (red) E14 cells indicates grafts are immature, but are positive for NSCs, NPCs 2 weeks after transplantation. ***C,*** Representative GFP+(green), NeuN+ (red) cells indicate grafts have differentiated into neuronal cells 4 weeks after transplantation. DAPI is depicted in blue.

3.3.3 Injecting E14 spinal cells into a KA lesion

In my final *in vivo* experiment, I aimed to further evaluate the cell injection parameters and investigate the survival of E14 spinal cells when transplanted into a KA lesion. Animals were injected with KA using the same parameters as previously determined and tested with a subset of behavioral tests three-weeks post-injury. The main goal of this experiment was to evaluate E14 cell survival following an SCI and whether cells remained at the injection sites or migrated. Two weeks post-KA injection, KA animals were split into two groups by an unblinded individual. Animals in the treatment group received three sets of bilateral injections in spinal L2-L4, with 500,000 cells/injection each, using the same injection parameters as KA. All cells were harvested and isolated on the day of injection. All control animals received saline injections. After three weeks, animals underwent a final round of behavioral testing and were sacrificed to evaluate graft survival (**Fig. 26**).

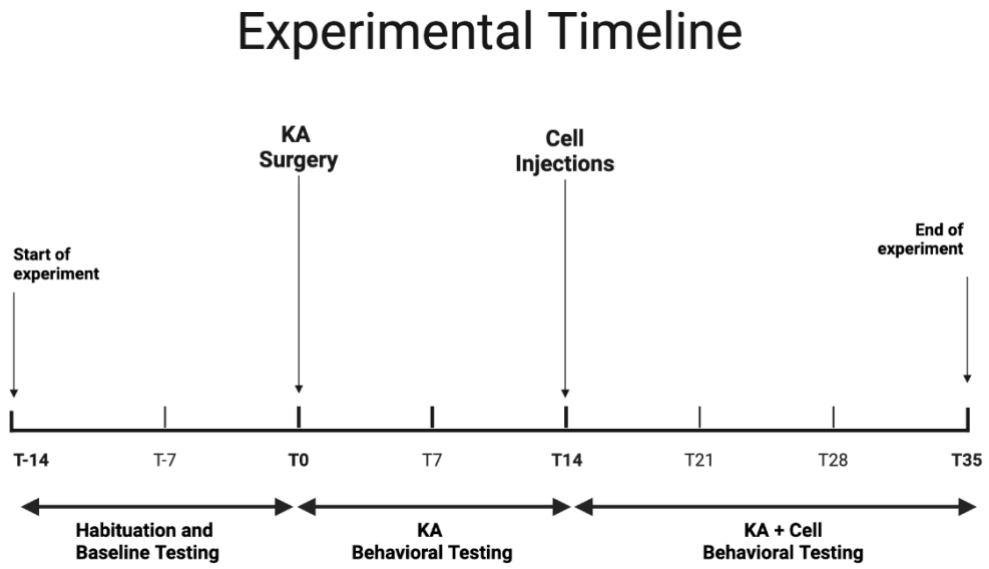

Figure 26. Timeline of fetal cell transplantation into KA lesion. Post-baseline behavioral testing, animals were injected with KA using the previously established injection coordinates. Behavioral testing followed after 7 and 14 days. Then, E14 spinal grafts were injected into the KA lesion 2 weeks after lesioning. Animals underwent final rounds of behavioral testing at 21, 28, 35 days prior to being sacrificed.

3.3.4 E14 spinal cells did not aid behavioral recovery three weeks post-injection into a KA lesion

First, to evaluate behavioral performance post-KA and cell injections, a subset of behavioral tests were selected to measure gross hindlimb function, coordination and balance, as well as sensory function. Three weeks post-cell injection, animals in both groups did not show significant differences in gross hindlimb function (**Fig. 27*A*:** KA = 8.83 ± 2.64, KA + cells = 8.40 ± 2.54, group p = 0.5879, 2-way ANOVA, n = 6 controls, n = 5 treatment animals). Only about half of the animals regained weight support after KA and saline/cell injections and could not participate in several of the behavioral tests. There were also no significant differences found in the BBB subscore, uneven ladder and inclined beam measuring coordination and balance **(Fig. 27*B-D*:** BBB subscore: KA = 3.67 ± 2.38, KA + cells = 3.80 ± 2.33, group p = 0.6886; uneven ladder % hindlimb slips: KA = 51.22 ± 21.84%, KA + cells = 76.67 ± 18.07%, group p = 0.5235; inclined beam completion: control = 50.00 ± 22.36%, KA + cells = 20.00 ± 20.00%, group p = 0.2252, 2-way ANOVAs, n = 6 KA, n = 5 KA + cell animals). Unfortunately, while not significant, there was a difference in inclined beam performance prior to treatment (completion for KA = 55.11 ± 18.59%, vs 20 ± 20% for KA + cells, n = 6 control, n = 5 treatment animals). Due to the high variation, there was no significance between these two groups two weeks post-KA-injection and three weeks post-treatment (**Fig. 27*D*:** group p at 14 days = 0.4634, group p at 35 days = 0.6227, 2-way ANOVA). Furthermore, sensory testing determined that there were no significant differences in light touch or nociception three weeks post-treatment (von Frey hair filament 1.4g response rate: KA = 40.00 ± 20.82%, KA + cells = 45.00 ± 15.00%, p = 0.8579; von Frey hair filament 60g response rate: KA = 76.67 ± 8.82%, KA + cells = 70.00 ± 20.00%, p = 0.7995, unpaired Welch's t-test, n = 3 control and n = 2 KA animals) or thermal sensitivity three weeks post-treatment (withdrawal latency: KA = 16.092 ± 1.203 sec, KA + cells = 16.644 ± 3.756 sec, p = 0.0.9083, unpaired Welch's t-test, n = 3 control and n = 2 KA animals). While this is likely too early a timepoint to observe any sensory shifts, we wanted to check all the same. Together these results indicate that cell injection two weeks post-injury did not improve hindlimb function, likely due to the short cell survival time (3 weeks).

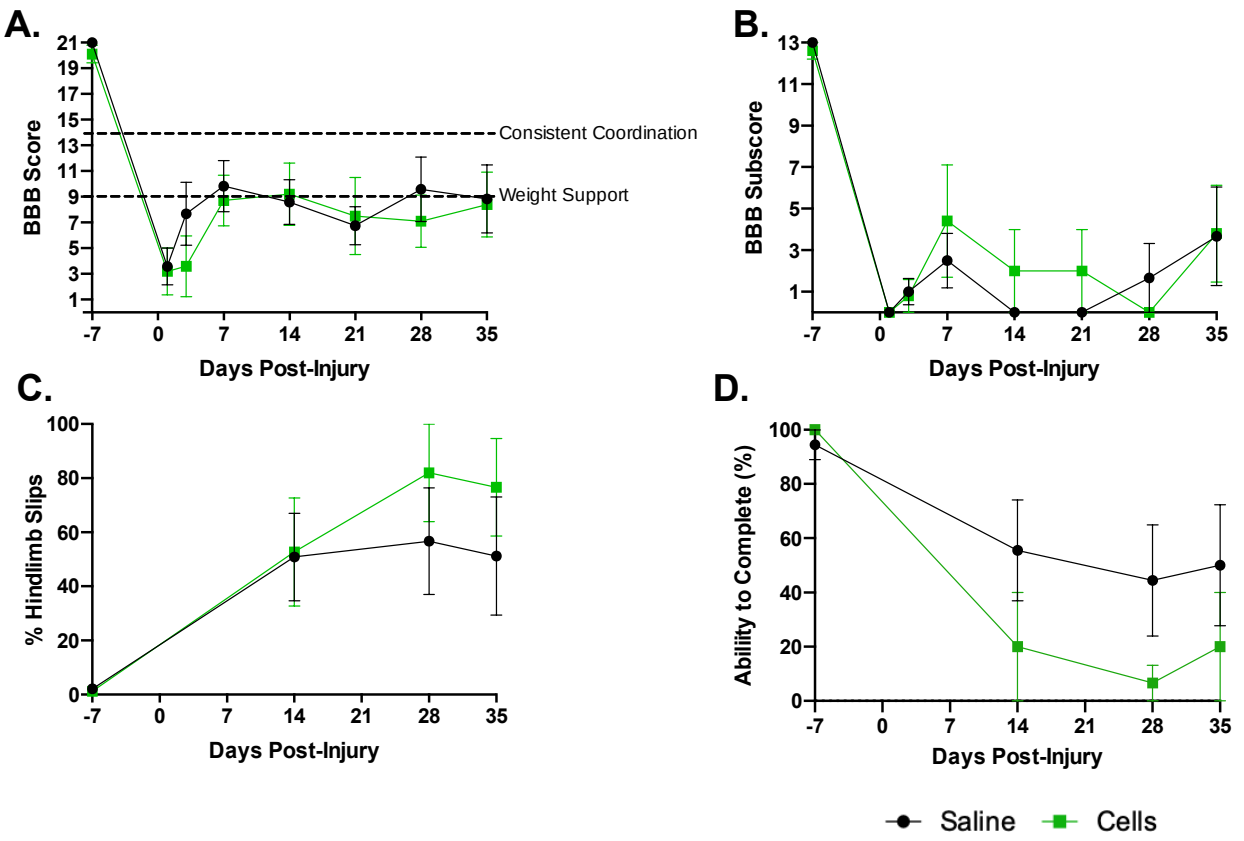

Figure 27. There were no significant differences in gross hindlimb function and coordination three weeks after E14 transplantation into a KA lesion. ***A,B*** There are no significant gross hindlimb and coordination differences after three weeks between the two groups (BBB score group p = 0.5879 BBB subscore group p = 0.6886). ***C,*** There were no significant differences in percent hindlimb slips on the uneven horizontal ladder (group p = 0.5235) ***D,*** The ability to complete the inclined beam was also not significantly different between the two groups (group p = 0.2252). All tests were performed using 2-way ANOVAs with repeated measures and Sidak's test, n = 6 control and n = 5 KA animals.

3.3.5 Histological analysis of transplanted E14 spinal cells into a KA-lesion shows high survival

Histological analysis of transplanted E14 spinal cells into a KA lesion demonstrated high survival rates into a KA-lesion three weeks post-transplantation. GFP+ cells were found in all transplanted animals. Cells spread on average over 1cm (10,500 ± 1,625µm, n = 5, data not shown) in the rostro-caudal axis. GFP+ cells were found in the dorsal and ventral white matter as well as the gray matter (**Fig. 28**). Due to the high density of GFP+ cells, it was not possible to count single cells. Future cell injections will need to adjust for the number of cells as it appeared that cells clustered in less dense areas. Additionally,

future experiments will need to better line up cell and KA injections. However, from these experiments it is clear that cells do not need additional growth factors to survive.

Preliminary stainings to evaluate graft maturity and cell differentiation showed that GFP+ cells did differentiate into NeuN+ cells (**Fig. 29**), however future experiments and histological analysis are required to evaluate the exact identity of E14 spinal cells transplanted into a KA lesion.

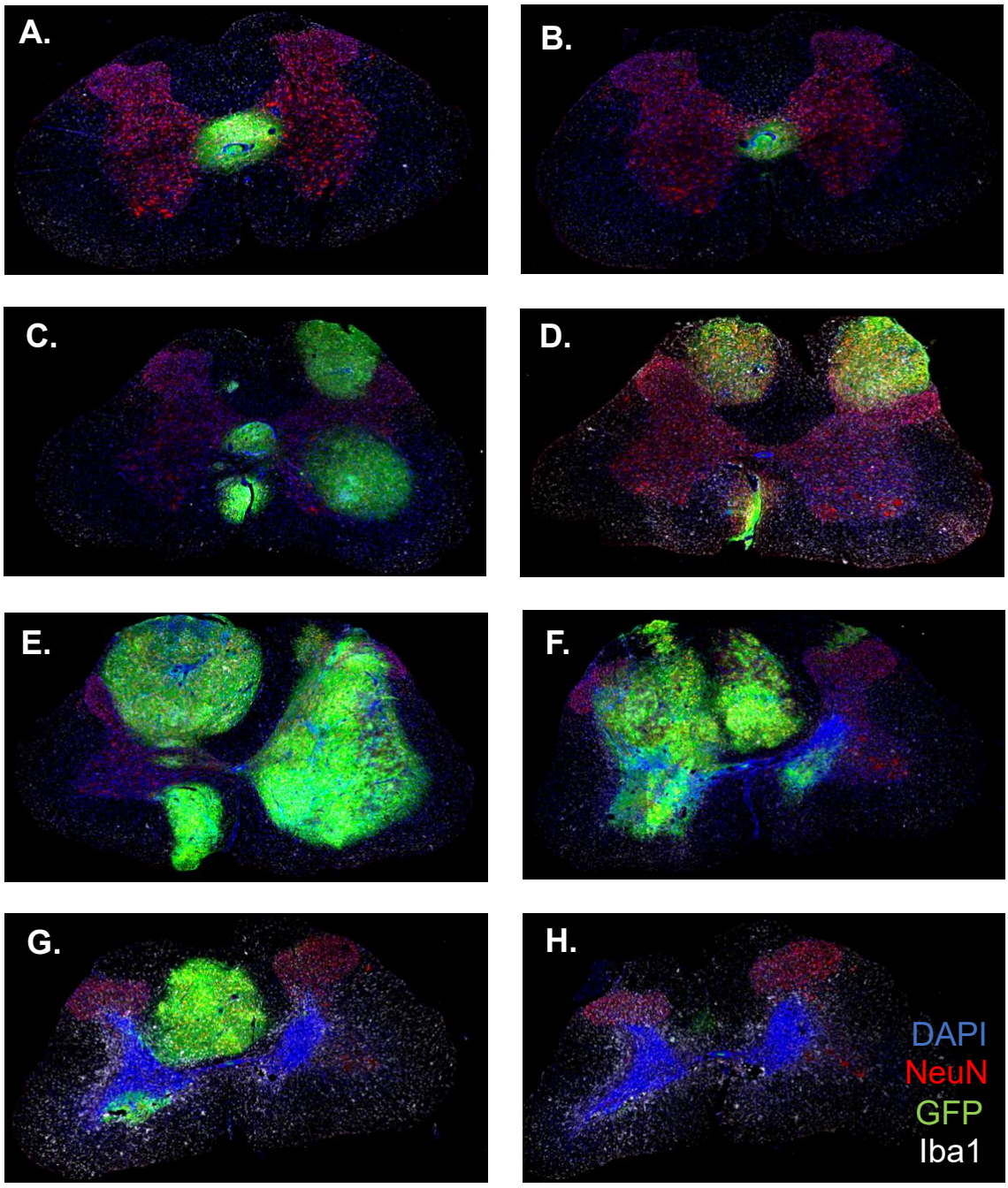

Figure 28. Sample images of graft extent in a representative KA-lesioned animal. Coronal sections stained for neurons (NeuN in red), transplanted cells (GFP in green), microglia and macrophages (Iba1 in magenta). In rostral (A) – to caudal (H) order. Grafted E14 cells spread both in the white and the gray matter in the rostrocaudal axis, partially filling the lesion site. DAPI+ nuclei are labeled in blue.

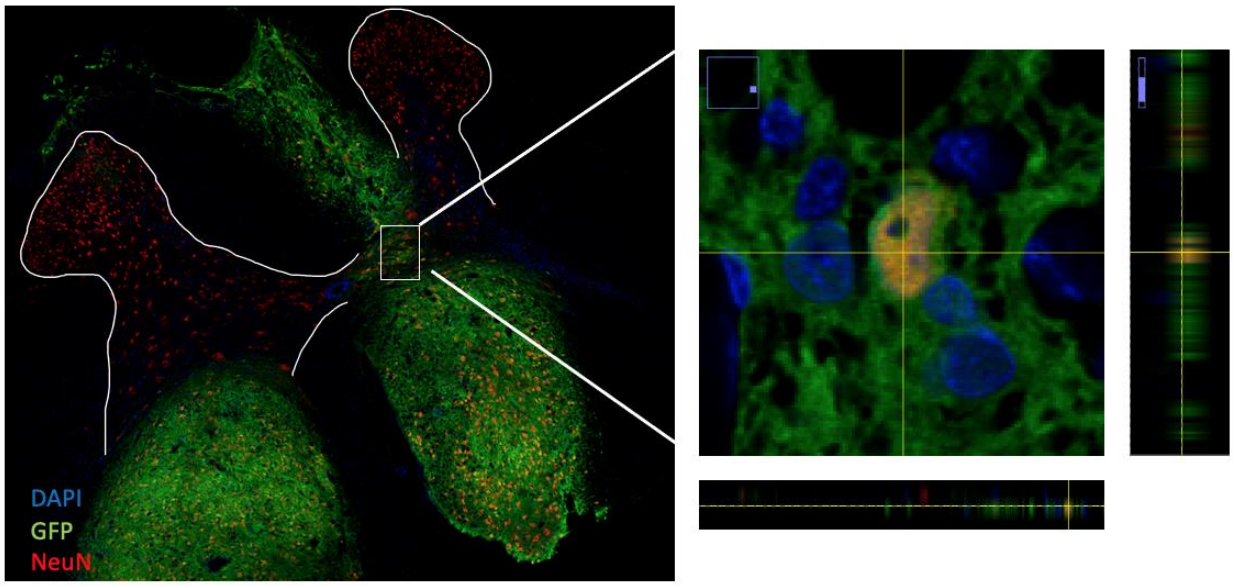

Figure 29. Grafted GFP+ cells differentiate into NeuN+ cells three weeks after transplantation into the KA-lesioned lumbar spinal cord. GFP+ (green), NeuN+ (red) cells were found both in the gray and white matter. DAPI+ nuclei are depicted in blue.

4 Discussion

The present work suggests that a SpIN loss in the lumbar gray matter following SCI significantly impacts coordination and provides an ideal model to evaluate the potential for E14 spinal grafts to restore lost function. By modifying and testing injection coordinates, I was able to use KA to target the intermediate gray matter from spinal L2-L4. Behavioral tests tailored to this specific lesion identified gross hindlimb, coordination, skilled walking, rhythmic walking, balance and gait deficits after two weeks. Deficits remained after three months, highlighting the stability of the lesion. Neuronal loss in both the rostrocaudal and dorsoventral axes significantly correlated with behavioral deficits. Number of motoneurons and white matter area at the lesion epicenters did not correlate with behavioral deficits, suggesting that the observed behavior was truly due to neuronal damage. With this fully characterized model, it is now possible to evaluate if E14 spinal cells can replace lost neurons and restore the above-mentioned deficits. E14 spinal cells have been previously shown to differentiate into gray matter (INs) both *in vitro* and *in vivo* (Dulin et al., 2018; Kumamaru et al., 2019). Initial transplantation experiments indicate E14 spinal cells survive well after three weeks. Future long-term experiments are required to evaluate their differentiation and functional potential. Sections have been adapted from (Kuehn et al., Manuscript in preparation) and were written by myself.

4.1 Tailoring the KA lesion model and behavioral tests to the experimental paradigm

4.1.1 Specificity of the KA lesion model: spinal level

There are many confounding factors that can influence a model's relevance and efficacy. For example, if behavioral tests are applied to a model that are not specific for that model or sensitive enough to distinguish small differences it will not provide sufficient information regarding functional recovery following SCI. Therefore significant time and effort was spent to establish and tailor this model to the animal and lesion paradigm with the appropriate behavioral tests. I aimed to create a spinal lumbar intermediate gray matter lesion in rats with specific behavioral readouts to track recovery. It was first

necessary to determine where to place the KA and cell injections in 10-week-old female, Fischer rats. It has been previously shown that vertebral level and spinal level do not align (ie vertebral level L1 does not necessarily correspond to spinal level L1 and this difference is more pronounced in the lumbar region compared to the cervical region) (Harrison et al., 2013; Hofstoetter et al., 2021; Moonen et al., 2016). KA injections by the Magnuson laboratory were targeted to vertebra T12 and T13 to target spinal L2 in male Sprague Dawley rats and resulted in significant behavioral deficits (Magnuson et al., 2005). As seen in our initial pilot experiments where injections were first focused on vertebra T12, there were no significant behavioral deficits. Following, histological analyses confirmed that the spinal level was indeed too far rostral, as this targeted the lower thoracic spinal cord rather than the upper to mid lumbar spinal cord. This variation could be due to the fact that male Sprague Dawley rats are much larger than 10-week-old female Fischer rats (300-370g vs 180-200g) or possible age or interspecies differences which cause a shift in the vertebrae – spinal cord alignment. Regardless, these findings may explain why no significant behavioral deficits were found in our pilot experiments as KA injections were targeted too far rostral. A previous study supports these results and have shown that gray matter damage to spinal level T8 caused no significant motor deficits (Magnuson et al., 1998; Magnuson et al., 2005). Together, our pilot experiments highlight the importance of establishing and testing models for specific sex, age, strain, and size of animals. These experiments have now shown that the intermediate gray matter in spinal levels L2-L4 under vertebral level T13 is crucial for locomotion in 10-week old female Fischer rats.

4.1.2 Specificity of the KA lesion model: targeting the intermediate gray matter

KA is an excitotoxin that has some dosage-dependent selectivity for INs over motoneurons (Kwak & Nakamura, 1995; Urca & Urca, 1990). Although I aimed to damage our target region, laminae V-VII, I cannot exclude the possibility of additional damage to surrounding laminae, particularly to lamina VIII. I confirmed that motoneurons and white matter remained primarily intact in this model and did not find significant sensory differences between the control and KA groups. As previously mentioned, neuronal damage to the dorsal horn can evoke pain-related behavior in mice (Yezierski et al., 1998)

and animals with pain in their hindlimbs display an altered gait including in duty cycle and stride length parameters (Deshpande et al., 2021; Pitzer et al., 2016). As our control animals have a normal pLDA gait score in comparison to other SCI models (Timotius et al., 2021) and there were no significant differences in mechanical or thermal sensitivity between the two groups after two weeks, I believe that KA did not affect the dorsal horn and impact our gait-related behavioral findings. These findings, therefore, indicate the specificity of our lesion and that damage to the regulatory SpINs which provide input to motoneurons resulted in the observed deficits.

4.1.3 Specificity of the KA lesion model: behavioral tests

Secondly, behavioral tests that could measure functions believed to be affected by the neuronal loss in our model were selected and tested. cFos stainings have shown that neurons in the intermediate laminae of the lumbar spinal cord are involved in locomotion and rotarod performance in both mice and rats (Ahn et al., 2006; Sathyamurthy et al., 2018). Furthermore, the Magnuson laboratory showed that KA injections into L2 of the lumbar spinal cord resulted in severe dorsal and intermediate gray matter damage, significantly affecting gross hindlimb function (Magnuson et al., 1998). Injections with 5mM KA resulted in a BBB score of about 4 after two weeks indicating animals only had slight movement of all three hindlimb joints, while injections with 2.5mM KA resulted in a BBB score of about 13 after two weeks, indicating animals had frequent to consistent front-and-hindlimb coordination and frequent to consistent weight-supported plantar steps (Basso et al., 1995; Magnuson et al., 1998). As our lesion model was centered on the intermediate gray matter in spinal levels L2-L4 of the lumbar cord, I selected tests that could evaluate locomotor function including coordination, balance and gait, beyond just gross hindlimb function.

Of all the behavioral tests used to quantify motor behavior, the BBB score/subscore, horizontal ladders, inclined beams and CatWalk tests were selected. Using the final injection coordinates, KA animals had an average BBB score of 11.2 after two weeks, indicating that they have weight-supported hindlimb steps but not fully coordinated locomotion. To further analyze hindimb function, I used the manual pawprint test which

proved to be unreliable and I could not calculate paw angle. I therefore selected the CatWalk to evaluate SCI gait-specific parameters. CatWalk analysis revealed significant differences in several temporal and static gait parameters. However, as with other SCI models (Leszczyńska et al., 2015), I also could not examine paw angle since KA animals did not leave perfect paw prints which is a requirement for this parameter. I also tested the backwards rotating rod due to its supposed sensitivity in measuring coordination in both the acute and chronic phases of mild and severe injuries (van Gorp et al., 2014). However, again due to high variability and lack of rodent motivation, this test was not further examined. Finally, I set up the inclined beams which proved to be a difficult, complex task measuring balance and coordination. In the final established injection parameters, the 1.9cm beam was challenging and discerning enough to eliminate further use of the 1.3cm beam.

To test for sensory deficits, the von Frey hair filament test was selected to measure mechanical sensitivity and the Hargreaves test was selected to measure thermal sensitivity. The soleus muscles of rat are innervated by the tibial and sural nerves, which enter the spinal cord between L3-L6 in Sprague Dawley rats (Siegel et al., 2007). A second study determined that the rat hindpaw dermatomes lie between L4-L5 also in Sprague Dawley rats (Takahashi et al., 2003). Therefore, the initial pilot experiments which targeted spinal levels rostral to L2, may explain why there were no significant sensory changes as they were too rostral. The established L2-L4 lesion resides in spinal levels associated with the rat hindpaw dermatomes. As mentioned earlier, there were no significant changes in mechanical or thermal sensitivity between the two groups. Signifying no significant sensory differences or damage to the dorsal horns with this model. Together these findings highlight the specificity of the tests selected for this lesion model in our 10-week-old, female Fischer rats, making it ideal to track appropriate function and recovery post-injury and treatment. Additionally, it allows for the evaluation of any abnormal connections or hypersensitivity that develops post-injury or potential treatment.

4.2 Lesioned intermediate SpINs spanning L2-L4 and at least 6mm in length produce significant behavioral deficits

Following analysis, I observed that the KA-animal lesion length in the rostro-caudal axis and laminae V-VII neuronal loss at spinal L2-L4 most influenced behavioral deficits. The average lumbar cord (L1-L6) of the adult *Rattus norvegicus* spans approximately 18mm. Spinal levels L2-L4 measure approximately 10mm, of which each spinal segment spanned slightly over 3mm (Nicolopoulos-Stournaras & Iles, 1983). Importantly, hindlimb muscles are innervated by motoneurons spanning several lumbar spinal levels. The muscles vastus medialis, vastus lateralis, gracillis, tibialis anterior, biceps femoris muscles are innervated by motoneurons from at least two spinal levels in spinal L2-L4 (Mohan et al., 2015; Wenger et al., 2016). It was determined that KA-lesioned animals needed to have a minimum intermediate gray matter lesion size of at least 6mm in the rostro-caudal length to produce consistent behavioral deficits using our behavioral tests. In lesions shorter than 6mm, SpINs and premotor circuitry in other spinal segments may be able to compensate for the neuronal loss, resulting in very minor or no behavioral deficits (these animals were excluded from the analysis). Beyond 6mm, we observed significant correlations between lesion size and locomotor function after two weeks. These findings suggest that the lesion size must span at least two spinal levels. This lesion is slightly larger than what has been previously published by the Magnuson lab (3.4mm or 5.5mm), however, this was a larger gray matter lesion which used 1.5µl of 5mM or 2.5mM KA per injection and also severely damaged the dorsal horns (Magnuson et al., 1998).

While lesion length in the rostro-caudal axis plays an important role, it does not appear to be the only determining criteria. For example, some animals have the same lesion length, but varying behavioral deficits. This may be due to the severity of the injury at given levels. I collaborated with Dr. Andreas Schwarz who developed two Random Forest classification models to classify animals as control or KA animals based solely on their behavioral performance after two weeks. This model classified all animals correctly, except for KA#1. This animal had a lesion size longer than 6mm (6125µm) with neuronal loss primarily in L3 and L4. All other animals with greater lesion lengths and neuronal loss were properly classified. The Random Forest classification and neuronal quantification

highlight that SpINs at L2 are integral to but not solely responsible for the observed behavioral loss. Additionally, many long-distance ascending propriospinal neurons reside in spinal level L2 (Brockett et al., 2013; English et al., 1985; Reed et al., 2006), which may also partially explain KA#1's high CatWalk performance. These findings support what has been previously published regarding circuitry critical to locomotion residing at this level in both the previously mentioned murine KA models and human SCI patients (Dimitrijevic et al., 1998; Hadi et al., 2000; Magnuson et al., 1999) and expands on them to show that just the intermediate gray matter alone from at least two spinal levels is sufficient for this deficit to be present.

4.3 CatWalk gait analysis reveals deficits in rhythm and pattern generation as well as propriospinal damage

The CatWalk measures dynamic and static gait parameters. Initial focus was placed on the pLDA score which draws on the nine parameters that best characterize thoracic contusion and hemisection SCI models. While both SCI models reside in the thoracic region, they target descending tracts at varying degrees. Such differences are lost in the BBB gross hindlimb score but are picked up in the pLDA score (Timotius et al., 2021). Work with collaborator Dr. Andreas Schwarz to rank which behavioral tests and parameters were most discriminant using a Gini Index confirmed that the CatWalk pLDA and subsequent parameters are highly predicative and that damage to gray matter in this particular region significantly alters gait.

Additionally, since circuitry crucial for locomotion resides in the upper lumbar cord, it was also expected to see significant differences in gait rhythm and pattern parameters. KA-injured animals have a longer stand time and shorter swing time, signifying rhythmic deficits. As in the thoracic and hemisection models, these differences were primarily seen in the forelimbs. Analysis of other individual CatWalk parameters revealed significant gait differences in both the fore-and-hindlimbs despite the KA injury residing only in the lumbar cord; particularly discriminant were forelimb parameters stride length, swing time and duty cycle. While these changes could be a compensatory mechanism, this may also be due to the uncoupling of the fore-and-hindlimbs. Both the cervical and lumbar cord contain rhythmic cellular components. Long descending and ascending propriospinal INs connect

these two segments. Their somas are located in laminae VII-VIII and they synapse either directly onto motoneurons or SpINs that then synapse onto motoneurons on the respective segments (including in spinal levels C6-C8 and L1-L3 (Pocratsky et al., 2020)). After SCI, this connection can be severed, and these centers are uncoupled. In this KA model, there was targeted neuronal loss in lamina VII and we cannot exclude possible damage in lamina VIII, where many ascending propriospinal somas reside (Frigon, 2017). KA damage to propriospinal INs connecting the cervical and lumbar enlargements may uncouple these two segments and result in forelimb changes.

There were also significant differences in pattern generation. The regularity index (RI) measures correctly sequenced footsteps and is used to analyze coordination recovery in mild to moderate injuries (Koopmans et al., 2005; Kuerzi et al., 2010; Shepard et al., 2021). As expected, KA-animals have a significantly lower RI, which indicates they have a lower paw-stepping quality and are less coordinated. It has been recently shown that silencing long ascending propriospinal INs in the uninjured cord partially decoupled the fore and hindlimbs (Pocratsky et al., 2020). However, after a thoracic contusion SCI, silencing long ascending propriospinal actually restored left and right spatiotemporal features, as well as the regularity index, improving coordination. This would lead one to assume that these SpINs hinder gait, however, it may be more likely that maladaptive plasticity following injury disrupted gait and silencing them prevented aberrant function (Shepard et al., 2021).

Additionally, KA-lesioned animals had significantly higher CA step sequences, as opposed to the more commonly seen AB sequence. Previous papers have reported speed can influence step sequence in mice and that a faster gait corresponds to AB sequence (Pitzer et al, 2021). As our KA-lesioned rats have significantly slower body speed, this change in gait pattern is not surprising.

Together, these results may suggest that KA-lesioned rats have local rhythmic/pattern and possibly long-distance propriospinal IN damage in the KA-lesioned animals that cannot be compensated for given the lack of recovery in the three-month study, making it an ideal model for cellular replacement therapy.

4.4 Damage to the lumbar spinal enlargement likely requires interventions other than endogenous plasticity

The aim of these experiments was to determine how essential the intermediate gray matter of the lumbar cord is for locomotion and if redundant pathways or other neurons can compensate for SpIN loss. Previous studies have shown that following SCI, propriospinal INs have the capacity to sprout and form new synaptic connections, with the potential to contribute to functional recovery in rodents (Stelzner, 2008; Zholudeva et al., 2018). The behavioral results of the study performed here may suggest that when propriospinal INs are lost there are no other intrinsic mechanisms that can recover lost motor function. Hindlimb deficits level off after two weeks and remain stable even after three months. In agreement, the two animals that did not have weight support after two weeks did not regain weight support after three months. Furthermore, behavioral deficits did not correlate with motoneuron loss or white matter white matter area at the lesion epicenters. Therefore, the results of this study indicate further neurorestorative therapies must be applied to SCI in spinal enlargements to restore function.

4.5 E14 spinal cells show potential to differentiate into gray matter interneurons

Prior to this experiment, cells have been transplanted into a lumbar KA SCI before. Cells from a neuronal progenitor cell line, RN33B derived from the rat embryonic raphe nuclei that had been retrovirally transduced with lac-Z, were transplanted into a spinal L3-L6 KA injury. Two weeks after transplantation, ß-gal morphological analysis revealed that while some cells differentiated into bipolar neurons, there was limited overall differentiation (Onifer et al., 1997). In an additional study, cells derived from E14 cerebral cortex were first cultured with fibroblast growth factor 2 (FGF2) and then transplanted 40 minutes or 4 weeks post-KA injury at L2. They found that between the two transplantation timepoints, there was no significant difference in cell survival. However, while they differentiated into neurons and glial cells *in vitro*, they also remained largely undifferentiated *in vivo* as immunohistological analysis revealed that most grafted cells were Nestin+ (Magnuson et al., 2001). While these results may suggest that a KA lesion

does not provide an environment conducive to appropriate cell differentiation, it is more likely given the data presented in this thesis that these cell types are not of appropriate origin to differentiate properly in the injured spinal cord. Supporting this, more recent studies using E14 spinal cells have shown that even when transplanted into the lesioned white matter in the cervical spinal cord, grafted neurons differentiate into gray matter SpINs and form gray matter laminae structured clusters (Dulin et al., 2018; Kadoya et al., 2016; Kumamaru et al., 2019).

4.6 E14 spinal cell transplantation must be repeated to evaluate functional potential

The aims of this initial E14 spinal cell transplantation experiment were to evaluate 1) grafted cell survival in the KA-damaged lumbar gray matter, 2) cell injection number and coordinates, as well as 3) if E14 spinal cells filled the gray matter lesion site. As these factors had to be tested prior to any differentiation and integration analysis, a short-term survival time point (3 weeks) post-grafting was chosen. I did not expect any significant changes in animal behavioral performance, however included behavioral tests to ensure that KA-animals were properly lesioned prior to grafting as well as to monitor recovery following a second surgery.

In this experiment, E14 spinal cells were grafted two weeks post-KA lesioning, a clinically relevant time point. This time point is after the peak inflammatory response (Rowland et al., 2008) which would aid cell survival and reduce additional growth/survival factors that may influence cell differentiation. After three weeks, the behavioral results did not reveal significant differences in gross hindlimb function, coordination or mechanical sensitivity. Again, this is not surprising, as it will likely take longer for cells to fully integrate themselves into host circuitry. It has been previously shown that transplanted E14 spinal cells into a C4 upper quadrant lesion in rats significantly improved forelimb function (the number of pellets eaten and the staircase reach level) starting five weeks after transplantation (Kadoya et al., 2016). E14 spinal cells transplanted into Fischer rats after a spinal C6 contusion injury started to significantly aid forelimb function 6 weeks after transplantation (Brock et al., 2018). Furthermore, Fischer rats with a T3 complete SCI

received E14 spinal grafts after two weeks. Five weeks post-transplantation, there was a significant increase in BBB score in transplanted animals, raising the average BBB score to 7, as opposed 1 for the controls, which indicates that animals have extensive movement in all three hindlimb joints as opposed to only slight movement in one or two joints (Basso et al., 1995; Lu et al., 2012). Given these previous studies which focused on bridging long-distance white matter relays, I predict that additional time is required to assess the functional potential of E14 grafts replacing lost neurons in a lumbar gray matter lesion.

The behavioral results of this experiment did not show significant differences between the two groups after cell transplantation. What did surprise us however, is that two weeks post-KA injection, the average BBB score for these animals was around 9. This is more similar to animals in the previous long-term experiment than that of the previous short-term experiment, which had an average BBB score of 11 two weeks post-KA injection While a two point difference may appear minor, a score of 9 signifies fully weight supported steps and is a requirement to perform all behavioral tests except for BBB. The surgery notes do not mention any obvious differences, and it does not appear to be due to when the stock was made and used, nor is it only due to lesion extent (as animals in the previous short-term experiment had the longest lesions). More in depth analysis into laminae damage is currently underway and may give a better understanding of where this variation is coming from. However, if this continues, I believe that KA concentration or volume may need to be changed. Otherwise it is more difficult to track functional recovery and efficacy of a treatment.

Furthermore, this experiment highlighted the need to consider beam performance as a crucial criterion prior to splitting up groups into treatment and control groups. Prior to the cell transplantation experiment, the von Frey hair filament performance was used to split animals into control and KA groups. This was partially due to increased performance variability in this test as well as time constraints. Other than the BBB test which was usually unaffected prior to injury, all additional motor tests require more time intensive analysis. For the cell transplantation experiment, the BBB score and von Frey hair filament performance were used prior to creating test groups. Unfortunately, while not significant, this resulted in group variation in the 14 day inclined beam performance

prior to treatment, making it difficult to evaluate treatment potential. As this test is highly sensitive in measuring function after our KA lesion, future cell transplantation experiments must consider beam performance as an essential criterion to split animals into control and treatment groups. Additionally, the Random Forest models developed by my collaborator Dr. Andreas Schwarz to classify animals prior to treatment will help evenly split animals into the control and treatment groups, ensuring that all animals are uniformly injured prior to treatment and that both groups have equivalent baseline performances.

4.7 E14 spinal cells survive well in a KA lesion without additional growth factors

Previously published E14 spinal transplantation experiments have evaluated E14 spinal cell potential to rebuild white matter relays. Here, we aim to investigate whether E14 spinal cells can survive and replace the lesioned gray matter. Analysis of the histological results of the cell transplantation experiment revealed that E14 spinal cells survive well following a gray matter injury. In fact, there were so many GFP+ cells, it was not possible to count single cells. Cells spread throughout the thoracolumbar cord, indicating that growth factors to aid cell survival are unnecessary for future transplantation experiments unlike in previous SCI models where E14 cells were grafted with additional growth factor cocktails (Lu et al., 2014; Robinson & Lu, 2017). While many cells were present in the gray matter, the majority were found in the white matter both in the dorsal and ventral hemispheres. This could be due to the high number of cells injected exceeding the space available for new cells to settle, proliferate and grow or that they prefer to settle in less dense areas. Another model has used white matter C4 dorsal column lesion transplanted with 1.2 x 10^6 E14 cells (Dulin et al., 2018). While in another study, 2 x 10^6 E14 cells were transplanted into a T10 full spinal transection in rats (Kadoya et al., 2016). In this newly developed KA model, despite the lesion length in the rostro-caudal axis, this lesion is more discrete than other more severe SCI models, suggesting that the number of transplanted cells (3 x 10^6, with 500,000 cells/injection) would need to be decreased. Regardless, it may be possible that grafted cells prefer white matter over gray matter. Previous studies have shown that a significantly greater numbers of axons from transplanted E14 spinal cells in a C5 hemisection were found in contact with host myelin

than would be expected by random extensions. These results were supported by further *in vitro* experiments where E14 spinal cells showed preferential and the greatest neurite outgrowth on myelin in comparison to PDL, contrary to previous work shown with adult dorsal root ganglia neurons (Poplawski et al., 2018). If this is the case, it is possible that E14 spinal cells prefer a myelin-based matrix, suggesting that perhaps either fibrinogen or thrombin should be used to retain cells in the gray matter. Furthermore, as there was no way to determine where exactly the KA injection was located both in the rostro-caudal and dorsal-ventral axes, the cell injection epicenter was not fully aligned with the KA-injection epicenter. To do so is technically very difficult, as there are no additional markers to visualize where exactly the KA-injections occurred. While the same coordinates for injections are used, any slight movement including the animal breathing leads to variability. It would be helpful to find a dye or marker to identify where KA was previously injected. I had considered a suture knot in the surrounding tissue around the spinal cord however this placement can change as the wound heals. This remains to be further explored in future experiments. Together, while specific injection parameters such as cell number, depth, and location in the rostro-caudal axis need to be further evaluated, it is evident from this study that E14 spinal cells survive well in a KA-lesioned cord and do not require additional growth factors to survive.

4.8 Grafts show potential for appropriate differentiation

These initial experiments have also shown that E14 spinal cells have the potential to differentiate into NeuN+ cells both in the white and gray matter in the uninjured cord as well as following a gray matter lesion and without the need of additional growth factors. This further supports and confirms the decision to use E14 spinal cells as the graft source, as well as the appropriate embryo age from which the cells were harvested. Future long-term experiments are required to evaluate if cells in the gray matter also differentiate into gray matter SpINs. Graft differentiation does not appear to be affected by donor sex (Pitonak et al., 2022). Previous studies have shown that E14 spinal cells survive and differentiate into gray matter sensory and motor SpINs that segregate into sensory and motor domains when transplanted into white matter lesions (Kumamaru et al., 2019).

Furthermore, the sensory SpINs form clusters representative of dorsal horn architecture (Dulin et al., 2018). It has been shown that E14 spinal cells differentiate into excitatory V2a neurons after being transplanted into a bilateral C4 dorsal SCI in rats (Kumamaru et al., 2019). It remains to be seen whether grafted E14 spinal cells also differentiate into V2a-derived $SC^{Vsx2:Hoxa10}$ INs, which have been shown to be crucial to locomotion after SCI (Kathe et al., 2022) and whether they aid functional recovery after a lumbar KA lesion. Grafts have been shown to receive appropriate nociceptive (calcitonin gene related peptide, CGRP+) fiber or descending motor (corticospinal tract, CST+) input and have shown extensive outgrowth into the host (Dulin et al., 2018; Kumamaru et al., 2019; Lu et al., 2012). Future experiments must evaluate E14 differentiation and connectivity following transplantation into a gray matter lesion in the lumbar cord. For example, H-reflex recordings would investigate whether grafted cells make connections with other INs and motoneurons and if so, indicate functional connections were made. Histological synaptophysin and post-synaptic density 95kDa (PSD-95) staining could investigate whether grafted neurons make glutamatergic synaptic connections with the host. Biotinylated dextran amine (BDA) injections into the ventrolateral white matter at T9 would reveal if long descending and ascending propriospinal INs make connections with grafts or vice-versa (Reed et al., 2009). CTB injections into the L2-L4 DRG would reveal if afferent fibers innervate grafts in spinal level L4. Bartha strain pseudorabies virus (PRV) injection into the sciatic nerve could reveal which grafted INs make direct connections with motoneurons (Jia et al., 2019; Kim et al., 2000). It will take a longer than two weeks to evaluate the potential for E14 spinal cells to replace lost cells and their connectivity within the host. Most importantly, their potential to aid functional recovery still needs to be determined in a long-term experiment.

4.9 Future Outlook

According to the European Multicenter Study about Spinal Cord Injury, the majority of spinal cord injuries occur at the cervical or thoracolumbar enlargements (EMSCI, 2022). These regions of the spinal cord contain highly diverse populations of local SpINs and propriospinal INs involved in sensory and motor function. The results of this study

highlight the role gray matter SpINs play in the lumbar enlargement. Furthermore, they do not seem to be compensated for by spontaneous remodeling. This study suggests that cellular replacement strategies must be implemented to restore function following a gray matter lumbar injury, as the most common lesions in patients (contusion and compression SCI injuries also cause damage to the gray matter. Our short-term experimental results show that E14 spinal cells survive well after injury. Future experiments exploring injection parameters, cell differentiation and long-term behavioral recovery will provide insight into whether or not E14 spinal cells are a candidate to aid recovery after a lumbar lesion. If so, induced pluripotent stem cell (iPSCs) could be differentiated into an E14 NSC/NPC state and thereby overcome potential graft rejection. Human spinal cord NSCs have been transplanted into a C7 hemisection primate model and shown to survive, differentiate into NeuN+ cells including pre-motor SpINs *in vivo* (Kumamaru et al., 2019). It still remains to be seen whether they can appropriately replace lesioned gray matter and aid functional recovery. This new SCI model with fully characterized behavioral deficits and sensitive neuronal quantification and classification models will help carefully evaluate the potential of a gray matter replacement therapy and aid future SCI treatment options.

5 References

Agrawal, S., & Fehlings, M. (1996). Mechanisms of secondary injury to spinal cord axons in vitro: role of Na+, Na(+)-K(+)-ATPase, the Na(+)-H+ exchanger, and the Na(+)-Ca2+ exchanger. *The Journal of Neuroscience*, *16*(2), 545-552. https://doi.org/10.1523/JNEUROSCI.16-02-00545.1996

Ahn, S. N., Guu, J. J., Tobin, A. J., Edgerton, V. R., & Tillakaratne, N. J. K. (2006). Use of c-fos to identify activity-dependent spinal neurons after stepping in intact adult rats. *Spinal Cord*, *44*(9), 547-559. https://doi.org/10.1038/sj.sc.3101862

Ahuja, C. S., Wilson, J. R., Nori, S., Kotter, M. R. N., Druschel, C., Curt, A., & Fehlings, M. G. (2017). Traumatic spinal cord injury. *Nat Rev Dis Primers*, *3*, 17018. https://doi.org/10.1038/nrdp.2017.18

Al-Zoubi, A., Jafar, E., Jamous, M., Al-Twal, F., Al-Bakheet, S., Zalloum, M., Khalifeh, F., Radi, S. A., El-Khateeb, M., & Al-Zoubi, Z. (2014). Transplantation of purified autologous leukapheresis-derived CD34+ and CD133+ stem cells for patients with chronic spinal cord injuries: long-term evaluation of safety and efficacy. *Cell Transplantation*, *23 Suppl 1*, S25-34. https://doi.org/10.3727/096368914X684899

Alam, M., Garcia-Alias, G., Jin, B., Keyes, J., Zhong, H., Roy, R. R., Gerasimenko, Y., Lu, D. C., & Edgerton, V. R. (2017). Electrical neuromodulation of the cervical spinal cord facilitates forelimb skilled function recovery in spinal cord injured rats. *Exp Neurol*, *291*, 141-150. https://doi.org/10.1016/j.expneurol.2017.02.006

Alaynick, W. A., Jessell, T. M., & Pfaff, S. L. (2011). SnapShot: spinal cord development. *Cell*, *146*(1), 178-178 e171. https://doi.org/10.1016/j.cell.2011.06.038

Alizadeh, A., Dyck, S. M., & Karimi-Abdolrezaee, S. (2019). Traumatic Spinal Cord Injury: An Overview of Pathophysiology, Models and Acute Injury Mechanisms. *Front Neurol*, *10*, 282. https://doi.org/10.3389/fneur.2019.00282

Arancio, O., & MacDermott, A. B. (1991). Differential distribution of excitatory amino acid receptors on embryonic rat spinal cord neurons in culture. *J Neurophysiol*, *65*(4), 899-913. https://doi.org/10.1152/jn.1991.65.4.899

Arancio, O., Yoshimura, M., Murase, K., & MacDermott, A. B. (1993). The distribution of excitatory amino acid receptors on acutely dissociated dorsal horn neurons from postnatal rats. *Neuroscience*, *52*(1), 159-167. https://doi.org/10.1016/0306-4522(93)90190-q

Assinck, P., Duncan, G. J., Hilton, B. J., Plemel, J. R., & Tetzlaff, W. (2017). Cell transplantation therapy for spinal cord injury. *Nat Neurosci*, *20*(5), 637-647. https://doi.org/10.1038/nn.4541

Basso, D. M., Beattie, M. S., & Bresnahan, J. C. (1995). A sensitive and reliable locomotor rating scale for open field testing in rats. *J Neurotrauma*, *12*(1), 1-21. https://doi.org/10.1089/neu.1995.12.1

Bear, M. F., Connors, B. W., & Paradiso, M. A. (2016). Neuroscience, Exploring the Brain. In (4th Edition ed.): Wolters Kluwer.

Berg, S., Kutra, D., Kroeger, T., Straehle, C. N., Kausler, B. X., Haubold, C., Schiegg, M., Ales, J., Beier, T., Rudy, M., Eren, K., Cervantes, J. I., Xu, B., Beuttenmueller, F., Wolny, A., Zhang, C., Koethe, U., Hamprecht, F. A., & Kreshuk, A. (2019). ilastik: interactive machine

learning for (bio)image analysis. *Nat Methods*, *16*(12), 1226-1232. https://doi.org/10.1038/s41592-019-0582-9

BioRender. (2021). *BioRender*.

Borgens, R. B., & Liu-Snyder, P. (2012). Understanding secondary injury. *Q Rev Biol*, *87*(2), 89-127. https://doi.org/10.1086/665457

Brock, J. H., Graham, L., Staufenberg, E., Im, S., & Tuszynski, M. H. (2018). Rodent Neural Progenitor Cells Support Functional Recovery after Cervical Spinal Cord Contusion. *Journal of Neurotrauma*, *35*(9), 1069-1078. https://doi.org/10.1089/neu.2017.5244

Brockett, E. G., Seenan, P. G., Bannatyne, B. A., & Maxwell, D. J. (2013). Ascending and descending propriospinal pathways between lumbar and cervical segments in the rat: evidence for a substantial ascending excitatory pathway. *Neuroscience*, *240*, 83-97. https://doi.org/10.1016/j.neuroscience.2013.02.039

Brown, T. G. (1914). On the nature of the fundamental activity of the nervous centres; together with an analysis of the conditioning of rhythmic activity in progression, and a theory of the evolution of function in the nervous system. *J Physiol*, *48*(1), 18-46. https://doi.org/10.1113/jphysiol.1914.sp001646

Brustein, E., & Rossignol, S. (1998). Recovery of locomotion after ventral and ventrolateral spinal lesions in the cat. I. Deficits and adaptive mechanisms. *J Neurophysiol*, *80*(3), 1245-1267. https://doi.org/10.1152/jn.1998.80.3.1245

Burda, J. E., & Sofroniew, M. V. (2014). Reactive gliosis and the multicellular response to CNS damage and disease. *Neuron*, *81*(2), 229-248. https://doi.org/10.1016/j.neuron.2013.12.034

Bush, T. G., Puvanachandra, N., Horner, C. H., Polito, A., Ostenfeld, T., Svendsen, C. N., Mucke, L., Johnson, M. H., & Sofroniew, M. V. (1999). Leukocyte infiltration, neuronal degeneration, and neurite outgrowth after ablation of scar-forming, reactive astrocytes in adult transgenic mice. *Neuron*, *23*(2), 297-308. https://doi.org/10.1016/s0896-6273(00)80781-3

Chen, B. K., Madigan, N. N., Hakim, J. S., Dadsetan, M., McMahon, S. S., Yaszemski, M. J., & Windebank, A. J. (2018). GDNF Schwann cells in hydrogel scaffolds promote regional axon regeneration, remyelination and functional improvement after spinal cord transection in rats. *J Tissue Eng Regen Med*, *12*(1), e398-e407. https://doi.org/10.1002/term.2431

Chen, Y., He, Y., & DeVivo, M. J. (2016). Changing Demographics and Injury Profile of New Traumatic Spinal Cord Injuries in the United States, 1972-2014. *Arch Phys Med Rehabil*, *97*(10), 1610-1619. https://doi.org/10.1016/j.apmr.2016.03.017

Cripps, R. A., Lee, B. B., Wing, P., Weerts, E., Mackay, J., & Brown, D. (2011). A global map for traumatic spinal cord injury epidemiology: towards a living data repository for injury prevention. *Spinal Cord*, *49*(4), 493-501. https://doi.org/10.1038/sc.2010.146

Crone, S. A., Quinlan, K. A., Zagoraiou, L., Droho, S., Restrepo, C. E., Lundfald, L., Endo, T., Setlak, J., Jessell, T. M., Kiehn, O., & Sharma, K. (2008). Genetic ablation of V2a ipsilateral interneurons disrupts left-right locomotor coordination in mammalian spinal cord. *Neuron*, *60*(1), 70-83. https://doi.org/10.1016/j.neuron.2008.08.009

Cusimano, M., Biziato, D., Brambilla, E., Donegà, M., Alfaro-Cervello, C., Snider, S., Salani, G., Pucci, F., Comi, G., Garcia-Verdugo, J. M., De Palma, M., Martino, G., & Pluchino, S.

(2012). Transplanted neural stem/precursor cells instruct phagocytes and reduce secondary tissue damage in the injured spinal cord. *Brain*, *135*(Pt 2), 447-460. https://doi.org/10.1093/brain/awr339

Dai, X., Noga, B. R., Douglas, J. R., & Jordan, L. M. (2005). Localization of spinal neurons activated during locomotion using the c-fos immunohistochemical method. *J Neurophysiol*, *93*(6), 3442-3452. https://doi.org/10.1152/jn.00578.2004

Davies, J. E., Pröschel, C., Zhang, N., Noble, M., Mayer-Pröschel, M., & Davies, S. J. (2008). Transplanted astrocytes derived from BMP- or CNTF-treated glial-restricted precursors have opposite effects on recovery and allodynia after spinal cord injury. *J Biol*, *7*(7), 24. https://doi.org/10.1186/jbiol85

Delaunay, D., Heydon, K., Cumano, A., Schwab, M. H., Thomas, J. L., Suter, U., Nave, K. A., Zalc, B., & Spassky, N. (2008). Early neuronal and glial fate restriction of embryonic neural stem cells. *J Neurosci*, *28*(10), 2551-2562. https://doi.org/10.1523/JNEUROSCI.5497-07.2008

Deshpande, D., Agarwal, N., Fleming, T., Gaveriaux-Ruff, C., Klose, C. S. N., Tappe-Theodor, A., Kuner, R., & Nawroth, P. (2021). Loss of POMC-mediated antinociception contributes to painful diabetic neuropathy. *Nat Commun*, *12*(1), 426. https://doi.org/10.1038/s41467-020-20677-0

DeVivo, M. J., & Chen, Y. (2011). Trends in new injuries, prevalent cases, and aging with spinal cord injury. *Arch Phys Med Rehabil*, *92*(3), 332-338. https://doi.org/10.1016/j.apmr.2010.08.031

Dimitrijevic, M. R., Gerasimenko, Y., & Pinter, M. M. (1998). Evidence for a spinal central pattern generator in humans. *Ann N Y Acad Sci*, *860*, 360-376. https://doi.org/10.1111/j.1749-6632.1998.tb09062.x

Donnelly, D. J., & Popovich, P. G. (2008). Inflammation and its role in neuroprotection, axonal regeneration and functional recovery after spinal cord injury. *Exp Neurol*, *209*(2), 378-388. https://doi.org/10.1016/j.expneurol.2007.06.009

Dulin, J. N., Adler, A. F., Kumamaru, H., Poplawski, G. H. D., Lee-Kubli, C., Strobl, H., Gibbs, D., Kadoya, K., Fawcett, J. W., Lu, P., & Tuszynski, M. H. (2018). Injured adult motor and sensory axons regenerate into appropriate organotypic domains of neural progenitor grafts. *Nat Commun*, *9*(1), 84. https://doi.org/10.1038/s41467-017-02613-x

EMSCI. (2022). *EMSCI* https://www.emsci.org

English, A. W., Tigges, J., & Lennard, P. R. (1985). Anatomical organization of long ascending propriospinal neurons in the cat spinal cord. *J Comp Neurol*, *240*(4), 349-358. https://doi.org/10.1002/cne.902400403

Faden, A. I., Demediuk, P., Panter, S. S., & Vink, R. (1989). The role of excitatory amino acids and NMDA receptors in traumatic brain injury. *Science*, *244*(4906), 798-800. https://doi.org/10.1126/science.2567056

Faulkner, J. R., Herrmann, J. E., Woo, M. J., Tansey, K. E., Doan, N. B., & Sofroniew, M. V. (2004). Reactive astrocytes protect tissue and preserve function after spinal cord injury. *J Neurosci*, *24*(9), 2143-2155. https://doi.org/10.1523/JNEUROSCI.3547-03.2004

Filous, A. R., & Schwab, J. M. (2018). Determinants of Axon Growth, Plasticity, and Regeneration in the Context of Spinal Cord Injury. *Am J Pathol*, *188*(1), 53-62. https://doi.org/10.1016/j.ajpath.2017.09.005

Fischer, I., Dulin, J. N., & Lane, M. A. (2020). Transplanting neural progenitor cells to restore connectivity after spinal cord injury. *Nat Rev Neurosci*, *21*(7), 366-383. https://doi.org/10.1038/s41583-020-0314-2

Fleming, J. C., Norenberg, M. D., Ramsay, D. A., Dekaban, G. A., Marcillo, A. E., Saenz, A. D., Pasquale-Styles, M., Dietrich, W. D., & Weaver, L. C. (2006). The cellular inflammatory response in human spinal cords after injury. *Brain*, *129*(Pt 12), 3249-3269. https://doi.org/10.1093/brain/awl296

Flynn, J. R., Graham, B. A., Galea, M. P., & Callister, R. J. (2011). The role of propriospinal interneurons in recovery from spinal cord injury. *Neuropharmacology*, *60*(5), 809-822. https://doi.org/10.1016/j.neuropharm.2011.01.016

Francius, C., Harris, A., Rucchin, V., Hendricks, T. J., Stam, F. J., Barber, M., Kurek, D., Grosveld, F. G., Pierani, A., Goulding, M., & Clotman, F. (2013). Identification of multiple subsets of ventral interneurons and differential distribution along the rostrocaudal axis of the developing spinal cord. *PLoS One*, *8*(8), e70325. https://doi.org/10.1371/journal.pone.0070325

Frigon, A. (2017). The neural control of interlimb coordination during mammalian locomotion. *J Neurophysiol*, *117*(6), 2224-2241. https://doi.org/10.1152/jn.00978.2016

Gosgnach, S., Lanuza, G. M., Butt, S. J., Saueressig, H., Zhang, Y., Velasquez, T., Riethmacher, D., Callaway, E. M., Kiehn, O., & Goulding, M. (2006). V1 spinal neurons regulate the speed of vertebrate locomotor outputs. *Nature*, *440*(7081), 215-219. https://doi.org/10.1038/nature04545

Grossman, R. G., Fehlings, M. G., Frankowski, R. F., Burau, K. D., Chow, D. S., Tator, C., Teng, A., Toups, E. G., Harrop, J. S., Aarabi, B., Shaffrey, C. I., Johnson, M. M., Harkema, S. J., Boakye, M., Guest, J. D., & Wilson, J. R. (2014). A prospective, multicenter, phase I matched-comparison group trial of safety, pharmacokinetics, and preliminary efficacy of riluzole in patients with traumatic spinal cord injury. *J Neurotrauma*, *31*(3), 239-255. https://doi.org/10.1089/neu.2013.2969

Guertin, P. A. (2009). The mammalian central pattern generator for locomotion. *Brain Res Rev*, *62*(1), 45-56. https://doi.org/10.1016/j.brainresrev.2009.08.002

Hadi, B., Zhang, Y. P., Burke, D. A., Shields, C. B., & Magnuson, D. S. (2000). Lasting paraplegia caused by loss of lumbar spinal cord interneurons in rats: no direct correlation with motor neuron loss. *J Neurosurg*, *93*(2 Suppl), 266-275. https://doi.org/10.3171/spi.2000.93.2.0266

Harrison, M., O'Brien, A., Adams, L., Cowin, G., Ruitenberg, M. J., Sengul, G., & Watson, C. (2013). Vertebral landmarks for the identification of spinal cord segments in the mouse. *Neuroimage*, *68*, 22-29. https://doi.org/10.1016/j.neuroimage.2012.11.048

Hayashi, M., Hinckley, C. A., Driscoll, S. P., Moore, N. J., Levine, A. J., Hilde, K. L., Sharma, K., & Pfaff, S. L. (2018). Graded Arrays of Spinal and Supraspinal V2a Interneuron Subtypes Underlie Forelimb and Hindlimb Motor Control. *Neuron*, *97*(4), 869-884 e865. https://doi.org/10.1016/j.neuron.2018.01.023

Hayes, R. L., Jenkins, L. W., & Lyeth, B. G. (1992). Neurotransmitter-mediated mechanisms of traumatic brain injury: acetylcholine and excitatory amino acids. *J Neurotrauma*, *9 Suppl 1*, S173-187. https://www.ncbi.nlm.nih.gov/pubmed/1350312

Hill, C. E., Beattie, M. S., & Bresnahan, J. C. (2001). Degeneration and sprouting of identified descending supraspinal axons after contusive spinal cord injury in the rat. *Exp Neurol*, *171*(1), 153-169. https://doi.org/10.1006/exnr.2001.7734

Ho, C. H., Triolo, R. J., Elias, A. L., Kilgore, K. L., DiMarco, A. F., Bogie, K., Vette, A. H., Audu, M. L., Kobetic, R., Chang, S. R., Chan, K. M., Dukelow, S., Bourbeau, D. J., Brose, S. W., Gustafson, K. J., Kiss, Z. H., & Mushahwar, V. K. (2014). Functional electrical stimulation and spinal cord injury. *Phys Med Rehabil Clin N Am*, *25*(3), 631-654, ix. https://doi.org/10.1016/j.pmr.2014.05.001

Hofstoetter, U. S., Perret, I., Bayart, A., Lackner, P., Binder, H., Freundl, B., & Minassian, K. (2021). Spinal motor mapping by epidural stimulation of lumbosacral posterior roots in humans. *iScience*, *24*(1), 101930. https://doi.org/10.1016/j.isci.2020.101930

Huang, H., Chen, L., Wang, H., Xi, H., Gou, C., Zhang, J., Zhang, F., & Liu, Y. (2006). Safety of fetal olfactory ensheathing cell transplantation in patients with chronic spinal cord injury. A 38-month follow-up with MRI. *Zhongguo Xiu Fu Chong Jian Wai Ke Za Zhi*, *20*(4), 439-443. https://www.ncbi.nlm.nih.gov/pubmed/16683452

Iwatsuki, K., Yoshimine, T., Kishima, H., Aoki, M., Yoshimura, K., Ishihara, M., Ohnishi, Y., & Lima, C. (2008). Transplantation of olfactory mucosa following spinal cord injury promotes recovery in rats. *Neuroreport*, *19*(13), 1249-1252. https://doi.org/10.1097/WNR.0b013e328305b70b

Jankowska, E., Lundberg, A., Roberts, W. J., & Stuart, D. (1974). A long propriospinal system with direct effect on motoneurones and on interneurones in the cat lumbosacral cord. *Exp Brain Res*, *21*(2), 169-194. https://doi.org/10.1007/BF00234388

Jia, F., Lv, P., Miao, H., Shi, X., Mei, H., Li, L., Xu, X., Tao, S., & Xu, F. (2019). Optimization of the Fluorescent Protein Expression Level Based on Pseudorabies Virus Bartha Strain for Neural Circuit Tracing. *Front Neuroanat*, *13*, 63. https://doi.org/10.3389/fnana.2019.00063

Kadoya, K., Lu, P., Nguyen, K., Lee-Kubli, C., Kumamaru, H., Yao, L., Knackert, J., Poplawski, G., Dulin, J. N., Strobl, H., Takashima, Y., Biane, J., Conner, J., Zhang, S. C., & Tuszynski, M. H. (2016). Spinal cord reconstitution with homologous neural grafts enables robust corticospinal regeneration. *Nat Med*, *22*(5), 479-487. https://doi.org/10.1038/nm.4066

Kathe, C., Skinnider, M. A., Hutson, T. H., Regazzi, N., Gautier, M., Demesmaeker, R., Komi, S., Ceto, S., James, N. D., Cho, N., Baud, L., Galan, K., Matson, K. J. E., Rowald, A., Kim, K., Wang, R., Minassian, K., Prior, J. O., Asboth, L., . . . Courtine, G. (2022). The neurons that restore walking after paralysis. *Nature*, *611*(7936), 540-547. https://doi.org/10.1038/s41586-022-05385-7

Kawaja, M. D., & Gage, F. H. (1991). Reactive astrocytes are substrates for the growth of adult CNS axons in the presence of elevated levels of nerve growth factor. *Neuron*, *7*(6), 1019-1030. https://doi.org/10.1016/0896-6273(91)90346-2

Kim, E.-S., Li, H., McCulloch, P. F., Morrison, L. A., Yoon, K.-W., & Xu, X. M. (2000). Spatial and temporal patterns of transneuronal labeling in CNS neurons after injection of pseudorabies virus into the sciatic nerve of adult rats. *Brain Research*, *857*(1-2), 41-55. https://doi.org/10.1016/S0006-8993(99)02332-X

Kitzman, P. H. (2009). Effectiveness of riluzole in suppressing spasticity in the spinal cord injured rat. *Neurosci Lett*, *455*(2), 150-153. https://doi.org/10.1016/j.neulet.2009.03.016

Kjell, J., & Olson, L. (2016). Rat models of spinal cord injury: from pathology to potential therapies. *Dis Model Mech*, *9*(10), 1125-1137. https://doi.org/10.1242/dmm.025833

Koch, S. C., Del Barrio, M. G., Dalet, A., Gatto, G., Gunther, T., Zhang, J., Seidler, B., Saur, D., Schule, R., & Goulding, M. (2017). RORbeta Spinal Interneurons Gate Sensory Transmission during Locomotion to Secure a Fluid Walking Gait. *Neuron*, *96*(6), 1419-1431 e1415. https://doi.org/10.1016/j.neuron.2017.11.011

Koopmans, G. C., Deumens, R., Honig, W. M., Hamers, F. P., Steinbusch, H. W., & Joosten, E. A. (2005). The assessment of locomotor function in spinal cord injured rats: the importance of objective analysis of coordination. *J Neurotrauma*, *22*(2), 214-225. https://doi.org/10.1089/neu.2005.22.214

Kretschmer, B. D., Kratzer, U., & Schmidt, W. J. (1998). Riluzole, a glutamate release inhibitor, and motor behavior. *Naunyn Schmiedebergs Arch Pharmacol*, *358*(2), 181-190. https://doi.org/10.1007/pl00005241

Kuehn, N., Schwarz, A., Beretta, C. A., Schwarte, Y., Schmitt, F., Motsch, M., Weidner, N., & Puttagunta, R. (Manuscript in preparation). Intermediate Gray Matter Interneurons in the Lumbar Spinal Cord Play a Critical and Necessary Role in Coordinated Locomotion. Sections of this thesis were adapted from (Kuehn et al, manuscript in prepration) and unless otherwise noted, were written and created by myself.

Kuerzi, J., Brown, E. H., Shum-Siu, A., Siu, A., Burke, D., Morehouse, J., Smith, R. R., & Magnuson, D. S. (2010). Task-specificity vs. ceiling effect: step-training in shallow water after spinal cord injury. *Exp Neurol*, *224*(1), 178-187. https://doi.org/10.1016/j.expneurol.2010.03.008

Kumamaru, H., Lu, P., Rosenzweig, E. S., Kadoya, K., & Tuszynski, M. H. (2019). Regenerating Corticospinal Axons Innervate Phenotypically Appropriate Neurons within Neural Stem Cell Grafts. *Cell Rep*, *26*(9), 2329-2339.e2324. https://doi.org/10.1016/j.celrep.2019.01.099

Kwak, S., & Nakamura, R. (1995). Selective degeneration of inhibitory interneurons in the rat spinal cord induced by intrathecal infusion of acromelic acid. *Brain Res*, *702*(1-2), 61-71. https://doi.org/10.1016/0006-8993(95)01000-6

Laliberte, A. M., Goltash, S., Lalonde, N. R., & Bui, T. V. (2019). Propriospinal Neurons: Essential Elements of Locomotor Control in the Intact and Possibly the Injured Spinal Cord. *Front Cell Neurosci*, *13*, 512. https://doi.org/10.3389/fncel.2019.00512

Lanuza, G. M., Gosgnach, S., Pierani, A., Jessell, T. M., & Goulding, M. (2004). Genetic identification of spinal interneurons that coordinate left-right locomotor activity necessary for walking movements. *Neuron*, *42*(3), 375-386. https://doi.org/10.1016/s0896-6273(04)00249-1

Lepore, A. C., Han, S. S., Tyler-Polsz, C. J., Cai, J., Rao, M. S., & Fischer, I. (2004). Differential fate of multipotent and lineage-restricted neural precursors following transplantation into the adult CNS. *Neuron Glia Biol*, *1*(2), 113-126. https://doi.org/10.1017/s1740925x04000213

Leszczyńska, A. N., Majczyński, H., Wilczyński, G. M., Sławińska, U., & Cabaj, A. M. (2015). Thoracic Hemisection in Rats Results in Initial Recovery Followed by a Late Decrement in Locomotor Movements, with Changes in Coordination Correlated with Serotonergic

Innervation of the Ventral Horn. *PLoS One*, *10*(11), e0143602. https://doi.org/10.1371/journal.pone.0143602

Lu, D. C., Niu, T., & Alaynick, W. A. (2015). Molecular and cellular development of spinal cord locomotor circuitry. *Front Mol Neurosci*, *8*, 25. https://doi.org/10.3389/fnmol.2015.00025

Lu, P., Graham, L., Wang, Y., Wu, D., & Tuszynski, M. (2014). Promotion of survival and differentiation of neural stem cells with fibrin and growth factor cocktails after severe spinal cord injury. *J Vis Exp*(89), e50641. https://doi.org/10.3791/50641

Lu, P., Wang, Y., Graham, L., McHale, K., Gao, M., Wu, D., Brock, J., Blesch, A., Rosenzweig, E. S., Havton, L. A., Zheng, B., Conner, J. M., Marsala, M., & Tuszynski, M. H. (2012). Long-distance growth and connectivity of neural stem cells after severe spinal cord injury. *Cell*, *150*(6), 1264-1273. https://doi.org/10.1016/j.cell.2012.08.020

Lundfald, L., Restrepo, C. E., Butt, S. J., Peng, C. Y., Droho, S., Endo, T., Zeilhofer, H. U., Sharma, K., & Kiehn, O. (2007). Phenotype of V2-derived interneurons and their relationship to the axon guidance molecule EphA4 in the developing mouse spinal cord. *Eur J Neurosci*, *26*(11), 2989-3002. https://doi.org/10.1111/j.1460-9568.2007.05906.x

Magnuson, D., Trinder, T., Zhang, Y. P., Burke, D., Morassutti, D., & Shields, C. (1998). Comparing Deficits Following Excitotoxic and Contusion Injuries in the Thoracic and Lumbar Spinal Cord of the Adult Rat. In (Vol. 156, pp. 191-204): Experimental Neurology.

Magnuson, D. S., Lovett, R., Coffee, C., Gray, R., Han, Y., Zhang, Y. P., & Burke, D. A. (2005). Functional consequences of lumbar spinal cord contusion injuries in the adult rat. *J Neurotrauma*, *22*(5), 529-543. https://doi.org/10.1089/neu.2005.22.529

Magnuson, D. S., Trinder, T. C., Zhang, Y. P., Burke, D., Morassutti, D. J., & Shields, C. B. (1999). Comparing deficits following excitotoxic and contusion injuries in the thoracic and lumbar spinal cord of the adult rat. *Exp Neurol*, *156*(1), 191-204. https://doi.org/10.1006/exnr.1999.7016

Magnuson, D. S. K., Zhang, Y. P., Cao, Q.-l., Han, Y., Burke, D. A., & Whittemore, S. R. (2001). Embryonic brain precursors transplanted into kainate lesioned rat spinal cord: . *Neuroreport*, *12*(5), 1015-1019. https://doi.org/10.1097/00001756-200104170-00030

Manley, N. C., Priest, C. A., Denham, J., Wirth, E. D., 3rd, & Lebkowski, J. S. (2017). Human Embryonic Stem Cell-Derived Oligodendrocyte Progenitor Cells: Preclinical Efficacy and Safety in Cervical Spinal Cord Injury. *Stem Cells Transl Med*, *6*(10), 1917-1929. https://doi.org/10.1002/sctm.17-0065

Martins, B. C., Torres, B. B. J., de Oliveira, K. M., Lavor, M. S., Osorio, C. M., Fukushima, F. B., Rosado, I. R., & de Melo, E. G. (2018). Association of riluzole and dantrolene improves significant recovery after acute spinal cord injury in rats. *Spine J*, *18*(3), 532-539. https://doi.org/10.1016/j.spinee.2017.10.067

Martins, L. A., Schiavo, A., Xavier, L. L., & Mestriner, R. G. (2022). The Foot Fault Scoring System to Assess Skilled Walking in Rodents: A Reliability Study. *Front Behav Neurosci*, *16*, 892010. https://doi.org/10.3389/fnbeh.2022.892010

Mayer-Proschel, M., Kalyani, A. J., Mujtaba, T., & Rao, M. S. (1997). Isolation of lineage-restricted neuronal precursors from multipotent neuroepithelial stem cells. *Neuron*, *19*(4), 773-785. https://doi.org/10.1016/s0896-6273(00)80960-5

McGeer, E. G., & McGeer, P. L. (1978). Some factors influencing the neurotoxicity of intrastriatal injections of kainic acid. *Neurochem Res*, *3*(4), 501-517. https://doi.org/10.1007/BF00966331
Metz, G. A., & Whishaw, I. Q. (2009). The ladder rung walking task: a scoring system and its practical application. *J Vis Exp*(28). https://doi.org/10.3791/1204
Mohan, R., Tosolini, A. P., & Morris, R. (2015). Segmental Distribution of the Motor Neuron Columns That Supply the Rat Hindlimb: A Muscle/Motor Neuron Tract-Tracing Analysis Targeting the Motor End Plates. *Neuroscience*, *307*, 98-108. https://doi.org/10.1016/j.neuroscience.2015.08.030
Moonen, G., Satkunendrarajah, K., Wilcox, J. T., Badner, A., Mothe, A., Foltz, W., Fehlings, M. G., & Tator, C. H. (2016). A New Acute Impact-Compression Lumbar Spinal Cord Injury Model in the Rodent. *J Neurotrauma*, *33*(3), 278-289. https://doi.org/10.1089/neu.2015.3937
Muroyama, Y., Fujihara, M., Ikeya, M., Kondoh, H., & Takada, S. (2002). Wnt signaling plays an essential role in neuronal specification of the dorsal spinal cord. *Genes Dev*, *16*(5), 548-553. https://doi.org/10.1101/gad.937102
Nagoshi, N., Nakashima, H., & Fehlings, M. G. (2015). Riluzole as a neuroprotective drug for spinal cord injury: from bench to bedside. *Molecules*, *20*(5), 7775-7789. https://doi.org/10.3390/molecules20057775
Nicholls, D. (2004). Mitochondrial Dysfunction and Glutamate Excitotoxicity Studied in Primary Neuronal Cultures. *Current Molecular Medicine*, *4*(2), 149-177. https://doi.org/10.2174/1566524043479239
Nicolopoulos-Stournaras, S., & Iles, J. F. (1983). Motor neuron columns in the lumbar spinal cord of the rat. *J Comp Neurol*, *217*(1), 75-85. https://doi.org/10.1002/cne.902170107
Nishimaru, H., Takizawa, H., & Kudo, N. (2000). 5-Hydroxytryptamine-induced locomotor rhythm in the neonatal mouse spinal cord in vitro. *Neurosci Lett*, *280*(3), 187-190. https://doi.org/10.1016/s0304-3940(00)00805-3
Nothias, F., & Peschanski, M. (1990). Homotypic fetal transplants into an experimental model of spinal cord neurodegeneration. *J Comp Neurol*, *301*(4), 520-534. https://doi.org/10.1002/cne.903010404
NSCISC. (2022). NSCISC National Spinal Cord Injury Statistics Center. In: University of Alabama at Birmingham.
Olney, J. W., Rhee, V., & Ho, O. L. (1974). Kainic acid: a powerful neurotoxic analogue of glutamate. *Brain Res*, *77*(3), 507-512. https://doi.org/10.1016/0006-8993(74)90640-4
Onifer, S. M., Cannon, A. B., & Whittemore, S. R. (1997). Altered differentiation of CNS neural progenitor cells after transplantation into the injured adult rat spinal cord. *Cell Transplantation*, *6*(3), 327-338. https://doi.org/10.1177/096368979700600315
Oyinbo, C. A. (2011). Secondary injury mechanisms in traumatic spinal cord injury: a nugget of this multiply cascade. *Acta Neurobiol Exp (Wars)*, *71*(2), 281-299. https://www.ncbi.nlm.nih.gov/pubmed/21731081
Percie du Sert, N., Hurst, V., Ahluwalia, A., Alam, S., Avey, M. T., Baker, M., Browne, W. J., Clark, A., Cuthill, I. C., Dirnagl, U., Emerson, M., Garner, P., Holgate, S. T., Howells, D. W., Karp, N. A., Lazic, S. E., Lidster, K., MacCallum, C. J., Macleod, M., . . . Wurbel, H. (2020). The

ARRIVE guidelines 2.0: Updated guidelines for reporting animal research. *PLoS Biol*, *18*(7), e3000410. https://doi.org/10.1371/journal.pbio.3000410

Pineau, I., & Lacroix, S. (2007). Proinflammatory cytokine synthesis in the injured mouse spinal cord: multiphasic expression pattern and identification of the cell types involved. *J Comp Neurol*, *500*(2), 267-285. https://doi.org/10.1002/cne.21149

Pitonak, M., Aceves, M., Kumar, P. A., Dampf, G., Green, P., Tucker, A., Dietz, V., Miranda, D., Letchuman, S., Jonika, M. M., Bautista, D., Blackmon, H., & Dulin, J. N. (2022). Effects of biological sex mismatch on neural progenitor cell transplantation for spinal cord injury in mice. *Nature Communications*, *13*(1), 5380. https://doi.org/10.1038/s41467-022-33134-x

Pitzer, C., Kuner, R., & Tappe-Theodor, A. (2016). Voluntary and evoked behavioral correlates in neuropathic pain states under different social housing conditions. *Molecular Pain*, *12*. https://doi.org/Artn 1744806916656635

10.1177/1744806916656635

Pocratsky, A. M., Burke, D. A., Morehouse, J. R., Beare, J. E., Riegler, A. S., Tsoulfas, P., States, G. J. R., Whittemore, S. R., & Magnuson, D. S. K. (2017). Reversible silencing of lumbar spinal interneurons unmasks a task-specific network for securing hindlimb alternation. *Nat Commun*, *8*(1), 1963. https://doi.org/10.1038/s41467-017-02033-x

Pocratsky, A. M., Shepard, C. T., Morehouse, J. R., Burke, D. A., Riegler, A. S., Hardin, J. T., Beare, J. E., Hainline, C., States, G. J., Brown, B. L., Whittemore, S. R., & Magnuson, D. S. (2020). Long ascending propriospinal neurons provide flexible, context-specific control of interlimb coordination. *Elife*, *9*. https://doi.org/10.7554/eLife.53565

Poplawski, G. H. D., Lie, R., Hunt, M., Kumamaru, H., Kawaguchi, R., Lu, P., Schafer, M. K. E., Woodruff, G., Robinson, J., Canete, P., Dulin, J. N., Geoffroy, C. G., Menzel, L., Zheng, B., Coppola, G., & Tuszynski, M. H. (2018). Adult rat myelin enhances axonal outgrowth from neural stem cells. *Sci Transl Med*, *10*(442). https://doi.org/10.1126/scitranslmed.aal2563

Popovich, P. G., Wei, P., & Stokes, B. T. (1997). Cellular inflammatory response after spinal cord injury in Sprague-Dawley and Lewis rats. *J Comp Neurol*, *377*(3), 443-464. https://doi.org/10.1002/(sici)1096-9861(19970120)377:3<443::aid-cne10>3.0.co;2-s

Preibisch, S., Saalfeld, S., & Tomancak, P. (2009). Globally optimal stitching of tiled 3D microscopic image acquisitions. *Bioinformatics*, *25*(11), 1463-1465. https://doi.org/10.1093/bioinformatics/btp184

Quadri, S. A., Farooqui, M., Ikram, A., Zafar, A., Khan, M. A., Suriya, S. S., Claus, C. F., Fiani, B., Rahman, M., Ramachandran, A., Armstrong, I. I. T., Taqi, M. A., & Mortazavi, M. M. (2020). Recent update on basic mechanisms of spinal cord injury. *Neurosurgical Review*, *43*(2), 425-441. https://doi.org/10.1007/s10143-018-1008-3

Reed, W. R., Shum-Siu, A., Onifer, S. M., & Magnuson, D. S. (2006). Inter-enlargement pathways in the ventrolateral funiculus of the adult rat spinal cord. *Neuroscience*, *142*(4), 1195-1207. https://doi.org/10.1016/j.neuroscience.2006.07.017

Reed, W. R., Shum-Siu, A., Whelan, A., Onifer, S. M., & Magnuson, D. S. K. (2009). Anterograde labeling of ventrolateral funiculus pathways with spinal enlargement connections in the adult rat spinal cord. *Brain Research*, *1302*, 76-84. https://doi.org/10.1016/j.brainres.2009.09.049

Reier, P. J., Perlow, M. J., & Guth, L. (1983). Development of embryonic spinal cord transplants in the rat. *Brain Res*, *312*(2), 201-219. https://doi.org/10.1016/0165-3806(83)90137-2

Robinson, J., & Lu, P. (2017). Optimization of trophic support for neural stem cell grafts in sites of spinal cord injury. *Exp Neurol*, *291*, 87-97. https://doi.org/10.1016/j.expneurol.2017.02.007

Rowald, A., Komi, S., Demesmaeker, R., Baaklini, E., Hernandez-Charpak, S. D., Paoles, E., Montanaro, H., Cassara, A., Becce, F., Lloyd, B., Newton, T., Ravier, J., Kinany, N., D'Ercole, M., Paley, A., Hankov, N., Varescon, C., McCracken, L., Vat, M., . . . Courtine, G. (2022). Activity-dependent spinal cord neuromodulation rapidly restores trunk and leg motor functions after complete paralysis. *Nat Med*, *28*(2), 260-271. https://doi.org/10.1038/s41591-021-01663-5

Rowland, J. W., Hawryluk, G. W., Kwon, B., & Fehlings, M. G. (2008). Current status of acute spinal cord injury pathophysiology and emerging therapies: promise on the horizon. *Neurosurg Focus*, *25*(5), E2. https://doi.org/10.3171/FOC.2008.25.11.E2

Ruder, L., Takeoka, A., & Arber, S. (2016). Long-Distance Descending Spinal Neurons Ensure Quadrupedal Locomotor Stability. *Neuron*, *92*(5), 1063-1078. https://doi.org/10.1016/j.neuron.2016.10.032

Sandner, B., Prang, P., Rivera, F. J., Aigner, L., Blesch, A., & Weidner, N. (2012). Neural stem cells for spinal cord repair. *Cell Tissue Res*, *349*(1), 349-362. https://doi.org/10.1007/s00441-012-1363-2

Sathyamurthy, A., Johnson, K. R., Matson, K. J. E., Dobrott, C. I., Li, L., Ryba, A. R., Bergman, T. B., Kelly, M. C., Kelley, M. W., & Levine, A. J. (2018). Massively Parallel Single Nucleus Transcriptional Profiling Defines Spinal Cord Neurons and Their Activity during Behavior. *Cell Rep*, *22*(8), 2216-2225. https://doi.org/10.1016/j.celrep.2018.02.003

Schindelin, J., Arganda-Carreras, I., Frise, E., Kaynig, V., Longair, M., Pietzsch, T., Preibisch, S., Rueden, C., Saalfeld, S., Schmid, B., Tinevez, J.-Y., White, D. J., Hartenstein, V., Eliceiri, K., Tomancak, P., & Cardona, A. (2012). Fiji: an open-source platform for biological-image analysis. *Nature Methods*, *9*(7), 676-682. https://doi.org/10.1038/nmeth.2019

Schinder, A. F., Olson, E. C., Spitzer, N. C., & Montal, M. (1996). Mitochondrial dysfunction is a primary event in glutamate neurotoxicity. *J Neurosci*, *16*(19), 6125-6133. https://doi.org/10.1523/JNEUROSCI.16-19-06125.1996

Shepard, C. T., Pocratsky, A. M., Brown, B. L., Van Rijswijck, M. A., Zalla, R. M., Burke, D. A., Morehouse, J. R., Riegler, A. S., Whittemore, S. R., & Magnuson, D. S. (2021). Silencing long ascending propriospinal neurons after spinal cord injury improves hindlimb stepping in the adult rat. *Elife*, *10*. https://doi.org/10.7554/eLife.70058

Sherrington, C. S. (1910). Flexion-reflex of the limb, crossed extension-reflex, and reflex stepping and standing. *J Physiol*, *40*(1-2), 28-121. https://doi.org/10.1113/jphysiol.1910.sp001362

Siegel, S. M., Lee, J. W., & Oaklander, A. L. (2007). Needlestick distal nerve injury in rats models symptoms of complex regional pain syndrome. *Anesthesia and Analgesia*, *105*(6), 1820-1829. https://doi.org/10.1213/01.ane.0000295234.21892.bc

Simonian, N. A., Getz, R. L., Leveque, J. C., Konradi, C., & Coyle, J. T. (1996). Kainic acid induces apoptosis in neurons. *Neuroscience*, *75*(4), 1047-1055. https://doi.org/10.1016/0306-4522(96)00326-0

Sliwinski, C., Nees, T. A., Puttagunta, R., Weidner, N., & Blesch, A. (2018). Sensorimotor Activity Partially Ameliorates Pain and Reduces Nociceptive Fiber Density in the Chronically Injured Spinal Cord. *J Neurotrauma*, *35*(18), 2222-2238. https://doi.org/10.1089/neu.2017.5431

Smith, A. J. (2020). Guidelines for planning and conducting high-quality research and testing on animals. *Lab Anim Res*, *36*, 21. https://doi.org/10.1186/s42826-020-00054-0

Srinivas, S., Wali, A. R., & Pham, M. H. (2019). Efficacy of riluzole in the treatment of spinal cord injury: a systematic review of the literature. *Neurosurg Focus*, *46*(3), E6. https://doi.org/10.3171/2019.1.FOCUS18596

Stelzner, D. J. (2008). Short-circuit recovery from spinal injury. *Nat Med*, *14*(1), 19-20. https://doi.org/10.1038/nm0108-19

Sternfeld, M. J., Hinckley, C. A., Moore, N. J., Pankratz, M. T., Hilde, K. L., Driscoll, S. P., Hayashi, M., Amin, N. D., Bonanomi, D., Gifford, W. D., Sharma, K., Goulding, M., & Pfaff, S. L. (2017). Speed and segmentation control mechanisms characterized in rhythmically-active circuits created from spinal neurons produced from genetically-tagged embryonic stem cells. *Elife*, *6*. https://doi.org/10.7554/eLife.21540

Stringer, C., Wang, T., Michaelos, M., & Pachitariu, M. (2021). Cellpose: a generalist algorithm for cellular segmentation. *Nat Methods*, *18*(1), 100-106. https://doi.org/10.1038/s41592-020-01018-x

Takahashi, Y., Chiba, T., Kurokawa, M., & Aoki, Y. (2003). Dermatomes and the central organization of dermatomes and body surface regions in the spinal cord dorsal horn in rats. *Journal of Comparative Neurology*, *462*(1), 29-41. https://doi.org/10.1002/cne.10669

Tator, C. H., & Koyanagi, I. (1997). Vascular mechanisms in the pathophysiology of human spinal cord injury. *J Neurosurg*, *86*(3), 483-492. https://doi.org/10.3171/jns.1997.86.3.0483

Timmer, J. R., Wang, C., & Niswander, L. (2002). BMP signaling patterns the dorsal and intermediate neural tube via regulation of homeobox and helix-loop-helix transcription factors. *Development*, *129*(10), 2459-2472. https://doi.org/10.1242/dev.129.10.2459

Timotius, I. K., Bieler, L., Couillard-Despres, S., Sandner, B., Garcia-Ovejero, D., Labombarda, F., Estrada, V., Müller, H. W., Winkler, J., Klucken, J., Eskofier, B., Weidner, N., & Puttagunta, R. (2021). Combination of Defined CatWalk Gait Parameters for Predictive Locomotion Recovery in Experimental Spinal Cord Injury Rat Models. *eNeuro*, *8*(2). https://doi.org/10.1523/ENEURO.0497-20.2021

Tran, A. P., Warren, P. M., & Silver, J. (2018). The Biology of Regeneration Failure and Success After Spinal Cord Injury. *Physiol Rev*, *98*(2), 881-917. https://doi.org/10.1152/physrev.00017.2017

Urca, G., & Urca, R. (1990). Neurotoxic effects of excitatory amino acids in the mouse spinal cord: quisqualate and kainate but not N-methyl-D-aspartate induce permanent neural damage. *Brain Res*, *529*(1-2), 7-15. https://doi.org/10.1016/0006-8993(90)90805-l

van Gorp, S., Leerink, M., Nguyen, S., Platoshyn, O., Marsala, M., & Joosten, E. A. (2014). Translation of the rat thoracic contusion model; part 2 - forward versus backward locomotion testing. *Spinal Cord*, *52*(7), 529-535. https://doi.org/10.1038/sc.2014.73

Viala, D., Buisseret-Delmas, C., & Portal, J. J. (1988). An attempt to localize the lumbar locomotor generator in the rabbit using 2-deoxy-[14C]glucose autoradiography. *Neurosci Lett*, *86*(2), 139-143. https://doi.org/10.1016/0304-3940(88)90560-5

Vierck, C. J., King, C. D., Berens, S. A., & Yezierski, R. P. (2013). Excitotoxic injury to thoracolumbar gray matter alters sympathetic activation and thermal pain sensitivity. *Exp Brain Res*, *231*(1), 19-26. https://doi.org/10.1007/s00221-013-3666-2

Wang, Q., Yu, S., Simonyi, A., Sun, G. Y., & Sun, A. Y. (2005). Kainic acid-mediated excitotoxicity as a model for neurodegeneration. *Mol Neurobiol*, *31*(1-3), 3-16. https://doi.org/10.1385/MN:31:1-3:003

Wang, S. J., Wang, K. Y., & Wang, W. C. (2004). Mechanisms underlying the riluzole inhibition of glutamate release from rat cerebral cortex nerve terminals (synaptosomes). *Neuroscience*, *125*(1), 191-201. https://doi.org/10.1016/j.neuroscience.2004.01.019

Wanner, I. B., Anderson, M. A., Song, B., Levine, J., Fernandez, A., Gray-Thompson, Z., Ao, Y., & Sofroniew, M. V. (2013). Glial scar borders are formed by newly proliferated, elongated astrocytes that interact to corral inflammatory and fibrotic cells via STAT3-dependent mechanisms after spinal cord injury. *J Neurosci*, *33*(31), 12870-12886. https://doi.org/10.1523/JNEUROSCI.2121-13.2013

Watson, C., Paxinos, G., & Kayaliuglu, G. (2009). *The Spinal Cord*. Elsevier Academic Press.

Watzlawick, R., Rind, J., Sena, E. S., Brommer, B., Zhang, T., Kopp, M. A., Dirnagl, U., Macleod, M. R., Howells, D. W., & Schwab, J. M. (2016). Olfactory Ensheathing Cell Transplantation in Experimental Spinal Cord Injury: Effect size and Reporting Bias of 62 Experimental Treatments: A Systematic Review and Meta-Analysis. *PLOS Biology*, *14*(5), e1002468. https://doi.org/10.1371/journal.pbio.1002468

Weber, J. (2004). Calcium Homeostasis Following Traumatic Neuronal Injury. *Current Neurovascular Research*, *1*(2), 151-171. https://doi.org/10.2174/1567202043480134

Wen, J., Sun, D., Tan, J., & Young, W. (2015). A consistent, quantifiable, and graded rat lumbosacral spinal cord injury model. *J Neurotrauma*, *32*(12), 875-892. https://doi.org/10.1089/neu.2013.3321

Wenger, N., Moraud, E. M., Gandar, J., Musienko, P., Capogrosso, M., Baud, L., Le Goff, C. G., Barraud, Q., Pavlova, N., Dominici, N., Minev, I. R., Asboth, L., Hirsch, A., Duis, S., Kreider, J., Mortera, A., Haverbeck, O., Kraus, S., Schmitz, F., . . . Courtine, G. (2016). Spatiotemporal neuromodulation therapies engaging muscle synergies improve motor control after spinal cord injury. *Nat Med*, *22*(2), 138-145. https://doi.org/10.1038/nm.4025

Whelan, P. J. (1996). Control of locomotion in the decerebrate cat. *Prog Neurobiol*, *49*(5), 481-515. https://doi.org/10.1016/0301-0082(96)00028-7

WHO, W. H. O. (2013). *Spinal Cord Injury*. WHO. https://www.who.int/news-room/fact-sheets/detail/spinal-cord-injury

Willison, A. G., Smith, S., Davies, B. M., Kotter, M. R. N., & Barnett, S. C. (2020). A scoping review of trials for cell-based therapies in human spinal cord injury. *Spinal Cord*, *58*(8), 844-856. https://doi.org/10.1038/s41393-020-0455-1

Wrathall, J. R., Teng, Y. D., & Choiniere, D. (1996). Amelioration of Functional Deficits from Spinal Cord Trauma with Systemically Administered NBQX, an Antagonist of Non-N-

methyl-D-aspartate receptors. *Experimental Neurology*, *137*(1), 119-126. https://doi.org/10.1006/exnr.1996.0012

Yezierski, P. R., Liu, S., Ruenes, L. G., Kajander, J. K., & Brewer, L. K. (1998). Excitotoxic spinal cord injury: behavioral and morphological characteristics of a central pain model. *Pain*, *75*(1), 141-155. https://doi.org/10.1016/S0304-3959(97)00216-9

Young, W. (1992). Role of calcium in central nervous system injuries. *J Neurotrauma*, *9 Suppl 1*, S9-25. https://www.ncbi.nlm.nih.gov/pubmed/1588635

Zavvarian, M. M., Hong, J., & Fehlings, M. G. (2020). The Functional Role of Spinal Interneurons Following Traumatic Spinal Cord Injury. *Front Cell Neurosci*, *14*, 127. https://doi.org/10.3389/fncel.2020.00127

Zhang, J., Lanuza, G. M., Britz, O., Wang, Z., Siembab, V. C., Zhang, Y., Velasquez, T., Alvarez, F. J., Frank, E., & Goulding, M. (2014). V1 and v2b interneurons secure the alternating flexor-extensor motor activity mice require for limbed locomotion. *Neuron*, *82*(1), 138-150. https://doi.org/10.1016/j.neuron.2014.02.013

Zhang, X. M., & Zhu, J. (2011). Kainic Acid-induced neurotoxicity: targeting glial responses and glia-derived cytokines. *Curr Neuropharmacol*, *9*(2), 388-398. https://doi.org/10.2174/157015911795596540

Zholudeva, L. V., & Lane, M. A. (2019). Transplanting Cells for Spinal Cord Repair: Who, What, When, Where and Why? *Cell Transplantation*, *28*(4), 388-399. https://doi.org/10.1177/0963689718824097

Zholudeva, L. V., Qiang, L., Marchenko, V., Dougherty, K. J., Sakiyama-Elbert, S. E., & Lane, M. A. (2018). The Neuroplastic and Therapeutic Potential of Spinal Interneurons in the Injured Spinal Cord. *Trends Neurosci*, *41*(9), 625-639. https://doi.org/10.1016/j.tins.2018.06.004